Precise determination of universal finite volume observables in the Gross-Neveu model

DISSERTATION

zur Erlangung des akademischen Grades
doctor rerum naturalium
(Dr. rer. nat.)
im Fach Physik

eingereicht an der
Mathematisch-Naturwissenschaftlichen Fakultät I
der Humboldt-Universität zu Berlin

von
Dipl. Phys. Tomasz Korzec
geboren am 28.11.1977 in Warschau

Präsident der Humboldt-Universität zu Berlin:
Prof. Dr. Christoph Markschies

Dekan der Mathematisch-Naturwissenschaftlichen Fakultät I:
Prof. Dr. Christian Limberg

Gutachter:

1. Prof. Dr. Ulrich Wolff
2. Dr. Rainer Sommer
3. Prof. Dr. Uwe Jens Wiese

eingereicht am:	28. September 2006
Tag der mündlichen Prüfung:	26. Januar 2007

Abstract

The Gross-Neveu model is a quantum field theory in two space time dimensions that shares many features with quantum chromo dynamics. In this thesis the continuum model and its discretized versions are reviewed and a finite volume renormalization scheme is introduced and tested. Calculations in the limit of infinitely many fermion flavors as well as perturbative computations are carried out. In extensive Monte-Carlo simulations of the one flavor and the four flavor lattice models with Wilson fermions a set of universal finite volume observables is calculated to a high precision. In the one flavor model which is equivalent to the massless Thirring model the continuum extrapolated Monte-Carlo results are confronted with an exact solution of the model.

Keywords:
Gross-Neveu model, Monte-Carlo, quantum field theory, lattice

Zusammenfassung

Bei dem Gross-Neveu Modell handelt es sich um eine in zwei Raumzeit-Dimensionen formulierte Quantenfeldtheorie, die einige Gemeinsamkeiten mit der Quantenchromodynamik aufweist. In der vorliegenden Arbeit wird zunächst ein Überblick über das Kontinuumsmodell sowie über diskretisierte Versionen gegeben. Ein Renormierungsschema wird eingeführt und getestet. Berechnungen im Grenzwert unendlich vieler Fermionfamilien und in Störungstheorie werden durchgeführt. In ausgiebigen Monte-Carlo Simulationen der Modelle mit einer und vier Fermionfamilien wird eine Reihe universeller Größen mit hoher Genauigkeit ermittelt. Simuliert wird eine Gitterversion des Modells mit Wilson-Fermionen. Für das Modell mit nur einer Fermionfamilie, welches zum masselosen Thirring-Modell äquivalent ist, werden die kontinuumsextrapolierten Ergebnisse mit einer exakten Lösung dieses Modells konfrontiert.

Schlagwörter:
Gross-Neveu Modell, Monte-Carlo, Quantenfeldtheorie, Gitter

Contents

Chapter 1

Overview

There is a theory which states that if ever anyone discovers exactly what the universe is for and why it is here, it will instantly disappear and be replaced by something even more bizarre and inexplicable.
There is another theory which states that this has already happened.

Douglas Adams

1.1 Introduction

The self-imposed goal of the physicist is to understand the underlying principles of the natural world and to be able to describe them mathematically. The mathematical model that has been developed in the second half of the 20th century in order to characterize the smallest known constituents of matter and the interactions among them is called the standard model of elementary particles. In this framework the relatively weak gravitational forces are neglected, while the electromagnetic, weak and strong forces as well as the miscellaneous elementary particles they act on are described by quantum field theories (QFTs). With a relatively small number of only 29 free parameters as an input the model is able to predict the whole spectrum of high energy phenomena, including the complete Hadron-spectrum. A vast amount of experimental data has been gathered over the last few decades and found to be in excellent agreement with the theoretical model.

It is in general impossible to solve problems in interacting QFTs exactly. Most calculations begin with some more or less justified approximations. To describe processes that happen at very high energies, as they are for instance realized in particle collider experiments, perturbation theory has emerged as a very useful and accurate tool. To describe the physics of strong interactions at lower energies where the involved coupling is rather large, other (i.e. nonperturbative) tools are required.

With the formulation of quantum chromo dynamics (QCD) on a space-time lattice [82] Wilson established the base for numerical simulations of quantum field theories. Unfortunately the Monte-Carlo methods that are utilized for the calculations are computationally extremely demanding. In fact, even though state of the art parallel supercomputers are utilized, it has not been possible so far to perform full QCD simulations. Despite considerable progress in algorithm efficiency and machine power, the most recent computations take into consideration only the three lightest quarks, run at unphysically large pion masses and on only moderately sized lattices. Nevertheless an impressive number of outstanding results has been achieved. The main fields of activity were so far the determination of the hadron spectrum, glueball spectroscopy, the investigation of the structure of hadrons (i.e. the calculation of structure functions), the running of the QCD-coupling α_S, the thermodynamics of QCD, the calculation of weak interaction matrix elements and many more. Most recent results are annually collected in the proceedings of the lattice conferences [39].

The high effort of realistic simulations makes the treatment of simpler, often lower dimensional "toy"-models attractive. Some of these models have a lot in common with QCD and can hence be used to study special aspects of the much more complicated theory at least qualitatively. The renormalizable two dimensional Gross-Neveu model [33] for instance is asymptotically free, has a complicated bound-state spectrum and features dynamical chiral symmetry breaking together with mass generation in the limit of an infinite number of flavors (large N limit). The Schwinger model [69] on the other hand is a two dimensional gauge theory which exhibits confinement and develops a chiral condensate but which in contrast to QCD is super-renormalizable. Such two dimensional models can be simulated with a satisfyingly high precision on simple personal computers using the same techniques that are well known from QCD. This makes them the perfect testbed for algorithms and a convenient laboratory in which different lattice-formulations of the same theory can be compared with each other.

Besides their role as toy-models, two dimensional systems are very interesting in their own right. Phenomena like bosonization [16], i.e. the quantum-equivalence between certain fermionic and bosonic systems exist only in two dimensions. Another 2d-feature is the impossibility of spontaneous breakdown of continuous symmetries. Instead, phase transitions of the Kosterlitz-Thouless type [51] can appear. In addition some of the models are integrable, which under certain assumptions made it possible to derive exact analytic results for certain observables (like the S-matrices [87, 43, 7] or the massgaps [25]). Some two dimensional quantum field theories have an application in the context of quasi one dimensional condensed matter systems. Particularly interesting in this regard is the equivalence between the $N = 2$ Gross-Neveu model and models that successfully describe con-

ducting polymers like trans-polyacetylene and cis-polyacetylene, or inhomogeneous superconductors [79, 13].

The main attention of this work goes to the formulation of finite volume renormalization schemes for the family of Gross-Neveu models, their testing in perturbation theory to one loop and at large-N and to the numerical calculation of numerous universal quantities to high accuracy by means of Monte-Carlo simulations. The layout is as follows:

After a short general introduction to quantum field theories on the lattice in chapter one the Gross-Neveu models are introduced (chapter two). A new renormalization scheme is proposed for the standard Gross-Neveu model, while for the chiral Gross-Neveu model a Schrödinger functional renormalization scheme similar to that used in QCD simulations [58, 74] is formulated. Chapter three is devoted to the different lattice formulations of these models. In chapter five a 1-loop perturbative calculation is presented in order to legitimate the renormalization scheme for the Gross-Neveu model with Wilson fermions. The core of the thesis (chapter six) deals with the Monte-Carlo simulation of the models.

Results and conclusions are presented at the end.

The large-N calculations of chapter four are more or less independent of the rest of the work. The results derived here contribute to the general understanding of the models and their discretized versions.

Parts of the results of this thesis have been published in [46, 50, 49].

1.2 Motivation of the thesis

Lattice field theory is by now a well established area of high energy physics. There are several reviews and text-books on this topic [48, 17, 60, 75, 67] which provide an excellent introduction to the field. The lattice approach is based on Feynman's path integral formalism in Euclidean space in which transition amplitudes from a state generated by the action of the time ordered operator O on the vacuum state $|\Omega\rangle$ to the vacuum are represented in terms of functional integrals

$$\langle\Omega|TO|\Omega\rangle = \frac{1}{Z}\int D\phi\, O[\phi]\, e^{-S[\phi]}\,, \tag{1.1}$$

where S is the Euclidean action of the field theory at hand and $\int D\phi$ is a (in the continuum usually ill-defined) functional integral measure. Z is a (in the continuum often infinite) normalization constant chosen such that $\langle\Omega|\Omega\rangle = 1$. The introduction of a space-time lattice regularizes the theory. On a finite lattice the functional integral turns into a very high dimensional ordinary integral, which can be evaluated with Monte-Carlo methods. Renormalized observables which not only have a finite value, but also a finite continuum limit can be defined.

In the path integral approach fermions are represented by Grassmann-valued fields, i.e.

$$\{\bar{\psi}(x), \bar{\psi}(y)\} = 0 \tag{1.2}$$
$$\{\bar{\psi}(x), \bar{\psi}(y)\} = 0 \tag{1.3}$$
$$\{\psi(x), \bar{\psi}(y)\} = 0\,, \qquad \forall x, y \tag{1.4}$$

$$\int d\bar{\psi}\,\bar{\psi} = \int d\psi\,\psi = 1 \tag{1.5}$$
$$\int d\bar{\psi}\,1 = \int d\psi\,1 = 0\,. \tag{1.6}$$

The incorporation of fermions into the Monte-Carlo simulations is a computationally very demanding task. The details of a lattice formulation of the Gross-Neveu models will be explained in chapter 3.

Since quantum field theories describe systems of arbitrarily many particles and the highly nonlinear interactions among them, it is not very astonishing, that only few results can be obtained analytically. Proofs usually rely on a basis of more or less well founded assumptions and many things remain unproven.

When a theory is set up on a lattice, there is much freedom in the formulation. Ideas borrowed from the theory of critical phenomena suggest that there are *universality classes* and that all lattice models which are in the same class can describe the same physics if the involved correlation lengths become very large in lattice units, i.e. when the continuum limit is taken. Since universality between different formulations is among the things that cannot be proven rigorously, discussions about the validity of certain approaches arise from time to time in the community. For instance the compatibility of results obtained in the staggered and in the Wilson formulation was questioned by S. Aoki on the year 2000 lattice conference [2]. His objections were addressed by C. Davies et al. [20] who explained the deviations by the contribution of subleading cutoff effects and found agreement after the employment of a more sophisticated fitting procedure.

Recently the validity of the so called rooted staggered fermion approach is discussed [71]. The corresponding action lacks locality which in turn arises doubts on the model's belonging to the correct universality class.

Of course numerical simulations cannot really prove that two models are equivalent. But if they are not, the simulations might find significant disagreement in quantities that are supposed to be universal. This is certainly only possible if the statistical errors on the results are small enough and the systematic errors under good control.

In this thesis a framework is set up in a two dimensional model, where the aforementioned questions can be addressed. Since the simulations in

this model are comparatively cheap, systematic errors arising from continuum extrapolations or finite size effects can be kept under control or completely eliminated, while the statistical errors may be as low as a fraction of one per mille.

Chapter 2

The Gross-Neveu models

2.1 Fermion interaction terms in two dimensions

In the discussion of the renormalizability of a given quantum field theory its symmetries play a key role. In the first part of this section the continuous and discrete symmetries of the Euclidean action of a free fermion in two space-time dimensions are summarized and afterwards possible interaction terms are introduced.

2.1.1 Symmetries of the free fermion action

The free action, is given by

$$S^{(0)} = \int d^2x \; \bar{\psi}(x)[\partial\!\!\!/ + m]\psi(x)\,. \tag{2.1}$$

In this short notation the Dirac and the flavor indices are suppressed. In places where it is favorable to have them explicit, Greek indices $(\alpha, \beta, \ldots)$ will denote the Dirac component (0 or 1) and Latin indices $(i, j, \ldots)$ will stand for the flavor component $(1 \ldots N)$. The free action is invariant under the following transformations

Euclidean symmetry

With a Euclidean metric instead of the Minkowski metric the Poincare group is replaced by the Euclidean group $E(2)$. The action is invariant under translations

$$x_\mu \to x_\mu + a_\mu \tag{2.2}$$

as well as under orthogonal transformations which would correspond to the boosts in a theory on a Minkowski space

$$x \to \Lambda x \qquad \Lambda \in O(2)\,. \tag{2.3}$$

One can parameterize a vector-representation of the $SO(2)$ group by

$$\Lambda = \begin{pmatrix} \cos(\alpha) & \sin(\alpha) \\ -\sin(\alpha) & \cos(\alpha) \end{pmatrix}. \tag{2.4}$$

Two component spinors transform according to

$$\begin{aligned} \psi(x) &\rightarrow e^{\frac{i}{2}\gamma_5\alpha}\psi(\Lambda x) \\ \bar{\psi}(x) &\rightarrow \bar{\psi}(\Lambda x)e^{-\frac{i}{2}\gamma_5\alpha}. \end{aligned} \tag{2.5}$$

Elements of the $O(2)$ with $\det\Lambda = -1$ are obtained by $SO(2)$ rotations followed by an axis reversal, i.e. either a parity transformation

$$\begin{aligned} \psi(x_0, x_1) &\rightarrow \mathcal{P}\psi(x_0, -x_1) \\ \bar{\psi}(x_0, x_1) &\rightarrow \bar{\psi}(x_0, -x_1)\mathcal{P}^\dagger \end{aligned} \tag{2.6}$$

or a time reversal transformation

$$\begin{aligned} \psi(x_0, x_1) &\rightarrow \mathcal{T}\psi(-x_0, x_1) \\ \bar{\psi}(x_0, x_1) &\rightarrow \bar{\psi}(-x_0, x_1)\mathcal{T}^\dagger \end{aligned} \tag{2.7}$$

The unitary matrices $\mathcal{P}$ and $\mathcal{T}$ have to satisfy

$$\begin{aligned} \mathcal{P}^\dagger\gamma_\mu\mathcal{P} &= (-1)^\mu \qquad \textit{and} \\ \mathcal{T}^\dagger\gamma_\mu\mathcal{T} &= (-1)^{\mu+1}. \end{aligned} \tag{2.8}$$

A convenient choice is $\mathcal{P} = \gamma_0$ and $\mathcal{T} = \gamma_1$.

Chiral symmetry

When the fermion fields are decomposed into their chiral components

$$\begin{aligned} \psi_R = P_R\psi \qquad & \bar{\psi}_R = \bar{\psi}P_L \\ \psi_L = P_L\psi \qquad & \bar{\psi}_L = \bar{\psi}P_R \end{aligned} \tag{2.9}$$

with the chiral projectors

$$P_R = \frac{1}{2}(\mathbb{1} + \gamma_5) \tag{2.10}$$

$$P_L = \frac{1}{2}(\mathbb{1} - \gamma_5), \tag{2.11}$$

the massless action falls into two separate terms which do not mix fields of different chirality

$$S^{(0)} = \int d^2x \ (\bar{\psi}_L(x)\partial\!\!\!/\psi_L(x) + \bar{\psi}_R(x)\partial\!\!\!/\psi_R(x)) \ . \tag{2.12}$$

It is invariant under independent unitary flavor transformations of the left-handed and the right-handed fields

$$\begin{array}{ll} \psi_{\mathrm{R}} \to V_{\mathrm{R}}\psi_{\mathrm{R}} & \bar{\psi}_{\mathrm{R}} \to \bar{\psi}_{\mathrm{R}}V_{\mathrm{R}}^{\dagger} \\ \psi_{\mathrm{L}} \to V_{\mathrm{L}}\psi_{\mathrm{L}} & \bar{\psi}_{\mathrm{L}} \to \bar{\psi}_{\mathrm{L}}V_{\mathrm{L}}^{\dagger} \end{array} \qquad V_{\mathrm{R}}, V_{\mathrm{L}} \in U(N)\,. \tag{2.13}$$

Since a mass term mixes the chiral components

$$\bar{\psi}m\psi = \bar{\psi}_{\mathrm{L}}m\psi_{\mathrm{R}} + \bar{\psi}_{\mathrm{R}}m\psi_{\mathrm{L}}\,, \tag{2.14}$$

in presence of degenerate masses (same mass for all flavors) the symmetry is broken down to the subgroup in which $V_{\mathrm{R}} = V_{\mathrm{L}}$, i.e. the vector transformations $U(N)_{\mathrm{V}}$. Should one decide to give every flavor its own unique mass ($m \to$ diagonal mass matrix), the symmetry would be further reduced to a $U(1)_{\mathrm{V}}$ for each flavor.

Charge conjugation

A discrete symmetry that interchanges ψ and $\bar{\psi}$ is given by the transformation

$$\begin{array}{rcl} \psi & \to & [\bar{\psi}C^{-1}]^{\top} \\ \bar{\psi} & \to & -[C\psi]^{\top}\,, \end{array} \tag{2.15}$$

with C fulfilling the following condition

$$-C^{-1}\gamma_{\mu}^{\top}C = \gamma_{\mu}\,. \tag{2.16}$$

With real and symmetric γ_0 and γ_1 the only choice (up to a multiplicative constant) is $C = \gamma_5$.

2.1.2 Possible interaction terms

In two dimensions the fermionic fields have mass dimension one half (which can be read off from the kinetic term), therefore the couplings of four fermion interaction terms are dimensionless and hence renormalizable (by power counting).

The most general local four fermion interaction term is

$$\Gamma_{\alpha\beta\gamma\delta}\, A_{ijkl}\, \bar{\psi}_{\alpha i}(x)\psi_{\beta j}(x)\bar{\psi}_{\gamma k}(x)\psi_{\delta l}(x)\,. \tag{2.17}$$

In the following it is discussed how the tensors Γ and A have to be restricted in order for the action to keep some of the symmetries of the free action.

If one wants to keep the $U(N)_{\mathrm{V}}$ flavor symmetry, the only possible choices for the tensor A are

$$A_{ijkl} = \delta_{ij}\delta_{kl} \qquad \text{or} \qquad A_{ijkl} = \delta_{il}\delta_{jk}\,. \tag{2.18}$$

The second possibility can be rewritten

$$\delta_{in}\delta_{jm} = \frac{1}{2}\sum_k \lambda^{(k)}_{ij}\lambda^{(k)}_{mn} + \frac{1}{N}\delta_{ij}\delta_{mn}\,, \tag{2.19}$$

where $\lambda^{(k)}$ are the generators of the $SU(N)$ group as defined in appendix A.5.

Another symmetry that should be respected by the interaction term is the Euclidean invariance. There are the following four possibilities to form a Lorentz scalar out of four spinors

$$\Gamma_{\alpha\beta\gamma\delta} = \begin{cases} \mathbb{1}_{\alpha\beta}\mathbb{1}_{\gamma\delta} \\ (\gamma_5)_{\alpha\beta}(\gamma_5)_{\gamma\delta} \\ \sum_\mu (\gamma_\mu)_{\alpha\beta}(\gamma_\mu)_{\gamma\delta} \\ \sum_\mu (\gamma_\mu\gamma_5)_{\alpha\beta}(\gamma_\mu\gamma_5)_{\gamma\delta} \end{cases} \tag{2.20}$$

The last two choices are proportional to each other, since two dimensions have the peculiarity that

$$\gamma_\mu\gamma_5 = i\epsilon_{\mu\nu}\gamma_\nu\,. \tag{2.21}$$

The possible interactions so far are

$$\begin{aligned} \mathcal{L}^{SS} &= (\bar\psi\psi)^2 & \mathcal{L}^{SS'} &= (\bar\psi\lambda^{(i)}\psi)(\bar\psi\lambda^{(i)}\psi) \\ \mathcal{L}^{PP} &= (\bar\psi\gamma_5\psi)^2 & \mathcal{L}^{PP'} &= (\bar\psi\gamma_5\lambda^{(i)}\psi)(\bar\psi\gamma_5\lambda^{(i)}\psi) \\ \mathcal{L}^{VV} &= (\bar\psi\gamma_\mu\psi)(\bar\psi\gamma_\mu\psi) & \mathcal{L}^{VV'} &= (\bar\psi\gamma_\mu\lambda^{(i)}\psi)(\bar\psi\gamma_\mu\lambda^{(i)}\psi)\,. \end{aligned} \tag{2.22}$$

But not all of them are independent. Fierz identities (see appendix B.2 for a more detailed calculation) can be used to eliminate three of them. For instance the identities

$$\mathcal{L}^{SS'} = -\frac{2+N}{N}\mathcal{L}^{SS} - \mathcal{L}^{PP} - \mathcal{L}^{VV} \tag{2.23}$$

$$\mathcal{L}^{PP'} = -\mathcal{L}^{SS} - \frac{2+N}{N}\mathcal{L}^{PP} + \mathcal{L}^{VV} \tag{2.24}$$

$$\mathcal{L}^{VV'} = -2\mathcal{L}^{SS} + 2\mathcal{L}^{PP} - \frac{2}{N}\mathcal{L}^{VV}\,. \tag{2.25}$$

can be used to write everything in the flavor-singlet-basis. Depending on which subset of interactions out of (2.22) is added to the free action, different (well known) models are obtained. The Thirring model [80] has just one flavor and the interaction term $\mathcal{L}^{VV}$ while the generalized $SU(N)$-Thirring [18] model has the terms $\mathcal{L}^{VV}$ and $\mathcal{L}^{VV'}$ and N flavors of fermions. In this work the main interest lies in the Gross-Neveu and the chiral Gross-Neveu models which are examined closer in the following two sections.

2.2 The Gross Neveu model

A very interesting model was studied by Gross and Neveu [33] already in the seventies. Its Euclidean action is given by

$$S^{\mathrm{GN}} = \int d^2x \left[\bar{\psi}(x) \partial\!\!\!/ \psi(x) - \frac{g^2}{2} \left(\bar{\psi}(x)\psi(x)\right)^2 \right]. \tag{2.26}$$

Depending on the number of flavors N the model reproduces other known models (or is believed to be in the same universality class).

- For $N = 1/2$ the model describes a free, massless fermion. Odd multiples of $1/2$ can be understood in the Majorana language (odd number of Majorana-components) which is explained in the next subsection. This correspondence is exact and holds also in a regularized theory, e.g. on a lattice.
- With $N = 1$ there is only one nonvanishing local four-fermion interaction possible due to the Grassmanian nature of the fields. Hence the 1-flavor Gross-Neveu model is identical to the massless Thirring model and to the 1-flavor chiral Gross-Neveu model. Also in this case the correspondence is completely rigorous. By bosonization techniques the Thirring model can be related to the bosonic sine-Gordon model [16, 76]. The latter equivalence is very non-trivial. Although there is no stringent mathematical prove for bosonization, the scenario is supported by numerous independent methods.
- With $N = 3/2$ the model is equivalent to the supersymmetric sine-Gordon model at the critical coupling [83]. The correspondence procedes via bosonization.
- $N = 2$ corresponds to two decoupled SU(2) Thirring models [34]. Again bosonization is needed to show the equivalence. This conjecture is supported by findings on the exact S-matrix of the model [43]. This system is also equivalent to models that are used to model quasi one dimensional condensed matter systems [79, 13].
- Finally for $N = 3$ bosonization relates the Gross-Neveu model to a $SU(4)$ Thirring model [34].

2.2.1 Symmetries of the Gross-Neveu model

Apart from Euclidean and charge conjugation symmetry the model has got a discrete chiral symmetry

$$\begin{aligned} \psi(x) &\rightarrow \gamma_5 \psi(x) \\ \bar{\psi}(x) &\rightarrow -\bar{\psi}(x)\gamma_5 \end{aligned} \tag{2.27}$$

and an $O(2N)$ flavor symmetry [19]. The latter is hidden but can be uncovered by a change of variables. Assuming that the chosen representation of the Clifford algebra has real γ_0 and γ_1 the substitution

$$\begin{pmatrix} \psi \\ \bar{\psi}^\top \end{pmatrix} = \frac{1}{\sqrt{2}} \begin{pmatrix} \xi_1 + i\xi_2 \\ C^\top \xi_1 - iC^\top \xi_2 \end{pmatrix} \tag{2.28}$$

where C is the charge-conjugation matrix introduced in 2.16, leads to the action

$$S^{GN'} = \int d^2x \left[\frac{1}{2} \xi^\top(x) C \partial\!\!\!/ \xi(x) - \frac{g^2}{8} \left(\xi^\top(x) C \xi(x) \right)^2 \right], \tag{2.29}$$

with a ξ field that has got $\mathcal{N} = 2N$ components. The $O(\mathcal{N})$ symmetry

$$\xi(x) \to R\xi(x), \qquad R \in O(\mathcal{N}) \tag{2.30}$$

has become apparent. This subgroup of the full chiral group is enough to render the model stable under renormalization. The γ_5-symmetry forbids a mass term, while the only four fermion term which is invariant under the large flavor symmetry is the one given in (2.26) and (2.29).

2.2.2 Auxiliary field actions

In large-N calculations and in simulations one often starts from an effective action in which the Grassmann-valued fermionic fields are already integrated out. This is possible only in theories where the action is quadratic in the fermionic variables. To bring the Gross-Neveu model into a suitable form the four-fermion interaction is traded for a boson-fermion interaction of the Yukava type. Depending on the value of N one can choose differently distributed bosonic fields (e.g. Ising-type or $U(1)$-fields). A choice which works for all values of N is a Gaussian auxiliary field. The identity[1]

$$1 = const \int D\sigma \ \exp\left[- \int d^2x \, \frac{1}{2g^2} \left(\sigma(x) + g^2 \bar{\psi}(x)\psi(x) \right)^2 \right] \tag{2.31}$$

can be inserted into the partition function giving

$$Z = \int D\bar{\psi} \, D\psi \, D\sigma \, e^{-S^{GN-aux}} \tag{2.32}$$

with the auxiliary-field action

$$S^{GN-aux} = \int d^2x \left(\bar{\psi}(x)[\partial\!\!\!/ + \sigma(x)]\psi(x) + \frac{\sigma(x)^2}{2g^2} \right). \tag{2.33}$$

[1] All this can be (and will be) made much more rigorous in the lattice-regularized model.

Fermionic correlation functions calculated in this statistical ensemble are identical to those calculated in the original model. In the Majorana-language one obtains

$$S^{GN-aux'} = \int d^2x \, \frac{1}{2}\left(\xi^\top(x)C[\partial\!\!\!/ + \sigma(x)]\xi(x) + \frac{\sigma(x)^2}{g^2}\right) \tag{2.34}$$

The integral over the fermionic fields yields a $\det[\partial\!\!\!/ + \sigma]^N$ in the Dirac language and the Pfaffian $Pf[C(\partial\!\!\!/ + \sigma)]^{\mathcal{N}}$ in the Majorana language. Of course this coincides for $\mathcal{N} = 2N$ and leads to a nonlocal effective action

$$S^{GN-eff} = \int d^2x \, \frac{\sigma(x)^2}{2g^2} - N \, \log \, \mathrm{d}et \, (\partial\!\!\!/ + \sigma) \, . \tag{2.35}$$

2.2.3 The Gross-Neveu model in the literature

Many interesting properties of the model have been established by various methods.

In the large-N limit the model exhibits asymptotic freedom and spontaneous breakdown of the discrete γ_5-symmetry together with dynamical mass generation [33]. The large-N expansion is also suitable to study the phase-diagram of the model at finite temperature and chemical potential [85, 68, 79]. Many calculations were extended beyond the leading order in the $1/N$-expansion [9].

The particle-spectrum has been calculated in the semi-classical approximation [19]. The $O(\mathcal{N})$-symmetric model (with $\mathcal{N} > 4$) is believed to contain kinks with the mass m_K as well as bound states of kinks with masses

$$m_n = 2m_K \, \sin \frac{\pi n}{\mathcal{N}-2}, \qquad 1 \leq n < \frac{\mathcal{N}}{2} - 1 \, . \tag{2.36}$$

Since the model belongs to the class of integrable quantum field theories, i.e. it has an infinite number of conservation laws on the classical level, the form of its S-matrix is very restricted. There is no particle production and the S-matrix factorizes into a product of two-particle S-matrices. The exact form of the S matrix for the elementary fermions has been proposed in [87]. The complete S-matrix has been given in [43].

The massgap was calculated exactly with the thermodynamic Bethe ansatz [27, 25] as well as in large N [26] .

The β-function of the model has been calculated up to three loops in dimensional regularization [81, 55, 32].

2.2.4 Observables

The main part of this work is concerned with Monte-Carlo simulations of the Gross-Neveu model, which can only be performed in a finite space-time box. To avoid systematical uncertainties due to finite size effects,

a finite volume renormalization scheme where the box size serves as a physical scale is employed. The work of the ALPHA collaboration [57, 58, 59] on the Schrödinger functional has shown that in such schemes precise continuum extrapolations become feasible. The Schrödinger functional has got Dirichlet boundary conditions in the temporal directions. The approach here is a little bit different.

Let the spatial extent of the space-time box be L and the temporal T with periodic boundary conditions in the spatial direction and antiperiodic in the temporal. The following observables are zero due to the γ_5-symmetry of the action (see appendix A.6 for the conventions concerning Fourier transformations)

$$\begin{aligned} k_S(x_0,p_1) &:= -\frac{2}{\mathcal{N}L}\left\langle \breve{\bar{\psi}}(x_0,-p_1)\breve{\psi}(0,p_1)\right\rangle && (2.37)\\ &= -\frac{1}{\mathcal{N}L}\left\langle \breve{\xi}^{\top}(x_0,-p_1)C\breve{\xi}(0,p_1)\right\rangle && (2.38)\\ \bar{k}_S(p_0,x_1) &:= -\frac{2}{\mathcal{N}T}\left\langle \hat{\bar{\psi}}(-p_0,x_1)\hat{\psi}(p_0,0)\right\rangle && (2.39)\\ &= -\frac{1}{\mathcal{N}T}\left\langle \hat{\xi}^{\top}(-p_0,x_1)C\hat{\bar{\xi}}(p_0,0)\right\rangle . && (2.40) \end{aligned}$$

They will be useful to define the "chiral point" in the regularized theory, when the regulator breaks the γ_5 symmetry (like the Wilson fermions on the lattice).

Other two point functions may be defined as

$$\begin{aligned} k_\mu(x_0,p_1) &:= -\frac{2}{\mathcal{N}L}\left\langle \breve{\bar{\psi}}(x_0,-p_1)\gamma_\mu\breve{\psi}(0,p_1)\right\rangle && (2.41)\\ &= -\frac{1}{\mathcal{N}L}\left\langle \breve{\xi}^{\top}(x_0,-p_1)C\gamma_\mu\breve{\xi}(0,p_1)\right\rangle && (2.42)\\ \bar{k}_\mu(p_0,x_1) &:= -\frac{2}{\mathcal{N}T}\left\langle \hat{\bar{\psi}}(-p_0,x_1)\gamma_\mu\hat{\psi}(p_0,0)\right\rangle && (2.43)\\ &= -\frac{1}{\mathcal{N}T}\left\langle \hat{\xi}^{\top}(-p_0,x_1)C\gamma_\mu\hat{\bar{\xi}}(p_0,0)\right\rangle . && (2.44) \end{aligned}$$

Some of these correlators vanish, e.g.

$$\begin{aligned} k_S(T/2,p_1) &= 0 \qquad \text{d}\textit{ue to time reversal + antiperiodicity} && (2.45)\\ k_1(x_0,0) &= 0 \qquad \text{d}\textit{ue to parity} && (2.46)\\ \bar{k}_1(p_0,L/2) &= 0 \qquad \text{d}\textit{ue to parity + periodicity}\,. && (2.47) \end{aligned}$$

Moreover the real parts of k_1 and $\bar{k}_0$ vanish for all arguments due to parity and time reversal symmetry respectively.

The corresponding renormalized quantities are defined by

$$\begin{aligned} (k_S)_R &= Z_\psi^{-1}k_S & \qquad (\bar{k}_S)_R &= Z_\psi^{-1}\bar{k}_S\\ (k_\mu)_R &= Z_\psi^{-1}k_\mu & \qquad (\bar{k}_\mu)_R &= Z_\psi^{-1}\bar{k}_\mu \end{aligned} \qquad (2.48)$$

with for instance

$$Z_\psi = k_0(T/2, 0)\,. \tag{2.49}$$

A renormalized coupling in this position space scheme can be defined by

$$\begin{aligned} g_R^2 \;=\; & Z_\psi^{-2}\frac{2}{TL}\Big\langle \breve{\bar{\psi}}(T/2)\gamma_5\breve{\bar{\psi}}^\top(0)\breve{\psi}^\top(T/2)\gamma_5\breve{\psi}(0) \\ & +\breve{\bar{\psi}}(0)\breve{\psi}(T/2)\breve{\bar{\psi}}(T/2)\breve{\psi}(0) \\ & +\breve{\bar{\psi}}(0)\breve{\psi}(T/2)\breve{\bar{\psi}}(0)\breve{\psi}(T/2)\Big\rangle\,. \end{aligned} \tag{2.50}$$

In this formula the flavors are not summed over - the four-point function is constructed from fields of the first flavor only. The definition seems a little bit long winded at the first sight, but looks much more natural when translated into the Majorana language

$$g_R^2 = Z_\psi^{-2}\frac{4}{TL}\left\langle \breve{\xi}_1^\top(T/2)C\breve{\xi}_1(0)\breve{\xi}_2^\top(T/2)C\breve{\xi}_2(0)\right\rangle\,. \tag{2.51}$$

Another useful observable is the current-current correlator

$$\breve{f}_{\mu\nu}(t, p_1) \coloneqq \left\langle \breve{j}_\mu(0, p_1)\breve{j}_\nu(t, -p_1)\right\rangle\,. \tag{2.52}$$

with

$$\breve{j}_\mu(x_0, p_1) = \int dx_1\; e^{-ip_1x_1}\, j_\mu(x) = \frac{1}{T}\sum_{p_0} e^{ip_0x_0}\,\tilde{j}_\mu(p) \tag{2.53}$$

and the conserved vector current

$$j_\mu(x) = \bar{\psi}(x)\gamma_\mu\psi(x)\,. \tag{2.54}$$

In the Thirring model (i.e. the Gross-Neveu model with $N = 1$) a calculation very similar to the one in section 2.3.1 but carried out explicitly in finite volume [84] with special care towards constant modes that were neglected in 2.3.1 allows it to calculate the current-current correlator analytically. The result for $p \neq 0$ is

$$\left\langle \tilde{j}_\mu(p)\tilde{j}_\nu(q)\right\rangle = \frac{2}{g^2 + 2\pi}\left[\delta_{\mu\nu} - \frac{p_\mu p_\nu}{p^2}\right]\delta(p + q)\,. \tag{2.55}$$

At zero momentum the afore mentioned constant modes play an important role. The result here is

$$\left\langle \tilde{j}_\mu(0)\tilde{j}_\mu(0)\right\rangle = TL\left[\frac{2}{g^2 + 2\pi} + f_\mu(g^2, \rho)\right], \tag{2.56}$$

with the aspect ratio $\rho = T/L$ and f_μ given by

$$f_0(g^2,\rho) = \rho\langle\langle m^2\rangle\rangle - \frac{2}{g^2+2\pi} \tag{2.57}$$

$$f_1(g^2,\rho) = \rho^{-1}\langle\langle n^2\rangle\rangle - \frac{2}{g^2+2\pi}\,. \tag{2.58}$$

The brackets $\langle\langle\cdot\rangle\rangle$ denote expectations with respect to the partition function

$$Z \propto \sum_{m,n} \alpha_{mn}\, \exp\left[-\frac{g^2}{4}(m^2\rho + n^2\rho^{-1})\right]. \tag{2.59}$$

The coefficients α_{mn} have been obtained numerically in [84], the largest ones for $\rho = 1$ being

m	n	α_{mn}
0	0	0.84721308
0	1	−0.35223659
0	2	0.00316424
0	3	−0.00000123
1	1	0.14644559
1	2	0.00131556
1	3	0.00000051
2	2	0.00001182

and $\alpha_{mn} = -1^{m+n}\alpha_{nm}$.

2.3 The chiral Gross-Neveu model

The chiral Gross-Neveu model is the two dimensional four fermion model whose interaction terms are invariant under an axial $U(1)$ transformation, i.e.

$$\begin{aligned} S^{\chi GN} = \int d^2x \Big\{ &\bar\psi \not\partial \psi - \frac{g_S^2}{2}\left[(\bar\psi\psi)^2 - (\bar\psi\gamma_5\psi)^2\right] \\ &- \frac{g_V^2}{2}\bar\psi\gamma_\mu\psi\bar\psi\gamma_\mu\psi)\Big\}. \end{aligned} \tag{2.60}$$

In general the second term with the coupling g_V is necessary in order to make the model renormalizable [88]. In the original work [33] however (as well as many other works) this term is omitted. As will be shown below, this is legal only if one is interested in the leading order of the large-N expansion of this model.

2.3.1 The current-current interaction term

In this section it is argued on a rather formal level that the coupling of the vector-vector term plays a special role and it is made plausible why it can be set to zero in leading-order large-N calculations. The formal manipulations on the path integral are similar to those in [61].

A Fierz-transformation (see appendix B.2) on the term $\frac{g_S^2}{2}(\mathcal{L}^{SS} - \mathcal{L}^{PP})$ brings the action into the form

$$\begin{aligned} S^{\chi GN} &= \int d^2x \left\{ \bar{\psi}\partial\!\!\!/\psi + \frac{g}{4}\bar{\psi}\lambda^{(i)}\gamma_\mu\psi\bar{\psi}\lambda^{(i)}\gamma_\mu\psi \right. \\ &\qquad \left. + \frac{g'}{2}\bar{\psi}\gamma_\mu\psi\bar{\psi}\gamma_\mu\psi \right\}, \end{aligned} \tag{2.61}$$

with $g = g_S^2$ and $g' = g_S^2/N - g_V^2$.

Of course also in this form auxiliary fields can be used to eliminate the four-fermion interactions. The identities

$$1 \propto \int DB \exp\left[-\int d^2x \, \frac{1}{2g'}(B_\mu + ig' j_\mu)(B_\mu + ig' j_\mu) \right] \tag{2.62}$$

$$1 \propto \int DA \exp\left[-\int d^2x \, \frac{1}{g}\left(A_\mu^i + i\frac{g}{2}J_\mu^i\right)\left(A_\mu^i + i\frac{g}{2}J_\mu^i\right) \right] \tag{2.63}$$

$$\begin{aligned} j_\mu &= \bar{\psi}\gamma_\mu\psi \\ J_\mu^i &= \bar{\psi}\gamma_\mu\lambda^{(i)}\psi \end{aligned}$$

with

$$DB = \prod_x dB_0(x)\, dB_1(x)\,, \qquad DA = \prod_{x,i} dA_0^i(x)\, dA_1^i(x) \tag{2.64}$$

allow it to write the generating functional (source terms suppressed) as

$$Z = \int D\bar{\psi}\, D\psi\, DB\, DA\, \exp\left[-\int d^2x\, \mathcal{L} \right] \tag{2.65}$$

with

$$\mathcal{L} = \bar{\psi}(\partial\!\!\!/ + i\mathcal{A}\!\!\!/ + iB\!\!\!/)\psi + \frac{2}{g}\mathrm{tr}^f(\mathcal{A}_\mu\mathcal{A}_\mu) + \frac{B_\mu B_\mu}{2g'}\,. \tag{2.66}$$

where

$$\mathcal{A}_\mu = \sum_i A_\mu^i \lambda^i \quad \in su(N)\,. \tag{2.67}$$

The auxiliary fields have to be transformed together with the fermions to preserve the symmetries. The $U(N)$ transformations take the form

$$\begin{aligned} \psi &\to U\psi \qquad\qquad U \in U(N) \\ \bar{\psi} &\to \bar{\psi}U^\dagger \\ \mathcal{A} &\to U\mathcal{A}U^\dagger \\ B &\to B \end{aligned} \tag{2.68}$$

while the axial $U(1)$ symmetry is given by

$$\begin{aligned} \psi &\rightarrow e^{i\gamma_5\theta}\psi \\ \bar{\psi} &\rightarrow \bar{\psi}e^{i\gamma_5\theta} \\ \mathcal{A} &\rightarrow \mathcal{A} \\ B &\rightarrow B\,. \end{aligned} \tag{2.69}$$

A linear change of variables in the path integral[2]

$$B_\mu(x) = \epsilon_{\mu\nu}\partial_\nu\phi(x) + \partial_\mu\eta(x) \qquad\qquad \epsilon_{01} = 1 \tag{2.70}$$

leads to

$$\begin{aligned} \mathcal{L} \rightarrow\ & \bar{\psi}[\partial\!\!\!/ + i\mathcal{A}\!\!\!/ + i(\partial\!\!\!/\eta) + i\epsilon_{\mu\nu}\gamma_\mu(\partial_\nu\phi)]\psi \\ & + \frac{2}{g}\mathrm{tr}^f(\mathcal{A}_\mu\mathcal{A}_\mu) + \frac{(\partial_\mu\phi)(\partial_\mu\phi) + (\partial_\mu\eta)(\partial_\mu\eta) + 2\epsilon_{\mu\nu}(\partial_\mu\eta)(\partial_\nu\phi)}{2g'}\,. \end{aligned}$$

The $i\bar{\psi}(\partial\!\!\!/\eta)\psi$ term can be removed by the variable transformation

$$\begin{aligned} \psi(x) &\rightarrow e^{-i\eta(x)}\psi(x) \\ \bar{\psi}(x) &\rightarrow \bar{\psi}(x)e^{i\eta(x)} \end{aligned} \tag{2.71}$$

and the $i\bar{\psi}\epsilon_{\mu\nu}\gamma_\mu(\partial_\nu\phi)\psi$ term vanishes after the transformation

$$\begin{aligned} \psi(x) &\rightarrow e^{-\gamma_5\phi(x)}\psi(x) \\ \bar{\psi}(x) &\rightarrow \bar{\psi}(x)e^{-\gamma_5\phi(x)}\,. \end{aligned} \tag{2.72}$$

Note that in 2d $-\partial\!\!\!/\gamma_5\phi = i\epsilon_{\mu\nu}\gamma_\mu\partial_\nu\phi$. The last transformation comes along with a non-trivial Jacobian (Fujikawa, see appendix B.3). The $2\epsilon_{\mu\nu}(\partial_\mu\eta)(\partial_\nu\phi)$ term does not contribute to the action (integrate by parts, assume $\eta(\infty) = 0$), so the generating functional factorizes into

$$Z = Z_1 Z_2 \tag{2.73}$$

with

$$Z_1 = \int D\bar{\psi}D\psi DA\ \exp\left[-\int d^2x\,\bar{\psi}[\partial\!\!\!/ + i\mathcal{A}\!\!\!/]\psi + \frac{2}{g}\mathrm{tr}^f(\mathcal{A}_\mu\mathcal{A}_\mu)\right] \tag{2.74}$$

$$Z_2 = \int D\eta D\phi\ \exp\left[-\int d^2x\left(\frac{\pi + iNg'}{2\pi g'}\partial_\mu\phi\partial_\mu\phi + \frac{1}{2g'}\partial_\mu\eta\partial_\mu\eta\right)\right] \tag{2.75}$$

Z_2 is just the partition function of a free scalar theory and hence g' does not renormalize. Moreover the relation $g' = g_S^2/N - g_V^2$ suggests, that in the limit $N \rightarrow \infty$ also g_V has a vanishing β-function. This means, that it can be safely set to zero.

[2] A more careful calculation would include a constant term on the r.h.s.

2.3.2 Ward identities

The chiral model satisfies an axial Ward identity (written here as an operator identity)

$$O(y)\,\partial_\mu \left[\bar{\psi}(x)\gamma_\mu\gamma_5\psi(x)\right] = 0\,, \qquad y \neq x\,. \tag{2.76}$$

When a small mass is introduced and the couplings of the $(\bar{\psi}\psi)^2$ and $(\bar{\psi}\gamma_5\psi)^2$ terms are unequal, the axial current is not conserved anymore

$$\begin{aligned} O(y)\,\partial_\mu \left[\bar{\psi}(x)\gamma_\mu\gamma_5\psi(x)\right] \;=\; & 2m\,O(y)\,\bar{\psi}(x)\gamma_5\psi(x) \\ & -2(g_{\mathrm{S}}^2 - g_{\mathrm{P}}^2)\,O(y)\,\bar{\psi}(x)\gamma_5\psi(x)\bar{\psi}(x)\psi(x) \end{aligned} \tag{2.77}$$

With Wilson fermions this Ward identity can be used to fix the additive mass renormalization constant and the ratio $g_{\mathrm{S}}/g_{\mathrm{P}}$. A careful and detailed treatment of the chiral Gross-Neveu model in the Schrödinger functional setup can be found in [53].

Chapter 3

The Gross-Neveu models on the lattice

Some kind of regularization is necessary if the theory is to be defined beyond a formal level. A popular regularization, and the only one that allows numerical simulations, is the lattice formulation. A space time lattice with spacing a is introduced. In a finite volume it will have a finite number $(L/a \times T/a)$ of sites. The fields $\bar{\psi}, \psi$ live only on the sites and derivatives of the fields are approximated by finite differences. Our lattice-notation is introduced in appendix A.1. Since one is eventually interested in the continuum limit, the lattice-actions that one may consider can differ by terms of order a, which vanish in the continuum limit. This freedom should be exploited to preserve as many of the continuum symmetries as possible.

A most naive action for the free fermion takes the form

$$S^{\mathrm{n}aive(0)} = a^2 \sum_x \bar{\psi}(x) \left[\tilde{\partial\!\!\!/} + m \right] \psi(x) \,. \tag{3.1}$$

It has the full chiral symmetry of the continuum action (2.1). The lattice however breaks most of the space-time symmetries. From the Euclidean group only rotations by 90 degrees, translations by whole lattice-spacings and axis reversals are preserved. This naive action has the well known problem of fermion-doubling [65]. For each flavor of the field ψ one obtains four degenerate "tastes" in the continuum limit. The problem can be understood already in the free theory. The propagator obtained from (3.1) is (see appendix A.1 for the lattice notation)

$$\langle \bar{\psi}(x)\psi(y) \rangle^{(0)} = - \int_{-\pi/a}^{\pi/a} \frac{d^2p}{(2\pi)^2} \, \frac{-i\mathring{p\!\!\!/} + m}{\mathring{p}^2 + m^2} e^{ip(y-x)} \,. \tag{3.2}$$

This is clearly a good approximation to the continuum expression 2.1 for momenta around zero. But also momenta around $(0, \pi/a)$, $(\pi/a, 0)$ and

$(\pi/a, \pi/a)$ give contributions that will not vanish in the continuum limit. It has been shown [70] that these contributions can be interpreted as three spare flavors (which are called tastes to distinguish them from the usual flavors).

The doubling problem is deeper and not restricted to the special action (3.1). The Nielsen-Ninomiya theorem [65] states that a lattice-regularization of a fermionic theory either breaks explicitly a part of the full chiral symmetry, or if not, that it will generate doublers. To be more precise one can consider some lattice Dirac operator D, so that the free massless action is given by

$$S = \int_{-\pi/a}^{\pi/a} \frac{d^2p}{(2\pi)^2}\, \tilde{\bar{\psi}}(-p)\tilde{D}(p)\psi(p)\,. \tag{3.3}$$

The statement of the Nielson-Ninomiya theorem is that the following criteria cannot be satisfied all at the same time:

- $\tilde{D}(p)$ is analytic and periodic (with period $2\pi/a$), which is required for D to be a local operator.
- For small momenta the lattice Dirac operator reproduces the continuum Dirac operator $\tilde{D}$, i.e.

$$\tilde{D}(p) = -i\not{p} + O(ap^2)\,. \tag{3.4}$$

- $\tilde{D}$ is invertible for all nonzero momenta within the Brillouin-zone, i.e. there are no doublers.
- $\tilde{D}$ anticommutes with γ_5, i.e.the chiral symmetry remains unbroken.

3.1 Wilson fermions

The oldest and best understood method to remove the doublers from the theory goes back to Wilson [82]. The naive lattice Dirac operator is supplemented with a second derivative term

$$\tilde{\not{\partial}} \to D_{\mathrm{W}} = \tilde{\not{\partial}} - \frac{ar}{2}\partial^*_\mu\partial_\mu\,, \tag{3.5}$$

where r is the Wilson parameter which is usually set to 1. The free propagator with massive Wilson fermions (bare mass m_0) is given by

$$\langle\bar{\psi}(x)\psi(y)\rangle^{(0)} = -\int_{\pi/a}^{\pi/a} \frac{d^2p}{(2\pi^2)}\, \frac{-i\mathring{\not{p}} + M(p)}{\mathring{p}^2 + M(p)^2} e^{ip(y-x)}\,, \tag{3.6}$$

with

$$M(p) = m_0 + \frac{ar}{2}\hat{p}^2 \,. \tag{3.7}$$

It has the correct continuum limit. The doublers get a mass which is proportional to the inverse lattice spacing.

The main drawback of Wilson fermions is, that in agreement with the Nielsen-Ninomiya theorem the chiral symmetry remains broken even for $m_0 \to 0$. Nevertheless it is believed [10] that a chiral continuum limit can be taken, but that the mass has to be carefully tuned along a critical line $m_0 = m_c(g_R^2)$. There are many ways to define such a line in an interacting theory. Usually one tunes the bare mass such that some chiral Ward identity (like the PCAC-relation) is fulfilled.

The action of the Gross-Neveu model with Wilson fermions is

$$\begin{aligned} S^{\mathrm{W}} &= a^2 \sum_x \left(\bar{\psi} D_{\mathrm{W}} \psi - \frac{g^2}{2} (\bar{\psi}\psi)^2 \right) && (3.8) \\ &= a^2 \sum_x \left(\frac{1}{2} \xi^\top C D_{\mathrm{W}} \xi - \frac{g^2}{8} (\xi^\top C \xi)^2 \right) && (3.9) \end{aligned}$$

and for the chiral Gross-Neveu model accordingly.

Since the $U(N)_{\mathrm{V}}$ symmetry is not affected by the Wilson term, it is possible to write down the exact Noether-current associated with this symmetry (see appendix B.1 for a short derivation). The singlet current is

$$\begin{aligned} j_\mu(x) &= \frac{1}{2} \left(\bar{\psi}(x) \gamma_\mu \psi(x+\hat{\mu}) + \bar{\psi}(x+\hat{\mu}) \gamma_\mu \psi(x) \right) \\ &- \frac{r}{2} \left(\bar{\psi}(x) \psi(x+\hat{\mu}) - \bar{\psi}(x+\hat{\mu}) \psi(x) \right) . \end{aligned} \tag{3.10}$$

Sometimes it is advantageous to use this definition of the current instead of the naive vector-current $j_\mu(x) = \bar{\psi} \gamma_\mu \psi(x)$. There exists of course no axial-vector Noether current with Wilson fermions.

3.2 Staggered fermions

Another very popular fermionic action was introduced in [77, 70]. The idea is to reduce the number of degrees of freedom per site in order to reduce the taste-degeneracy. Although most of the following derivation of the free fermion staggered action can be found in the literature [44, 67], it will be reviewed here rather carefully, because a detailed understanding of the procedure is necessary in order to introduce interactions into the formalism and to formulate suitable observables.

3.2.1 Free fermions

The derivation starts from the naively discretized action of the free massless field theory (3.1). In this section we use lattice units ($a = 1$), hence

$$S^{\mathrm{naive}(0)} = \frac{1}{2} \sum_{x,\mu} (\bar{\psi}(x)\gamma_\mu \psi(x+\hat{\mu}) - \bar{\psi}(x)\gamma_\mu \psi(x-\hat{\mu}))\,. \tag{3.11}$$

One way to obtain a staggered formulation is the "spin-diagonalization". The variables are locally changed according to

$$\psi(x) = T(x)\chi(x) \tag{3.12}$$
$$\bar{\psi}(x) = \bar{\chi}(x)T^\dagger(x) \tag{3.13}$$

where $T(x)$ are unitary 2×2 matrices chosen such that

$$T^\dagger(x)\gamma_\mu T(x+\hat{\mu}) = \eta_\mu(x)\mathbb{1}, \qquad \eta_\mu \in \mathbb{C}\,. \tag{3.14}$$

A popular choice, which has the useful property that $T(x-\hat{\mu}) = T(x+\hat{\mu})$, is

$$T(x) = \gamma_0^{x_0}\gamma_1^{x_1}\,. \tag{3.15}$$

With this choice the so called staggered-phases η take the values

$$\eta_\mu(x) \coloneqq T^\dagger(x)\gamma_\mu T(x+\hat{\mu}) = (-1)^{\mu\, x_0} \tag{3.16}$$

After the change of variables the action is diagonal in spin

$$S^{\mathrm{naive}(0)} = \frac{1}{2} \sum_{x,\alpha,\mu} \eta_\mu(x) \left[\bar{\chi}_\alpha(x)\chi_\alpha(x+\hat{\mu}) - \bar{\chi}_\alpha(x)\chi_\alpha(x-\hat{\mu})\right]\,. \tag{3.17}$$

So far the action is still equivalent to the naive action with its fermion doubling problem. The step to staggered fermions is to omit the summation over the Dirac index α, i.e. to reduce χ and $\bar{\chi}$ from a 2-component to a single component field. The difficult part is to show that this new action describes in its continuum limit free fermions. These must be represented by spinors

and not by a single-component field. One introduces a coarse lattice (here labeled by big letters e.g. X, Y)

$$x_\mu = 2X_\mu + \rho_\mu\,, \tag{3.18}$$

where ρ_μ can have the values 0 and 1, and defines a four-component field

$$\chi_\rho(X) = \chi(2X + \rho)\,. \tag{3.19}$$

To express the action in terms of the χ_ρ-fields it is necessary to know how to map $\chi(2X + \rho \pm \hat{\mu})$ to χ_ρ when $|\rho + \hat{\mu}| > 1$. A reasonable way to do it is

$$\chi(2X + \rho + \hat{\mu}) = \sum_{\rho'} [\delta_{\rho+\hat{\mu},\rho'}\chi_{\rho'}(X) + \delta_{\rho-\hat{\mu},\rho'}\chi_{\rho'}(X + \hat{\mu})] \tag{3.20}$$

$$\chi(2X + \rho - \hat{\mu}) = \sum_{\rho'} [\delta_{\rho-\hat{\mu},\rho'}\chi_{\rho'}(X) + \delta_{\rho+\hat{\mu},\rho'}\chi_{\rho'}(X - \hat{\mu})]\,. \tag{3.21}$$

Now the action can be brought into the form

$$S^{stag(0)} = \frac{1}{2}\sum_{X,\rho,\rho'} \bar{\chi}_\rho(X)\left[\sum_\mu \left(\Gamma^\mu_{\rho\rho'}\tilde{\partial}_\mu + \frac{1}{2}\Gamma^{5\mu}_{\rho\rho'}\Delta_\mu\right)\right]\chi_{\rho'}(X) \tag{3.22}$$

with

$$\Gamma^{(\mu)}_{\rho\rho'} = [\delta_{\rho+\hat{\mu},\rho'} + \delta_{\rho-\hat{\mu},\rho'}]\eta_\mu(\rho)\,, \tag{3.23}$$

$$\Gamma^{(5\mu)}_{\rho\rho'} = [\delta_{\rho-\hat{\mu},\rho'} - \delta_{\rho+\hat{\mu},\rho'}]\eta_\mu(\rho)\,. \tag{3.24}$$

And the symbols $\tilde{\partial}$ and Δ_μ stand for the symmetric first and second lattice derivatives in lattice units

$$\tilde{\partial}_\mu f(X) = \frac{1}{2}[f(X + \hat{\mu}) - f(X - \hat{\mu})] \tag{3.25}$$

$$\Delta_\mu f(X) = f(X + \hat{\mu}) + f(X - \hat{\mu}) - 2f(X) \tag{3.26}$$

In two dimensions it is easy to write down the Γ-matrices explicitly[1]

$$\Gamma^{(0)} = \begin{pmatrix} 0 & 0 & 1 & 0 \\ 0 & 0 & 0 & 1 \\ 1 & 0 & 0 & 0 \\ 0 & 1 & 0 & 0 \end{pmatrix} \qquad \Gamma^{(1)} = \begin{pmatrix} 0 & 1 & 0 & 0 \\ 1 & 0 & 0 & 0 \\ 0 & 0 & 0 & -1 \\ 0 & 0 & -1 & 0 \end{pmatrix} \tag{3.27}$$

$$\Gamma^{(50)} = \begin{pmatrix} 0 & 0 & -1 & 0 \\ 0 & 0 & 0 & -1 \\ 1 & 0 & 0 & 0 \\ 0 & 1 & 0 & 0 \end{pmatrix} \qquad \Gamma^{(51)} = \begin{pmatrix} 0 & -1 & 0 & 0 \\ 1 & 0 & 0 & 0 \\ 0 & 0 & 0 & 1 \\ 0 & 0 & -1 & 0 \end{pmatrix}. \tag{3.28}$$

[1]The explicit form of the Γ matrices depends on the order in which the components of the χ_ρ field appear. The choice here is: $\chi = (\chi_{(00)}, \chi_{(01)}, \chi_{(10)}, \chi_{(11)})$.

These matrices satisfy the following anticommutation relations

$$\begin{aligned} \{\Gamma^\mu, \Gamma^\nu\} &= 2\delta_{\mu\nu} && (3.29)\\ \{\Gamma^\mu, \Gamma^{5\nu}\} &= 0 && (3.30)\\ \{\Gamma^{5\mu}, \Gamma^{5\nu}\} &= -2\delta_{\mu\nu}\,, && (3.31) \end{aligned}$$

which happen to be the same as those satisfied by $\gamma_\mu \otimes \mathbb{1}$ and $\gamma_5 \otimes \gamma_5\gamma_\mu$. If (3.22) can be brought by a variable transformation into a form in which the usual kinetic term is recovered (up to lattice artifacts), then free staggered fermions have indeed the correct classical continuum limit. The unitary transformation to achieve this is

$$\begin{aligned} q_{\alpha i} &= \frac{1}{\sqrt{2}} \sum_\rho U_{\alpha i,\rho} \chi_\rho(X) \\ \bar{q}_{\alpha i} &= \frac{1}{\sqrt{2}} \sum_\rho \bar{\chi}_\rho(X) U^\dagger_{\rho,\alpha i}\,, && (3.32) \end{aligned}$$

with

$$U_{\alpha i,\rho} = \frac{1}{\sqrt{2}} (T_\rho)_{\alpha i} \tag{3.33}$$

and $T_\rho = T(\rho) = \gamma_0^{\rho_0}\gamma_1^{\rho_1}$ like in (3.15). In terms of the new variables the action reads

$$S^{stag(0)} = \sum_{X,\alpha,\beta,i,j,\mu} \bar{q}_{\alpha i}(X) \Big[(\gamma_\mu)_{\alpha\beta}\delta_{ij}\tilde{\partial} + (\gamma_5)_{\alpha\beta}(\gamma_5\gamma_\mu)_{ij}\Delta_\mu \Big] q_{\beta j}(X) \tag{3.34}$$

and the usual kinetic term for two-spinors with components labeled by α is recognized. The index i/j can be interpreted as an additional flavor index, thus the fermion doubling is reduced. Instead of 4 tastes for each original flavor there are 2 tastes. The second derivative term, which is similar to a Wilson term but that is neither diagonal in spin- nor in taste-space, comes with a power of the lattice spacing due to dimensional reasons.

3.2.2 Symmetries of the free staggered action

The symmetries of the free staggered action can be discussed either in the χ-basis, or in the basis with flavored q-fields which of course is equivalent. In the χ-basis the following symmetries can be identified

Translations

The action is invariant under translations

$$\begin{aligned} \chi(x) &\to \zeta_\mu(x)\chi(x+\hat{\mu}) \\ \bar{\chi}(x) &\to \zeta_\mu(x)\bar{\chi}(x+\hat{\mu}) && (3.35) \end{aligned}$$

with

$$\zeta_\mu(x) = (-1)^{(1-\mu)x_1}\,. \tag{3.36}$$

Rotations

The action is also invariant under 90° rotations

$$\begin{aligned} \chi(x_0, x_1) &\rightarrow \rho(x)\chi(x_1, -x_0) \\ \bar{\chi}(x_0, x_1) &\rightarrow \rho(x)\bar{\chi}(x_1, -x_0) \end{aligned} \tag{3.37}$$

with

$$\rho(x) = i(-1)^{x_0 x_1} . \tag{3.38}$$

Axis reversals

Two other discrete symmetries are given by parity

$$\begin{aligned} \chi(x_0, x_1) &\rightarrow \chi(x_0, -x_1) \\ \bar{\chi}(x_0, x_1) &\rightarrow \bar{\chi}(x_0, -x_1) \end{aligned} \tag{3.39}$$

and by time reversal

$$\begin{aligned} \chi(x_0, x_1) &\rightarrow \eta_1(x)\chi(-x_0, x_1) \\ \bar{\chi}(x_0, x_1) &\rightarrow \eta_1(x)\bar{\chi}(-x_0, x_1) . \end{aligned} \tag{3.40}$$

Charge conjugation

The action is invariant under charge conjugation in the form

$$\chi(x) \rightarrow \epsilon(x)\bar{\chi}(x) \tag{3.41}$$

$$\bar{\chi}(x) \rightarrow -\epsilon(x)\chi(x) , \tag{3.42}$$

with

$$\epsilon(x) = (-1)^{x_0 + x_1} . \tag{3.43}$$

Chiral symmetry

If the second derivative term in (3.34) were absent, the action would be invariant under the full chiral group. This taste-breaking term reduces the invariance significantly. Written with χ-fields, the massless action connects only even sites with odd sites, so there is a symmetry

$$\chi(x) \rightarrow U_{\mathrm{e}}\, \chi(x) , \qquad \bar{\chi}(x) \rightarrow \bar{\chi}(x)\, U_{\mathrm{o}}^{\dagger} \qquad \textit{for even } x \tag{3.44}$$

$$\chi(x) \rightarrow U_{\mathrm{o}}\, \chi(x) , \qquad \bar{\chi}(x) \rightarrow \bar{\chi}(x)\, U_{\mathrm{e}}^{\dagger} \qquad \textit{for odd } x , \tag{3.45}$$

with independent $U_{\mathrm{e}}, U_{\mathrm{o}} \in U(N/2)$. A mass term $\propto \bar{\chi}\chi$ would break this symmetry down to the diagonal subgroup $U_{\mathrm{e}} = U_{\mathrm{o}}$.

In the language of the flavored fields the generators

$$\mathbb{1}^{(2\times2)} \otimes \mathbb{1}^{(2\times2)} \otimes \mathbb{1}^{(N/2\times N/2)} \tag{3.46}$$
$$\mathbb{1}^{(2\times2)} \otimes \mathbb{1}^{(2\times2)} \otimes \lambda^{(k)} \tag{3.47}$$
$$\gamma_5 \otimes \gamma_5 \otimes \mathbb{1}^{(N/2\times N/2)} \tag{3.48}$$
$$\gamma_5 \otimes \gamma_5 \otimes \lambda^{(k)} \tag{3.49}$$

give rise to transformations that leave the action invariant. The first matrix acts in spin-space, the second in taste-space and the third on the $N/2$ explicit flavor components. $\lambda^{(k)}$ are the $N^2/4-1$ generators of the $SU(N/2)$. The generators (3.46) and (3.47) generate vector transformations which would not be affected by a (degenerate) mass term. The remaining generators generate nonsinglet (γ_5 is traceless) axial transformations.

The massless staggered action is invariant under the interchange

$$\chi(x) \leftrightarrow \bar{\chi}(x)\,. \tag{3.50}$$

This symmetry is equivalent to a charge conjugation followed by a particular transformation from the chiral group, namely $U_\mathrm{o} = \mathbb{1}$ and $U_\mathrm{e} = e^{i\pi}$.

3.2.3 The mass term and interactions

In order to introduce interaction terms and to formulate observables it is useful to translate the fermion-bilinears

$$\bar{q}q, \qquad \bar{q}\gamma_5 q \qquad \mathit{and} \qquad \bar{q}\gamma_\mu q \tag{3.51}$$

from the flavored basis to the χ-basis. For simplicity reasons the number of flavors is chosen to be $N = 2$. A generalization to all even numbers is straightforward, but would unnecessarily complicate the notation. In the following the matrix Γ is one of $\{\gamma_0, \gamma_1, \gamma_5, \mathbb{1}\}$. A bilinear translates according to

$$\sum_{\alpha,\beta,i,j} \bar{q}_{\alpha i}\Gamma_{\alpha\beta}\mathbb{1}_{ij}q_{\beta j} \tag{3.52}$$
$$= \frac{1}{2}\sum_{\rho,\xi} \bar{\chi}_\rho \underbrace{\sum_{\alpha,\beta,i,j} U^\dagger_{\rho,\alpha i}\Gamma_{\alpha\beta}\mathbb{1}_{ij}U_{\beta j,\xi}}_{\Lambda_{\rho,\xi}} \chi_\xi\,. \tag{3.53}$$

Insertion of the definition of U from (3.33) yields

$$\Lambda_{\rho,\xi} = \sum_{\alpha\beta ij} \frac{1}{2}\left[\gamma_0^{\rho_0}\gamma_1^{\rho_1}\right]_{\alpha i}\Gamma_{\alpha\beta}\mathbb{1}_{ij}\left[\gamma_0^{\xi_0}\gamma_1^{\xi_1}\right]_{\beta j}\,. \tag{3.54}$$

That means

$$\Lambda = \frac{1}{2}\begin{pmatrix} tr\Gamma & tr(\Gamma\gamma_1) & tr(\Gamma\gamma_0) & tr(\Gamma\gamma_0\gamma_1) \\ tr(\Gamma\gamma_1^\top) & tr(\Gamma\gamma_1^\top\gamma_1) & tr(\Gamma\gamma_0\gamma_1^\top) & tr(\Gamma\gamma_0\gamma_1^\top\gamma_1) \\ tr(\gamma_0^\top\Gamma) & tr(\gamma_0^\top\Gamma\gamma_1) & tr(\gamma_0^\top\Gamma\gamma_0) & tr(\gamma_0^\top\Gamma\gamma_0\gamma_1) \\ tr(\gamma_0^\top\Gamma\gamma_1^\top) & tr(\gamma_0^\top\Gamma\gamma_1^\top\gamma_1) & tr(\gamma_0^\top\Gamma\gamma_0\gamma_1^\top) & tr(\gamma_0^\top\Gamma\gamma_0\gamma_1^\top\gamma_1) \end{pmatrix} \tag{3.55}$$

So, depending on what is substituted for Γ, when the Clifford-algebra and properties of the trace are exploited, one finds explicitly

$$\Gamma = \mathbb{1}: \qquad \Lambda_{\rho,\xi} = \begin{pmatrix} 1 & 0 & 0 & 0 \\ 0 & 1 & 0 & 0 \\ 0 & 0 & 1 & 0 \\ 0 & 0 & 0 & 1 \end{pmatrix} = \mathbb{1}_{\rho_0\xi_0}\,\mathbb{1}_{\rho_1\xi_1} \tag{3.56}$$

$$\Gamma = \gamma_5: \qquad \Lambda_{\rho,\xi} = \begin{pmatrix} 0 & 0 & 0 & -i \\ 0 & 0 & -i & 0 \\ 0 & i & 0 & 0 \\ i & 0 & 0 & 0 \end{pmatrix} = \sigma^{(2)}_{\rho_0\xi_0}\,\sigma^{(1)}_{\rho_1\xi_1} \tag{3.57}$$

$$\Gamma = \gamma_0: \qquad \Lambda_{\rho,\xi} = \begin{pmatrix} 0 & 0 & 1 & 0 \\ 0 & 0 & 0 & 1 \\ 1 & 0 & 0 & 0 \\ 0 & 1 & 0 & 0 \end{pmatrix} = \sigma^{(1)}_{\rho_0\xi_0}\,\mathbb{1}_{\rho_1\xi_1} \tag{3.58}$$

$$\Gamma = \gamma_1: \qquad \Lambda_{\rho,\xi} = \begin{pmatrix} 0 & 1 & 0 & 0 \\ 1 & 0 & 0 & 0 \\ 0 & 0 & 0 & -1 \\ 0 & 0 & -1 & 0 \end{pmatrix} = \sigma^{(3)}_{\rho_0\xi_0}\,\sigma^{(1)}_{\rho_1\xi_1}, \tag{3.59}$$

with the usual Pauli matrices $\sigma^{(i)}$.

The easiest application is to translate the mass term. One readily finds

$$\sum_X \bar{q}(X) m\,[\mathbb{1}\otimes\mathbb{1}]\,q(X) = \frac{1}{2}\sum_x \bar{\chi}(x) m \chi(x)\,. \tag{3.60}$$

For the interaction term $\mathcal{L}^{SS}$ one finds

$$\sum_X \left(\bar{q}(X)[\mathbb{1}\otimes\mathbb{1}]q(X)\right)^2 = \frac{1}{4}\sum_X \left(\sum_\rho \bar{\chi}(2X+\rho)\chi(2X+\rho)\right)^2. \tag{3.61}$$

To obtain a form which preserves the staggered translation invariance (3.35) it is necessary to introduce a discretization error of order a by writing

$$\mathcal{L}^{SS} = \frac{1}{16}\sum_x \left(\sum_\rho \bar{\chi}(x+\rho)\chi(x+\rho)\right)^2. \tag{3.62}$$

This form of the Gross-Neveu interaction term has already been proposed in [15] and carefully examined in [40]. Similarly for the other four-fermion interaction terms one obtains

$$\begin{aligned}\mathcal{L}^{PP} &= -\frac{1}{16}\sum_x \Big[\bar\chi(x+\hat 0)\chi(x+\hat 1) - \bar\chi(x+\hat 1)\chi(x+\hat 0) \\ &\qquad +\bar\chi(x+\hat 0+\hat 1)\chi(x) - \bar\chi(x)\chi(x+\hat 0+\hat 1)\Big]^2 \qquad (3.63)\\ \mathcal{L}^{VV} &= -\frac{1}{16}\sum_x \Big[\bar\chi(x)\chi(x+\hat 0) + \bar\chi(x+\hat 0)\chi(x) \\ &\qquad +\bar\chi(x+\hat 1)\chi(x+\hat 0+\hat 1) + \bar\chi(x+\hat 0+\hat 1)\chi(x+\hat 1)\Big]^2 \\ &\qquad +\Big[\bar\chi(x+\hat 0)\chi(x+\hat 0+\hat 1) + \bar\chi(x+\hat 0+\hat 1)\chi(x+\hat 0) \\ &\qquad -\bar\chi(x)\chi(x+\hat 1) - \bar\chi(x+\hat 1)\chi(x)\Big]^2 \qquad (3.64)\end{aligned}$$

In simulations the equivalent actions with auxiliary fields are used. An interaction term of the form

$$\frac{g^2}{2}\sum_x \frac{1}{16}\left(\sum_{\rho,\xi}\bar\chi(x+\rho)\,\Lambda_{\rho,\xi}\,\chi(x+\xi)\right)^2 \qquad (3.65)$$

is eliminated by the introduction of a scalar field σ and the corresponding terms in the auxiliary-field-action are

$$\sum_x \frac{8\sigma^2(x)}{g^2} + \sum_x\sum_{\rho,\xi}\sigma(x)\,\bar\chi(x+\rho)\,\Lambda_{\rho,\xi}\,\chi(x+\xi)\,. \qquad (3.66)$$

This means that the Gross-Neveu model with N flavors in the continuum limit can be described by the action[2]

$$S^{GN-stag} = \sum_{x,y}\sum_{i=1}^{N/2}\bar\chi_i(x)K(x,y)\chi_i(y) + \sum_x\frac{8\sigma(x)^2}{g^2} \qquad (3.67)$$

with the fermion matrix

$$K(x,y) = \frac{1}{2}\sum_\mu \eta_\mu(x)[\delta_{x+\hat\mu,y} - \delta_{x-\hat\mu,y}] + \sum_\rho \sigma(x-\rho)\delta_{x,y}\,. \qquad (3.68)$$

The action is invariant under translations, rotations, axis reversals and the discrete chiral symmetry as defined in section 3.2.2, provided that the

[2]The reordering of the terms which is necessary to write the action as a quark bilinear, works in this way only for periodic and antiperiodic boundary conditions.

auxiliary field transforms as follows

$$\begin{aligned}
\text{t}\textit{ranslations}: \quad & \sigma(x) && \to \sigma(x+\hat{\mu}) && (3.69)\\
90^o\ \textit{rotations}: \quad & \sigma(x_0,x_1) && \to \sigma(x_1,-x_0-a) && (3.70)\\
\text{p}\textit{arity}: \quad & \sigma(x_0,x_1) && \to \sigma(x_0,-x_1-a) && (3.71)\\
\text{t}\textit{ime reversal}: \quad & \sigma(x_0,x_1) && \to \sigma(-x_0-a,x_1) && (3.72)\\
\textit{charge conjugation}: \quad & \sigma(x) && \to -\sigma(x)\,. && (3.73)
\end{aligned}$$

Similar to a mass-term, interaction breaks the chiral symmetry $U(N/2)_\mathrm{e} \times U(N/2)_\mathrm{o}$ down to the diagonal subgroup. However unlike a mass-term it preserves the discrete chiral symmetry, which makes the model stable against additive mass renormalizations.

The fermion-matrix K is real and hence its eigenvalues are either real or come in complex-conjugate pairs. The determinant of K is not necessarily positive. This is easily seen in the large g limit, when only configurations contribute, where $\sigma(x)$ is large. Then the kinetic part of the operator can be neglected and the determinant is given by $\prod_x \sum_\rho \sigma(x-\rho)$ with Gaussian distributed σ-fields, which can of course become negative.

Chiral Gross-Neveu model

The auxiliary field action of the chiral Gross-Neveu model with staggered fermions is

$$\begin{aligned}
S^{\chi\mathrm{GN-}\textit{stag}} &= \sum_{x,y,i} \bar{\chi}_i(x) K(x,y) \chi_i(y) + \sum_x \left(\frac{8\sigma(x)^2}{g_\mathrm{S}^2} + \frac{8\Pi(x)^2}{g_\mathrm{P}^2} + \frac{8A_\mu(x)A_\mu(x)}{g_\mathrm{V}^2} \right)\\
K(x,y) &= \frac{1}{2}\sum_\mu \eta_\mu(x)[\delta_{x+\hat{\mu},y} - \delta_{x-\hat{\mu},y}]\\
&\quad + \sum_\rho \sigma(x-\rho)\,\delta_{x,y} + \sum_{\rho,\xi} i\Pi(x-\rho)\,\sigma^{(2)}_{\rho_0\xi_0}\sigma^{(1)}_{\rho_1\xi_1}\delta_{x-\rho+\xi,y}\\
&\quad + \sum_{\rho,\xi} A_0(x-\rho)\,\sigma^{(1)}_{\rho_0\xi_0}\mathbb{1}_{\rho_1\xi_1}\delta_{x-\rho+\xi,y}\\
&\quad + \sum_{\rho,\xi} A_1(x-\rho)\,\sigma^{(3)}_{\rho_0\xi_0}\sigma^{(1)}_{\rho_1\xi_1}\delta_{x-\rho+\xi,y}\,. \qquad (3.74)
\end{aligned}$$

Not even for $g_\mathrm{S}^2 = g_\mathrm{P}^2$ the axial $U(1)$ symmetry of the continuum model is realized with staggered fermions, and that is why in this model, like in the Wilson case a tuning of the ratio of the two couplings is necessary to approach the correct continuum limit. The additive mass renormalization however is not necessary, since the $\chi \leftrightarrow \bar{\chi}$ symmetry is realized.

In literature [35, 36] often a model is studied which preserves the remnant staggered chiral $U(1)$ symmetry. This however is not the singlet $U(1)$

of what is commonly called the chiral Gross-Neveu model. Moreover this model cannot be easily simulated with standard techniques, because its fermion matrix is neither real nor (anti)hermitian. Therefore usually a model with fermionic weight $\det(K^\dagger K)$ is simulated instead of the desired $\det K^2$ in order to be able to introduce pseudo fermion fields.

3.2.4 Observables

The observables defined in 2.2.4 can be translated into the staggered formalism in a similar way as the interaction terms. With Wilson fermions the observables k_S and $\bar{k}_S$ can be used to fix the chiral point. With staggered fermions no additive mass renormalization is required and therefore these observables should vanish at every lattice spacing automatically.

$$\begin{aligned} k_S(X_0,p_1) &= -\frac{2a^2}{NL}\sum_{X_1Y_1} e^{i2(X_1-Y_1)p_1}\,\langle\bar{\chi}(2X_0,2X_1)\chi(0,2Y_1)\rangle \\ &= \frac{a^2}{L}\sum_{X_1Y_1} e^{i2(X_1-Y_1)p_1}\,\langle K^{-1}(0,2Y_1;2X_0,2X_1)\rangle^{aux} \qquad (3.75) \\ \bar{k}_S(p_0,X_1) &= -\frac{2a^2}{NT}\sum_{X_0Y_0} e^{i2(X_0-Y_0)p_0}\,\langle\bar{\chi}(2X_0,2X_1)\chi(2Y_0,0)\rangle \\ &= \frac{a^2}{T}\sum_{X_0Y_0} e^{i2(X_0-Y_0)p_0}\,\langle K^{-1}(2Y_0,0;2X_0,2X_1)\rangle^{aux}\,. \qquad (3.76) \end{aligned}$$

In fact, these observables are odd under the interchange $\bar{\chi} \leftrightarrow \chi$, which is a symmetry of the action (3.2.2) and therefore vanish. For k_μ and $\bar{k}_\mu$ the transcription produces

$$\begin{aligned} k_0(X_0,p_1) &= -\frac{a^2}{NL}\sum_{X_1Y_1} e^{i2(X_1-Y_1)p_1}\langle\bar{\chi}(2X_0+a,2X_1)\chi(0,2Y_1) \\ &\qquad +\bar{\chi}(2X_0-a,2X_1)\chi(0,2Y_1)\rangle \\ &= \frac{a^2}{2L}\sum_{X_1Y_1} e^{i2(X_1-Y_1)p_1}\langle K^{-1}(0,2Y_1;2X_0+a,2X_1) \qquad (3.77) \\ &\qquad +K^{-1}(0,2Y_1;2X_0-a,2X_1)\rangle^{aux} \qquad (3.78) \\ \bar{k}_1(p_0,X_1) &= -\frac{a^2}{NT}\sum_{X_0Y_0} e^{i2(X_0-Y_0)p_0}\langle\bar{\chi}(2X_0,2X_1+a)\chi(2Y_0,0) \\ &\qquad +\bar{\chi}(2X_0,2X_1-a)\chi(2Y_0,0)\rangle \qquad (3.79) \\ &= \frac{a^2}{2T}\sum_{X_0Y_0} e^{i2(X_0-Y_0)p_0}\langle K^{-1}(2X_0,0;2X_0,2X_1+a) \\ &\qquad +K^{-1}(2Y_0,0;2X_0,2X_1-a)\rangle^{aux}\,. \qquad (3.80) \end{aligned}$$

The renormalized coupling defined in (2.51) as well as current current correlators are more involved.

3.2.5 Staggered fermions with an odd number of flavors

Staggered fermions do not remove all doublers. In two dimensions at least 2 flavors emerge in the continuum limit. A theory with for instance $N = 1$ cannot be described without further manipulations. A popular approach in QCD-simulations is to integrate out the fermions and take a square (or fourth) root of the resulting fermion determinant. A Gross-Neveu model with N flavors would be described by the effective action

$$S^{GN-rooted} = \sum_x \frac{8\sigma(x)^2}{g^2} - \frac{N}{4} \mathrm{Tr} \log K^\dagger K \,. \tag{3.81}$$

For odd N a corresponding local action formulated in terms of the Grass"-mann-fields does not exist which raises questions with respect to the universality of such theories [12, 71].

3.3 Ginsparg-Wilson Fermions

It was discovered in [31] that a lattice-Dirac operator that would satisfy the Ginsparg-Wilson relation

$$\gamma_5 D + D\gamma_5 = aD\gamma_5 D \,, \tag{3.82}$$

would be consistent with the Nielson-Ninomiya theorem while breaking chiral symmetry only in a "mild" way. The operator on the right hand side is local and it vanishes if applied to solutions of the Dirac equation $D\psi = 0$.

Nowadays several operators that satisfy all the criterions of the Nielson-Ninomiya theorem and in addition eq. (3.82) are known. None of them is ultralocal, but they are local in the sense that the interaction strength between distant points dies off exponentially with the distance in lattice units. This is considered enough to guarantee universality. Three prominent examples are given by the Fixed-Point (or classically perfect) action [37], the domain-wall fermions [42] and the overlap fermions [63].

An important observation by M. Lüscher [56] was that although Gins"-parg-Wilson Fermions do break chiral symmetry, there exists a modified chiral symmetry which remains unbroken on the lattice. This symmetry is (here an infinitesimal rotation by ϵ)

$$\begin{aligned} \psi &\rightarrow \psi + i\epsilon\hat{\gamma}_5\psi \\ \bar{\psi} &\rightarrow \bar{\psi} + i\epsilon\bar{\psi}\gamma_5 \,, \end{aligned} \tag{3.83}$$

with $\hat{\gamma}_5$ that approaches γ_5 in the continuum limit

$$\hat{\gamma}_5 = \gamma_5(1 - aD)\,. \tag{3.84}$$

With such a symmetry at hand, it suggests itself to discretize fields and operators in a way which preserves the transformation properties that they have in the continuum. With the chiral projectors

$$P_{\mathrm{R}} = \frac{1}{2}(1 + \gamma_5) \qquad P_{\mathrm{L}} = \frac{1}{2}(1 - \gamma_5) \tag{3.85}$$

$$\hat{P}_{\mathrm{R}} = \frac{1}{2}(1 + \hat{\gamma}_5) \qquad \hat{P}_{\mathrm{L}} = \frac{1}{2}(1 - \hat{\gamma}_5) \tag{3.86}$$

$$\tag{3.87}$$

The chiral components can be defined as

$$\psi_{\mathrm{L}} = \hat{P}_{\mathrm{L}}\psi \qquad \psi_{\mathrm{R}} = \hat{P}_{\mathrm{R}}\psi \tag{3.88}$$

$$\bar{\psi}_{\mathrm{L}} = \bar{\psi}P_{\mathrm{R}} \qquad \bar{\psi}_{\mathrm{R}} = \bar{\psi}P_{\mathrm{L}}\,. \tag{3.89}$$

The four fermion interaction terms that have the correct transformation properties are

$$\mathcal{L}^{SS} = (\bar{\psi}_{\mathrm{L}}\psi_{\mathrm{R}} + \bar{\psi}_{\mathrm{R}}\psi_{\mathrm{L}})^2 \qquad = \left(\bar{\psi}\left[1 - \frac{a}{2}D\right]\psi\right)^2 \tag{3.90}$$

$$\mathcal{L}^{PP} = (\bar{\psi}_{\mathrm{L}}\psi_{\mathrm{R}} - \bar{\psi}_{\mathrm{R}}\psi_{\mathrm{L}})^2 \qquad = \left(\bar{\psi}\gamma_5\left[1 - \frac{a}{2}D\right]\psi\right)^2 \tag{3.91}$$

$$\mathcal{L}^{VV} = \left(\bar{\psi}_{\mathrm{L}}\gamma_\mu\psi_{\mathrm{R}} + \bar{\psi}_{\mathrm{R}}\gamma_\mu\psi_{\mathrm{L}}\right)^2 \qquad = \left(\frac{1}{2}\bar{\psi}\left[\gamma_\mu - \hat{\gamma}_5\gamma_\mu\gamma_5\right]\psi\right)^2\,. \tag{3.92}$$

Of course auxiliary fields can be introduced. The auxiliary field action for the chiral Gross-Neveu model with Ginsparg-Wilson fermions reads

$$\begin{aligned} S^{\chi GN-GW} \;=\; & \sum_x \bar{\psi}\Big[D + \sigma\left(1 - \frac{a}{2}D\right) + i\Pi\gamma_5\left(1 - \frac{a}{2}D\right) \\ & \qquad + \frac{1}{2}A_\mu\left(\gamma_\mu - \hat{\gamma}_5\gamma_\mu\gamma_5\right)\Big]\psi \\ & + \sum_x\left(\frac{\sigma^2 + \Pi^2}{2g_{\mathrm{S}}^2} + \frac{A_\mu A_\mu}{2g_{\mathrm{V}}^2}\right), \end{aligned} \tag{3.93}$$

and for the Gross-Neveu model accordingly.

Under the Lüscher symmetry the auxiliary fields σ and Π transform according to

$$\begin{pmatrix}\sigma\\ \Pi\end{pmatrix} \;\rightarrow\; \begin{pmatrix}1 & 2\epsilon\\ -2\epsilon & 1\end{pmatrix}\begin{pmatrix}\sigma\\ \Pi\end{pmatrix}, \tag{3.94}$$

while A_μ is invariant. This behavior is exactly the same as in the continuum theory.

Chapter 4

Large-N calculations

Both the Gross-Neveu and the chiral Gross-Neveu are large-N expandable. Already in the leading order of this expansion very interesting properties of the models can be observed. The Gross-Neveu model with discrete chiral symmetry at $N \to \infty$ is asymptotically free, exhibits spontaneous symmetry breakdown and dynamical mass generation [33]. None of these features can be seen in perturbation theory (in g) no matter how high its order is. In the chiral Gross-Neveu model with Wilson fermions there exists an Aoki-phase [1]. Recently this study has been extended to the case with twisted-mass fermions [62] and a phase-structure similar to that observed in QCD was found.

This chapter plays a somewhat special role in this thesis. It does not intersect very much with the other sections, and the results presented here origin from an early stage of the work where it was important to get comfortable with the model and its different discretizations.

A universal finite volume quantity very similar to the Lüscher-Weisz-Wolff (LWW) coupling [57] is calculated in the large N limit of the continuum theory as well as in its lattice versions with three different fermion-discretizations. The LWW-coupling has originally been introduced as the dimensionless product of the finite-volume massgap and the spatial volume in two dimensional $O(N)$-invariant nonlinear σ-models. The observable that is used here is the product of the finite volume fermion mass $m(L)$ with the spatial volume L. One can obtain a value of $m(L)L$ for each L or more precisely for each value of the dimensionless volume-parameter $m(\infty)L$, where $m(\infty)$ is the fermion mass in infinite volume which will be denoted simply by m from here on.

4.1 Continuum theory

For the Large-N calculation the notation is slightly changed. A rescaled bare coupling $\lambda = Ng^2$ is used and the action of the Gross-Neveu model

reads

$$S = \int_0^T dt \int_{-L/2}^{+L/2} dx \left(\bar{\psi} \partial\!\!\!/ \psi - \frac{\lambda}{2N} (\bar{\psi}\psi)^2 \right) \tag{4.1}$$

After introduction of the usual auxiliary scalar field σ the partition function takes the form

$$Z = \int D\sigma \, \exp\left[-N \left(\frac{1}{2\lambda} \int\int dt\, dx \, \sigma^2 - \mathrm{T}r \, \log(\partial\!\!\!/ + \sigma) \right) \right] \tag{4.2}$$

The large-N expansion is a saddle-point expansion. In the $N \to \infty$ limit the classical solution for the σ-field (here called m) which is defined by

$$\left. \frac{\delta S}{\delta \sigma} \right|_{\sigma = m(L)} = 0 \,, \tag{4.3}$$

dominates. In higher orders of the expansion fluctuations around the saddle-point are taken into account and a power series in $1/N$ is obtained. The present work restricts itself to the leading order which although rather straightforward already yields some interesting nontrivial results.

If one is interested in the phase structure of the model in the presence of a chemical potential and at finite temperature, it is necessary to find also the space (or even space and time) dependent saddle-point solutions [24, 68], which can have non trivial topologies. Here however it is enough to look for solutions of (4.3) with constant fields σ, i.e. with action

$$S^{eff}(\sigma) = \frac{NLT}{2\lambda} \sigma^2 - N \, \mathrm{T}r \, \log(\partial\!\!\!/ + \sigma) \,. \tag{4.4}$$

Hence for S to be extremal σ has to satisfy the gap equation

$$\frac{\sigma}{\lambda} = \frac{1}{TL} \mathrm{T}r (\partial\!\!\!/ + \sigma)^{-1} = \frac{1}{L} \sum_{p_1} \int_{-\infty}^{+\infty} \frac{dp_0}{2\pi} \frac{2\sigma}{p_0^2 + p_1^2 + \sigma^2} \,. \tag{4.5}$$

In this step a geometry was chosen where $T = \infty$ and L is finite with the boundary conditions $\psi(x_0, x_1 + L) = e^{i\theta} \psi(x_0, x_1)$ which include periodic and antiperiodic b.c. as special cases. That means that the spatial momenta to sum over are $p_1 = (2n\pi + \theta)/L$, $n = 0, \pm 1, \pm 2, \ldots$). The solution $\sigma = 0$ corresponds to a local maximum of the action. To find the minima $\sigma \neq 0$ is assumed. Dividing both sides by σ, performing the integral and introducing a sharp cutoff Λ for the spatial momentum (i.e. $n = 0, \pm 1, \pm 2, \ldots, \pm n_{max}$) yields

$$\frac{1}{\lambda} = \frac{1}{L} \sum_{|p_1| < \Lambda} \frac{1}{\sqrt{p_1^2 + \sigma^2}} \tag{4.6}$$

In infinite volume the solutions

$$\pm\sigma = \frac{\Lambda}{\sinh\frac{\pi}{\lambda}} \equiv m \tag{4.7}$$

$$\Rightarrow \quad m \approx \Lambda \exp(-\frac{\pi}{\lambda}), \tag{4.8}$$

are found. This equation shows that the Gross-Neveu model is asymptotically free at large N. In fact, the model keeps this property for all $N > 1$.

To calculate the finite volume mass $m(L)$ it is necessary to remove the cutoff and at the same time adjust the bare coupling such that the physical volume is kept constant. One way too proceed is to solve (4.7) for λ and substitute this expression into the finite-volume gap-equation. Thereafter the $\Lambda = 2\pi n_{max}/L \to \infty$ limit can be taken while mL is kept fixed.

The equation

$$\frac{L}{\pi} = \sum_{|n+\frac{\theta}{2\pi}|\leq n_{max}} \frac{1}{\sqrt{(n+\theta)^2(\frac{2\pi}{L})^2+\sigma^2}} \frac{1}{\mathrm{arcsinh}(\frac{2\pi n_{max}}{mL})} \tag{4.9}$$

gives implicitly the solution $\sigma = m(L)$ which has a finite $n_{max} \to \infty$ limit and thus a value of $m(L)L$ can be calculated for any value of mL (at least numerically). One observation is, that there exists a "critical volume" L_c below which the gap equation has only the solution $\sigma = 0$, i.e. no symmetry breaking takes place. This volume depends on the boundary conditions and is given by

$$L_c = \frac{4\pi}{m} \exp\left[-\frac{\pi}{|\theta|} - \gamma - \sum_{n=1}^{\infty}\left(\frac{\theta}{2\pi}\right)^{2n} \zeta(2n+1)\right],$$

where γ is the Euler-Mascheroni-constant and ζ the Riemann-zeta-function. This observation is not entirely new - in fact for the case of antiperiodic boundaries, where the finite volume can be interpreted as a finite temperature (while the spatial volume is infinite), the finite-temperature transition found by Wolff [85] is exactly recovered. That a spontaneous symmetry breaking can take place in finite volume at all is a special feature of the $N \to \infty$ limit. At finite N the symmetry remains unbroken because tunneling between the two minima can take place.

The results are plotted in figure 4.1.

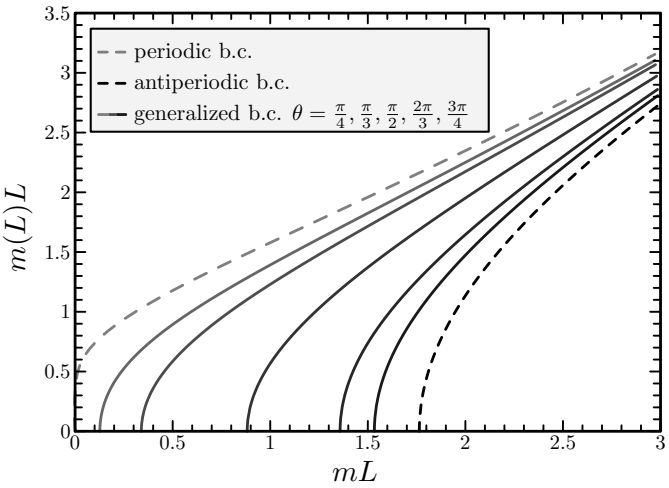

Figure 4.1: $m(L)L$ as a function of mL for different boundary conditions.

The same calculation can be carried out for the chiral Gross-Neveu model. The effective potential is given by

$$V^{eff} = \beta L \frac{\sigma^2 + \Pi^2}{2\lambda} - \mathrm{T}r \log(\not{\partial} + \sigma + i\gamma_5 \Pi) \tag{4.10}$$

where σ and Π are the auxiliary fields associated with $\mathcal{L}^{\mathrm{SS}}$ and $\mathcal{L}^{\mathrm{PP}}$. As argued in section 2.3.1 the interaction term $\mathcal{L}^{\mathrm{VV}}$ can be dropped at leading order of the large-N expansion.

The trace can be rewritten

$$\begin{aligned}
\mathrm{T}r \log(\not{\partial} + c) &= \beta L \int \frac{d^2k}{(2\pi)^2} e^{-ikx}\, \mathrm{tr} \log(\not{\partial} + \sigma + i\gamma_5 \Pi) e^{ikx} && (4.11)\\
&= \beta L \int \frac{d^2k}{(2\pi)^2} e^{-ikx}\, \mathrm{tr} \log(i\not{k} + \sigma + i\gamma_5 \Pi) e^{ikx} && (4.12)\\
&= \beta L \int \frac{d^2k}{(2\pi)^2} \log(k^2 + \Pi^2 + \sigma^2)\,. && (4.13)
\end{aligned}$$

For the last step the spin-part of the trace was evaluated using the eigenvalues of $i\not{k} + \sigma + i\gamma_5\Pi$ which are: $\lambda_\pm = \sigma \pm i\sqrt{k^2 + \Pi^2}$. Hence the effective potential

$$V^{eff} = \beta L \frac{\sigma^2 + \Pi^2}{2\lambda} - \beta L \int \frac{d^2k}{(2\pi)^2} \log(k^2 + \Pi^2 + \sigma^2) \tag{4.14}$$

is manifestly invariant under chiral rotations.

To find extrema of the effective potential $V^{eff}(\rho = \sqrt{\sigma^2 + \Pi^2})$, the gap equation

$$\frac{dV^{eff}}{d\rho} = \frac{\rho}{\lambda} - \int \frac{d^2k}{(2\pi)^2} \frac{2\rho}{k^2 + \rho^2} = 0 \tag{4.15}$$

has to be solved, which happens to be exactly the same as in the discrete model. The $1/N$ corrections in the chiral model are not easy to obtain. The expansion is plagued by infrared singularities which require a special treatment [47].

4.2 Wilson fermions

Instead of imposing a cutoff on spatial momenta only as done in the last section, it is also possible to regularize the theory on a space-time lattice. Here Wilson's approach to represent the fermions is applied. As described in section 3.1 the main disadvantage of Wilson-fermions is, that chiral symmetry is explicitly broken. As a consequence additive mass renormalization is required in order to be able to take a continuum limit in which this symmetry is restored. In the continuum theory the effective potential 4.4 is symmetric ($S^{eff}(\sigma) = S^{eff}(-\sigma)$) due to the γ_5-symmetry. With Wilson fermions this symmetry is lost, but one can fix the additive mass renormalization constant by the requirement, that both minima of the effective potential lie on the exactly same level. The dynamically generated fermion mass m can be defined as half of the distance between the two minima. In the continuum limit, where the symmetry of the effective potential is expected to become restored this definition coincides with that of section 4.1.

With Wilson fermions the effective potential to leading order in large-N is given by

$$\begin{aligned} V_{\mathrm{e}ff} &= \frac{\sigma^2}{2\lambda} - \frac{1}{LT}\mathrm{T}r\,\log(D_{\mathrm{W}} + \sigma + m_0) \\ &= \frac{\sigma^2}{2\lambda} - \iint\limits_{-\pi/a}^{+\pi/a} \frac{d^2p}{(2\pi)^2} \log\left[\mathring{p}^2 + M(p)^2\right], \end{aligned} \tag{4.16}$$

with the usual definitions of $\mathring{p}$, $\hat{p}$ and $M(p) = m_0 + \sigma + \frac{r}{2}a\hat{p}^2$ (see appendix A.1). Its shape for some values of m_0 around m_c is shown in figure 4.2. It has been shown in [3] that below a certain value of the coupling there are three distinct values of m_0 for which the minima of the potential become degenerate. The situation is shown schematically in figure 4.3. The fermion doubling with naive fermions in two dimensions leads to three additional fermion tastes with momenta around $(0, \pi/a)$, $(\pi/a, 0)$ and $(\pi/a, \pi/a)$. With Wilson fermions, depending on how the bare mass is tuned, either the taste around $(0, 0)$ or one of these additional tastes can become massless in the continuum limit, while the others become infinitely heavy. The different branches in figure 4.3 correspond to these different choices. In this work the continuum limit is taken in such a way that only the taste around the point $(0, 0)$ of the Brillouin zone survives the limit.

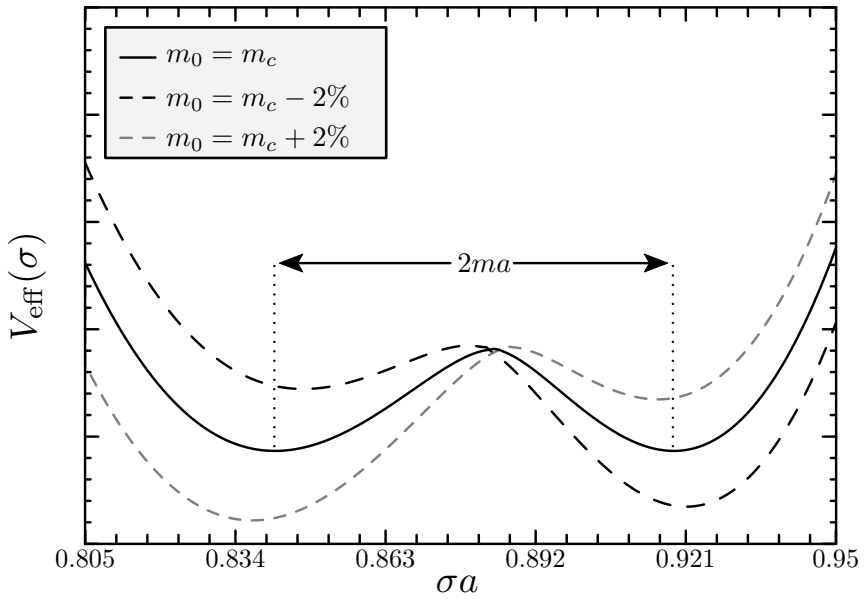

Figure 4.2: The effective potential with Wilson-fermions for three values of m_0 at and around $m_0 = m_c$

The nearly linear behavior of m_c vs λ can be easily understood. An equally suitable condition for the critical mass, which should differ from the one used here only by cutoff effects, could be to demand that the slope of the effective potential at $\sigma = -m_c$ is zero (i.e. there is the local maximum). From this condition one obtains

$$m_c = \frac{\lambda}{LT} \mathrm{Tr}\left[D_{\mathrm{W}}^{-1}\right], \tag{4.17}$$

i.e. the linear behavior is exact in this scheme. Fixing the critical mass by the requirement that the two minima are at the same level has however some practical advantages. The critical masses differ from (4.17) only by lattice artifacts and thats why the behavior in figure 4.3 is not perfectly linear (but almost).

In appendix C.1 some numerical estimates of m_c and the corresponding values of m are summarized. The data is the Wilson-fermion-equivalent of eq. (4.7).

As in the continuum theory the next step is to switch to finite volume. On a lattice of spatial extent L, i.e. L/a sites, for some of the known values of $mL = ma \cdot L/a$ the corresponding $m(L)L$ is calculated. For this the bare mass has to be tuned to its critical value on a finite lattice which differs slightly from the infinite lattice value. Then $2m(L)L$ is given by the distance between the two degenerate minima of the effective potential. In figure 4.4 some of the lattice results are compared to continuum results.

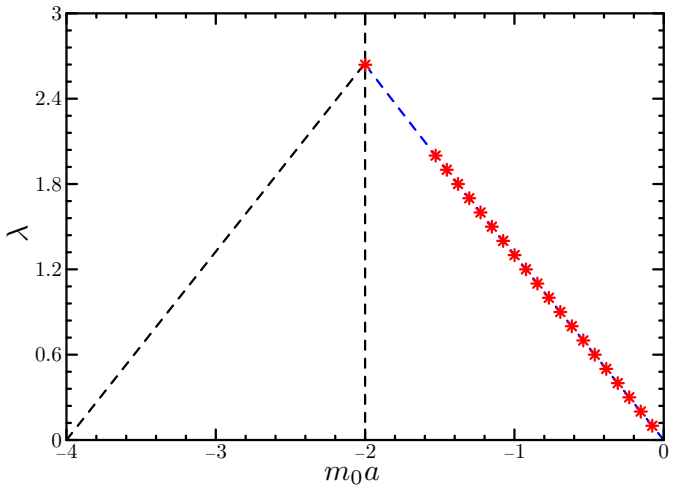

Figure 4.3: Critical values of m_0 for different couplings. The dashed branch which corresponds to the physical fermion mode is a polynomial fit (3. degree) to the numerical results (asterisks). Black dashed lines show schematically the situation for the other modes.

Also with different choices of the boundaries (different θ) the continuum results are reproduced by the $a \to 0$ limit of the theory discretized with Wilson fermions.

In figure 4.6 it is shown how the continuum limit is approached and the results obtained with Wilson fermions are compared to those with staggered fermions. In asymptotically free theories the leading lattice artifacts can be described by Symanzik's effective theory [78]. With unimproved Wilson fermions cutoff effects of order a are expected [72]. The plot suggests $O(a^2)$, i.e. the coefficient of the linear term is either very small or absent.

The treatment of the chiral Gross-Neveu model with Wilson fermions requires some care. It has been found out in [3] that in this model not only the mass needs an additive renormalization, but also the ratio of the couplings of the two interaction terms needs to be adjusted properly in order to recover a chirally symmetric effective potential in the continuum limit. Since this result is quite important for this thesis, the whole calculation is repeated in great detail and can be found in the appendix B.4.2.

4.3 Staggered fermions

With the staggered action for the Gross-Neveu model as introduced in section 3.2 the effective potential is

$$V^{eff} = \frac{\sigma^2}{\lambda} - \frac{1}{16LT}\mathrm{Tr}\left[\log K\right] , \tag{4.18}$$

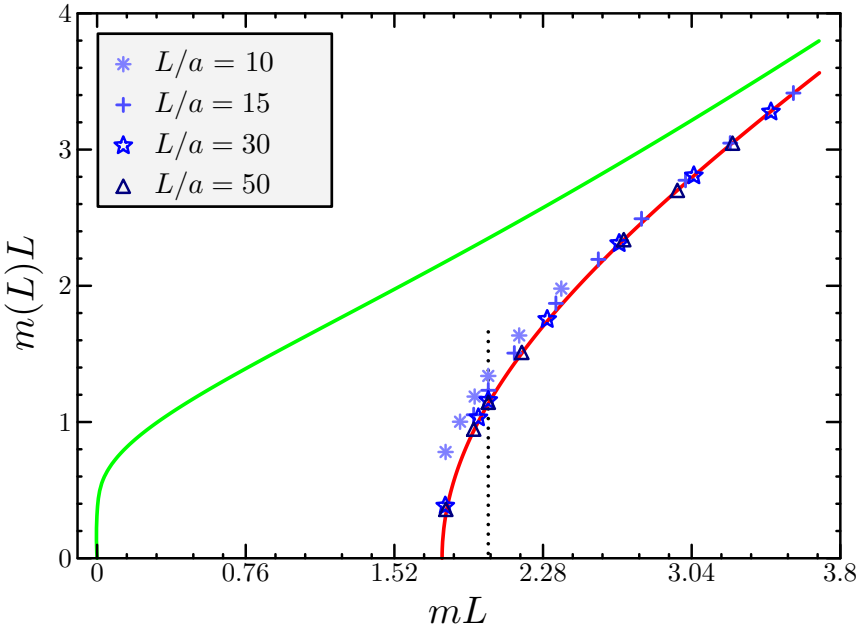

Figure 4.4: Comparison of lattice (Wilson fermions) and continuum results. The dotted black line indicates the mL value along which the approach to the continuum is shown in fig. 4.6. The green and red lines are continuum solutions. The lattice data and the red curve had antiperiodic, the green curve periodic b.c.

where K is the fermion matrix defined in eq. (3.68). The infinite volume gap-equation

$$\frac{1}{\lambda} = \frac{1}{2}\iint_{-\pi}^{\pi} \frac{d^2k}{(2\pi)^2} \frac{1}{\mathring{k}^2 + (4\sigma)^2} \tag{4.19}$$

can be expressed in terms of hypergeometric functions [6] .

$$\frac{1}{\lambda} = \frac{1}{\sqrt{64\sigma^2(16\sigma^2+2)}}\, {}_2F_1\left(\frac{1}{2},\frac{1}{2};1;-\frac{1}{16\sigma^2(16\sigma^2+2)}\right). \tag{4.20}$$

Assuming that the solution $\sigma = m$ gets small close to the continuum limit ($\lambda \to 0$), one can large-z expand ${}_2F_1(1/2,1/2;1;z)$ and obtains in the leading order

$$a\,m = \frac{1}{\sqrt{2}} \exp\left[-\frac{\pi}{\lambda}\right], \tag{4.21}$$

which coincides with the solution in the continuum 4.7. This means that indeed in the continuum limit N flavors are produced out of a staggered action with fields that have only $N/2$ components (at least at large N).

The same procedure as with Wilson fermions (only much easier, because no mass-tuning is necessary) leads to the curves $m(L)L$ vs mL which have a universal continuum limit. The result is plotted in figure 4.5. The approach to the continuum at some particular value of mL is displayed in figure 4.6.

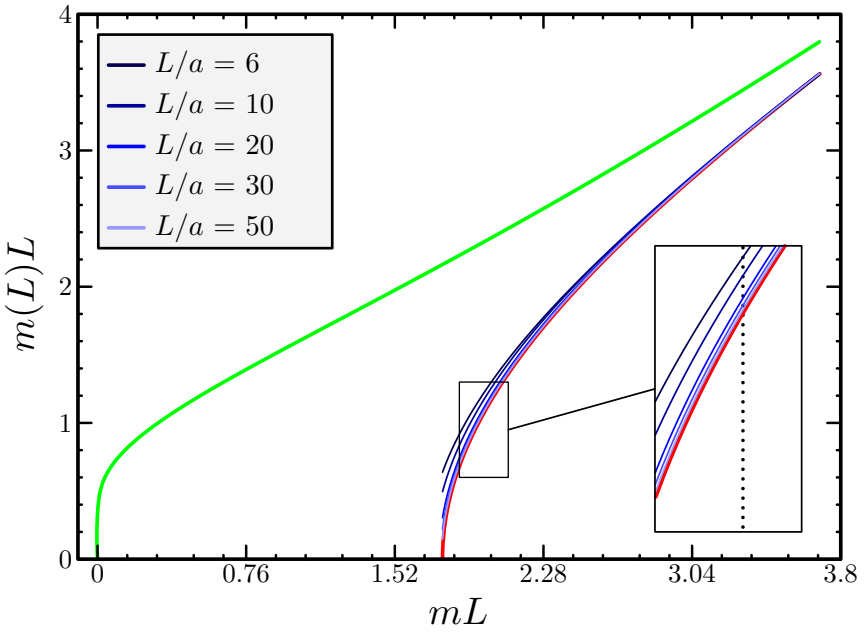

Figure 4.5: $m(L)L$ vs mL curves obtained with staggered fermions on different lattices. The red line is the corresponding continuum solution. The dotted vertical line indicates the mL value for which the approach to the continuum is plotted in figure 4.6. The light green line indicates the continuum solution with periodic b.c. while all the other curves had antiperiodic b.c.

4.4 Overlap fermions

With the exact chiral symmetry of overlap fermions, the calculation for the chiral Gross-Neveu model (without the $\mathcal{L}^{VV}$ term which can be dropped at large N) can be carried out as in the continuum.

After the introduction of auxiliary fields, the fermions can be integrated out and one ends up with the partition function ($\lambda = g_s^2/N$)

$$Z = \int D\sigma D\Pi \exp\Big\{ - N \sum_x a^2 \frac{\sigma^2 + \Pi^2}{2\lambda} + N \,\mathrm{Tr}\, \log\Big[D + \sigma\Big(1 - \frac{a}{2}D\Big) + i\Pi\gamma_5\Big(1 - \frac{a}{2}D\Big)\Big]\Big\}$$

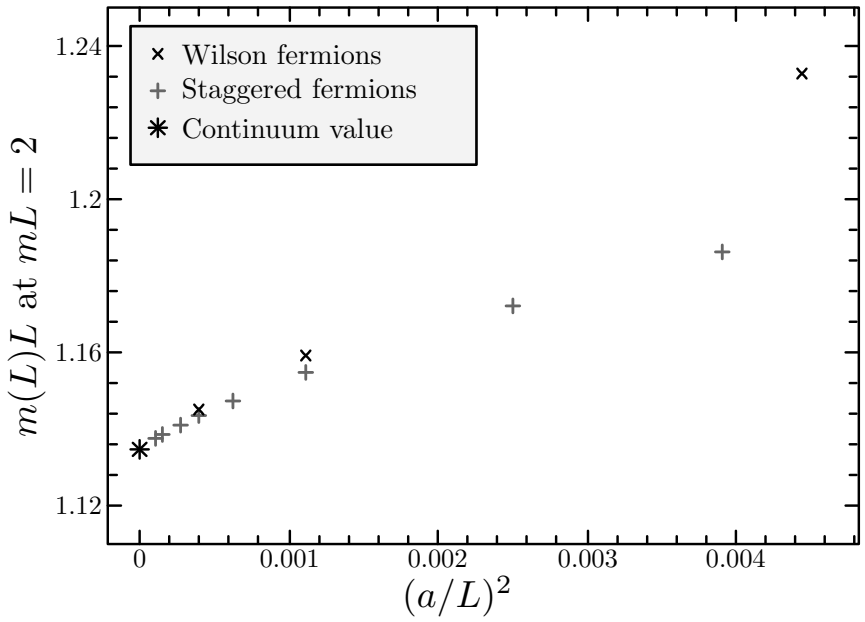

Figure 4.6: The approach to the continuum at some value of mL ($mL = 2$) and antiperiodic b.c. for Wilson and staggered fermions.

This form is suitable for a large-N expansion. To carry out the leading order for the finite volume mass-gap it is necessary to find the extrema of the action, which are assumed to occur at constant σ and Π fields.

For constant fields the trace can be written as

$$\begin{aligned} & \mathrm{T}r\, \log\left[D + \sigma\left(1 - \frac{a}{2}D\right) + i\Pi\gamma_5\left(1 - \frac{a}{2}D\right)\right] \\ = & \iint_{-\pi/a}^{+\pi/a} \frac{d^2p}{(2\pi)^2} \sum_x a^2 e^{-ipx}\, \mathrm{tr}^s\, \log\left[D + \sigma\left(1 - \frac{a}{2}D\right) + i\Pi\gamma_5\left(1 - \frac{a}{2}D\right)\right] e^{ipx} \\ = & TL \iint_{-\pi/a}^{+\pi/a} \frac{d^2p}{(2\pi)^2}\, \mathrm{tr}^s\, \log\left[\tilde{D}(p) + \sigma\left(1 - \frac{a}{2}\tilde{D}(p)\right) + i\Pi\gamma_5\left(1 - \frac{a}{2}\tilde{D}(p)\right)\right] \end{aligned} \tag{4.22}$$

where

$$a\tilde{D}(p) = 1 - \left[1 - \frac{a^2}{2}\hat{p}^2 - ia\mathring{\not{p}}\right]\left[1 + \frac{a^4}{2}\hat{p}_0^2\hat{p}_1^2\right]^{-\frac{1}{2}} . \tag{4.23}$$

After the evaluation of the spin-trace the rotational symmetry of the effective potential becomes manifest

$$V^{eff}(\sigma, \Pi) = \frac{\sigma^2 + \Pi^2}{2\lambda} + \iint_{-\pi/a}^{+\pi/a} \frac{d^2p}{(2\pi)^2} \log\left\{C_1(p)\left(\sigma^2 + \Pi^2\right) + C_2(p)\right\} , \tag{4.24}$$

with the not very illuminating abbreviations

$$\begin{aligned} C_1(p) &= \frac{1}{2}\left(1+\frac{1-\frac{a^2}{2}\hat{p}^2}{(1+\frac{a^4}{2}\hat{p}_0^2\hat{p}_1^2)^{\frac{1}{2}}}\right)^2+\frac{a^2}{4}\frac{\overset{\circ}{p}^2}{1+\frac{a^4}{2}\hat{p}_0^2\hat{p}_1^2} \\ C_2(p) &= \frac{1}{a^2}\left(1-\frac{1-\frac{a^2}{2}\hat{p}^2}{(1+\frac{a^4}{2}\hat{p}_0^2\hat{p}_1^2)^{\frac{1}{2}}}\right)^2+\frac{\overset{\circ}{p}^2}{1+\frac{a^4}{2}\hat{p}_0^2\hat{p}_1^2}\,. \end{aligned}$$

As in the continuum case the variable $\rho^2 = \sigma^2 + \Pi^2$ can be introduced and minima of the potential can be found by solving the gap-equation

$$\frac{1}{\lambda} - \iint_{-\pi/a}^{+\pi/a} \frac{d^2p}{(2\pi)^2}\frac{2}{\rho^2+\frac{C_2(p)}{C_1(p)}} = 0 \tag{4.25}$$

In correspondence to the discrete Gross-Neveu model the solutions can be interpreted as a dynamically acquired fermion mass m. Solutions of the gap-equation in infinite volume allow it to construct the functional dependence between m and λ numerically. This can be used to get rid of the parameter λ in the finite-volume gap-equation which is given by eq. (4.25) only that the integral over the spatial momentum is replaced by the appropriate momentum sum. At fixed mL the value of $m(L)L$ has got a finite continuum limit. Fig. 4.7 shows the curves $m(L)L$ vs. mL for a sequence of lattice spacings. Fig. 4.8 shows the approach to the continuum at a fixed value of mL.

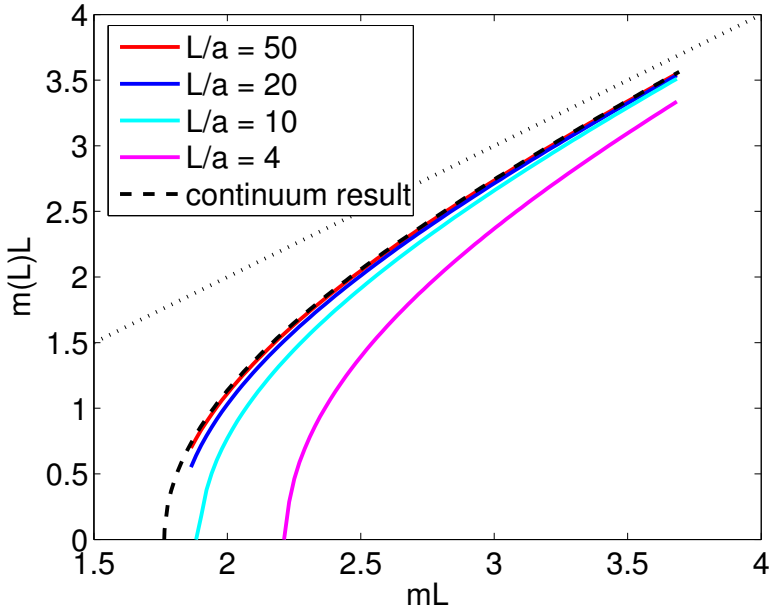

Figure 4.7: Curves $m(L)L$ as a function of mL for a sequence of lattice spacings. Antiperiodic boundary conditions were employed in the spatial direction.

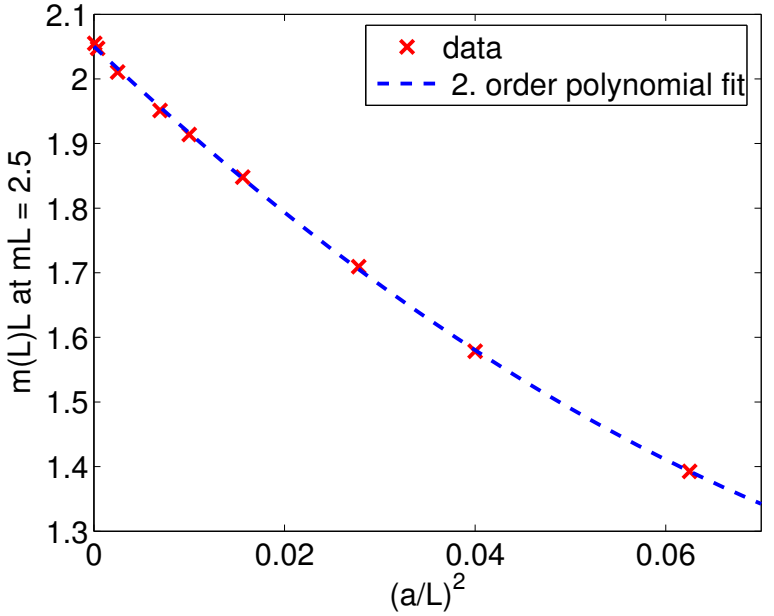

Figure 4.8: Approach of $m(L)L$ to its continuum value at $mL = 2.5$

Chapter 5

Perturbative renormalization of the Gross-Neveu model

In this chapter the renormalization procedure of the Gross-Neveu model is carried out to one-loop using Wilson-lattice-perturbation theory. The results derived here serve three main purposes:

- Values of continuum extrapolated universal quantities can be compared to results obtained in different schemes thus validating our approach.
- At finite lattice spacing and small bare coupling the Monte-Carlo simulations must reproduce the perturbative results. This allows for very nontrivial tests of the simulation code.
- Perturbative results for the critical mass and the renormalized coupling help significantly in tuning the simulation parameters in order to stay on a line of constant physics while taking the continuum limit.

For the calculation the "Majorana language" (as defined in 2.29) is used. It seems to be the natural choice in this model and calculations are slightly easier than in the form with Dirac fields.

The perturbative renormalization of the chiral model in the Schrödinger functional renormalization scheme is described in great detail in [53] and therefore omitted in this thesis.

5.1 Lattice perturbation theory

The expectation value of an observable is defined by

$$\langle O \rangle = \frac{\int D\xi \, O \, e^{-S^{(0)}+g^2 S^{(I)}}}{\int D\xi \, e^{-S^{(0)}+g^2 S^{(I)}}}, \tag{5.1}$$

where $S^{(0)}$ is the free, massive Wilson-action

$$S^{(0)} = \frac{a^2}{2} \sum_x \xi^\top(x) C [D_W + m_0] \xi(x) \,, \tag{5.2}$$

and $S^{(I)} = \sum_x \frac{a^2}{8} (\xi^\top(x) C \xi(x))^2$ is the Gross-Neveu interaction term. For small couplings the exponential can be Taylor-expanded around $g^2 = 0$ and the bare perturbation series

$$\begin{aligned} \langle O \rangle &= \langle O \rangle^{(0)} \\ &+ g^2 \left(\left\langle O S^{(I)} \right\rangle^{(0)} - \langle O \rangle^{(0)} \left\langle S^{(I)} \right\rangle^{(0)} \right) \\ &+ g^4 \Big(\left\langle O S^{(I)} S^{(I)} \right\rangle^{(0)} - \langle O \rangle^{(0)} \left\langle S^{(I)} S^{(I)} \right\rangle^{(0)} - 2 \left\langle O S^{(I)} \right\rangle^{(0)} \left\langle S^{(I)} \right\rangle^{(0)} \\ &\qquad + 2 \langle O \rangle^{(0)} \left\langle S^{(I)} \right\rangle^{(0)} \left\langle S^{(I)} \right\rangle^{(0)} \Big) \\ &+ O(g^6) \,, \end{aligned} \tag{5.3}$$

is obtained. Here $\langle . \rangle^{(0)}$ denotes the expectation value in the free theory. With the knowledge of the free propagator

$$\langle \tilde{\xi}_{\alpha i}(p) \tilde{\xi}_{\beta j}(q) \rangle^{(0)} = -\delta(p+q) \delta_{i,j} \left[\tilde{G}(p) C^{-1} \right]_{\alpha\beta} \tag{5.4}$$

$$\tilde{G}(p) = \frac{-i \mathring{\not{p}} + M(p)}{\mathring{p}^2 + M(p)^2} \tag{5.5}$$

and the Wick theorem, equation (5.3) can be evaluated for arbitrary observables.

For our observables the half Fourier-transformed propagators are of more use.

$$\breve{G}(x_0, p_1) = \frac{1}{T} \sum_{p_0} e^{i p_0 x_0} \tilde{G}(p) \quad \textit{and} \quad \hat{G}(p_0, x_1) = \frac{1}{L} \sum_{p_1} e^{i p_1 x_1} \tilde{G}(p) \tag{5.6}$$

Analytic expressions for these propagators were obtained in [84]. This calculation is repeated in appendix B.5. The result is

$$\breve{G}(x_0, p_1) = h_0(x_0, p_1) \gamma_1 + h_+(x_0, p_1) P_+ + h_-(x_0, p_1) P_- \tag{5.7}$$

$$\hat{G}(p_0, x_1) = \bar{h}_0(p_0, x_1) \gamma_0 + \bar{h}_+(p_0, x_1) Q_+ + \bar{h}_-(p_0, x_1) Q_- \,, \tag{5.8}$$

with the projectors $P_\pm = \frac{1}{2}(\mathbb{1} \pm \gamma_0)$ and $Q_\pm = \frac{1}{2}(\mathbb{1} \pm \gamma_1)$. The coefficient functions are given by

$$h_\pm(x_0, p_1) = (1 + M_1) f(x_0, p_1) - f(x_0 \pm a, p_1) \tag{5.9}$$

$$h_0(x_0, p_1) = -i \mathring{p}_1 f(x_0, p_1) \tag{5.10}$$

$$\bar{h}_\pm(p_0, x_1) = (1 + M_0) \bar{f}(p_0, x_1) - \bar{f}(p_0, x_1 \pm a) \tag{5.11}$$

$$\bar{h}_0(p_0, x_1) = -i \mathring{p}_0 \bar{f}(p_0, x_1) \tag{5.12}$$

with $M_\mu = m_0 + \frac{a}{2}\hat{p}_\mu^2$ and the scalar functions

$$f(x_0, p_1) = \frac{-1}{2(1+M_1)\sinh(\alpha)} \frac{\sinh(\alpha(t-T/2))}{\cosh(\alpha T/2)} \tag{5.13}$$

$$\bar{f}(p_0, x_1) = \frac{1}{e^{2\bar{\alpha}}-1} \frac{\cosh(\bar{\alpha}(x_1 - L/2))}{\sinh(\bar{\alpha}L/2)}\,. \tag{5.14}$$

Finally the angles α and $\bar{\alpha}$ are determined by

$$\alpha = \mathrm{a}cosh\left(\frac{1}{2}\left(1 + M_1 + \frac{1+\mathring{p}_1^2}{1+M_1}\right)\right) \tag{5.15}$$

$$\bar{\alpha} = \mathrm{a}cosh\left(\frac{1}{2}\left(1 + M_0 + \frac{1+\mathring{p}_0^2}{1+M_0}\right)\right). \tag{5.16}$$

5.2 Two point functions

For $k_S = k_S^{(0)} + g^2 k_S^{(1)} + O(g^4)$ and the related k_μ, $\bar{k}_S$ and $\bar{k}_\mu$ (For the definition see section 2.2.4) one obtains

$$k_S^{(0)}(x_0, p_1) = h_+(x_0, p_1) + h_-(x_0, p_1) \tag{5.17}$$

$$k_0^{(0)}(x_0, p_1) = h_+(x_0, p_1) - h_-(x_0, p_1) \tag{5.18}$$

$$\bar{k}_S^{(0)}(p_0, x_1) = \bar{h}_+(p_0, x_1) + \bar{h}_-(p_0, x_1) \tag{5.19}$$

$$\bar{k}_1^{(0)}(p_0, x_1) = \bar{h}_+(p_0, x_1) - \bar{h}_-(p_0, x_1) \tag{5.20}$$

at tree level. The one loop correction to k_S is given by the Feynman-diagram in figure 5.1 (The Feynman rules and a detailed example-calculation can be found in appendix B.6) which is equivalent to

$$k_S^{(1)} = -\frac{\mathcal{N}-1}{2L} a \sum_{y_0, q_1} \mathrm{tr}\left[\breve{G}(x_0 - y_0, p_1)\breve{G}(y_0, -p_1)\right] \mathrm{tr}\left[\breve{G}(0, q_1)\right]. \tag{5.21}$$

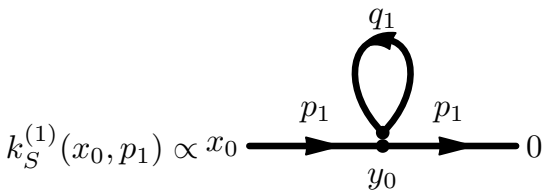

Figure 5.1: The one loop diagram contributing to k_S.

This can be further simplified leading to the following expressions

$$\begin{aligned}
k_S^{(1)}(x_0,p_1) &= -(\mathcal{N}-1)\sum_{y_0}\Big(h_+(x_0-y_0,p_1)h_+(y_0,p_1) \\
&\qquad +h_-(x_0-y_0,p_1)h_-(y_0,p_1) \\
&\qquad -2h_0(x_0-y_0,p_1)h_0(y_0,p_1)\Big)K \qquad (5.22)\\
k_0^{(1)}(x_0,p_1) &= -(\mathcal{N}-1)\sum_{y_0}\Big(h_+(x_0-y_0,p_1)h_+(y_0,p_1) \\
&\qquad -h_-(x_0-y_0,p_1)h_-(y_0,p_1)\Big)K \qquad (5.23)\\
\bar{k}_S^{(1)}(p_0,x_1) &= -(\mathcal{N}-1)\sum_{y_1}\Big(\bar{h}_+(p_0,x_1-y_1)\bar{h}_+(p_0,y_1) \\
&\qquad +\bar{h}_-(p_0,x_1-y_1)\bar{h}_-(p_0,y_1) \\
&\qquad -2\bar{h}_0(p_0,x_1-y_1)\bar{h}_0(p_0,y_1)\Big)K \qquad (5.24)\\
\bar{k}_1^{(1)}(p_0,x_1) &= -(\mathcal{N}-1)\sum_{y_1}\Big(\bar{h}_+(p_0,x_1-y_1)\bar{h}_+(p_0,y_1) \\
&\qquad -\bar{h}_-(p_0,x_1-y_1)\bar{h}_-(p_0,y_1)\Big)K\,. \qquad (5.25)
\end{aligned}$$

The dimensionless numerical constant K is given by

$$K = \frac{a}{2LT}\sum_{q_0,q_1} tr\left[\tilde{G}(q)\right] = \frac{a}{2L}\sum_{q_1} tr\left[\check{G}(0,q_1)\right]. \qquad (5.26)$$

If the value of K is known for a series of lattices, the continuum limit and the leading lattice artifacts can be extracted numerically. For this extraction the method introduced in [11] is used. The numerical values that enter the procedure and the final result are summarized in table C.6 in the appendix C.2. The result is (for $L = T$, $m_0 = 0$, all quoted digits are significant)

$$K = K_0 + 0.2821\frac{a^4}{L^4} + O(a^6), \qquad K_0 = 0.3849001794598\,. \qquad (5.27)$$

5.3 Perturbative renormalization

To obtain finite and universal results in the continuum limit with Wilson-fermions it is necessary to fix the additive mass renormalization constant, the multiplicative wave-function renormalization constant and to take the limit while keeping some renormalized coupling fixed.

The additive mass renormalization can be fixed by the requirement that the quantity k_S or $\bar{k}_S$ vanishes for some choice of the arguments (at which it does not vanish due to some other symmetry). These quantities are plotted in figure 5.2

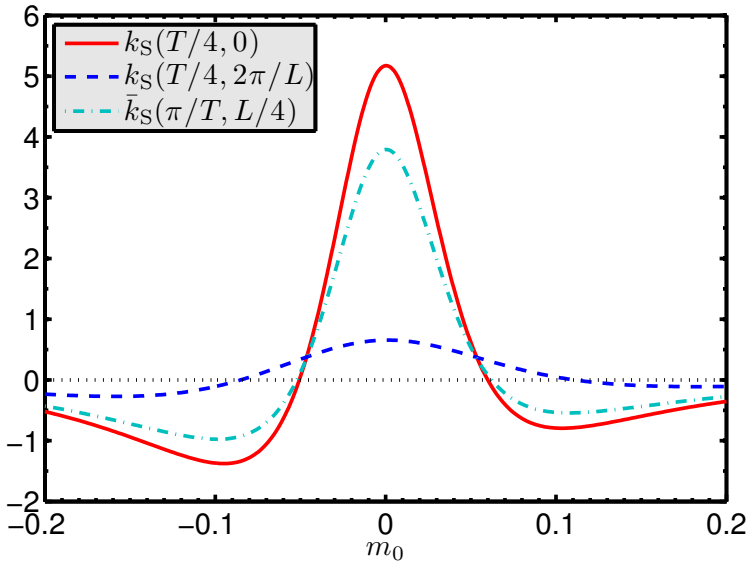

Figure 5.2: Sensitivity of k_S and $\bar{k}_S$ to the bare mass m_0 for different choices of arguments. The plot shows the one loop result for the $\mathcal{N} = 8$ Gross-Neveu model on a 48×48 lattice with the bare coupling set to $g = 0.4$. The situation is qualitatively the same for all values of the coupling in the interval $g \in [0, 1]$.

for several choices of arguments. From this plot and similar plots with different choices of $\mathcal{N}$, g, L/a it appears, that $k_S(T/4, 0)$ is most sensitive to changes of the bare mass in the regions of interest. Moreover quantities at higher momentum are expected to have bigger lattice artifacts. Therefore in this work the additive mass renormalization is fixed by

$$k_S(T/4,0)|_{m_0=m_c} \stackrel{!}{=} 0\,. \tag{5.28}$$

At zero spatial momentum and with $m_0 = 0$ expression (5.9) simplifies to

$$h_+(x_0,0) = \frac{1}{2} \qquad \text{for } x_0 \in 0\ldots T-1 \tag{5.29}$$

$$h_-(x_0,0) = -\frac{1}{2} \qquad \text{for } x_0 \in 1\ldots T\,. \tag{5.30}$$

Hence from equation (5.17) one obtains at tree level

$$m_c^{(0)} = 0\,. \tag{5.31}$$

The one loop correction is fixed by

$$m_c^{(1)} \left.\frac{\partial k_S(T/4,0)}{\partial m_0}\right|_{m_0=m_c^{(0)}} + \left. k_S^{(1)}(T/4,0)\right|_{m_0=m_c^{(0)}} \stackrel{!}{=} 0\,. \tag{5.32}$$

Carrying out the derivative one finds

$$\left.\frac{\partial k(T/4,0)}{\partial m_0}\right|_{m_0=m_c^{(0)}} = \frac{T}{4}\,, \tag{5.33}$$

while the 1-loop diagram simplifies to

$$\left.k_{\mathrm{S}}^{(1)}(T/4,0)\right|_{m_0=m_c^{(0)}} = \frac{(\mathcal{N}-1)T}{4a}K\,. \tag{5.34}$$

Hence the first correction to the critical mass is

$$m_c^{(1)} = -\frac{(\mathcal{N}-1)}{a}K\,. \tag{5.35}$$

That means that at one loop the leading cutoff-effects for the critical mass are only proportional to $(L/a)^4$ in this scheme.

To fix the wave function renormalization constant Z_ψ one can require $(k_0)_R(T/2,0) = Z_\psi^{-1}k_0(T/2,0)$ to assume the value 1 at $m_0 = m_c$. With this requirement one obtains at tree level

$$Z_\psi^{(0)} = \left.k_0^{(0)}(T/2,0)\right|_{m_0=m_c^{(0)}} = \frac{1}{2}+\frac{1}{2} = 1\,. \tag{5.36}$$

To obtain the one loop correction it is necessary to know

$$\left.\frac{\partial k_0^{(0)}(T/2,0)}{\partial m_0}\right|_{m_0=m_c^{(0)}} = -a \tag{5.37}$$

and

$$\left.k_0^{(1)}(T/2,0)\right|_{m_0=m_c^{(0)}} = -(\mathcal{N}-1)K\,. \tag{5.38}$$

So the 1-loop correction to the renormalization constant is absent

$$\begin{aligned} Z_\psi^{(1)} &= m_c^{(1)}\left.\frac{\partial k_0^{(0)}(T/2,0)}{\partial m_0}\right|_{m_0=m_c^{(0)}} + \left.k_0^{(1)}(T/2,0)\right|_{m_0=m_c^{(0)}} \\ &= 0\,. \end{aligned} \tag{5.39}$$

The absence of a divergence is in agreement with [55]. In the scheme that was used by those authors (i.e. dimensional regularization) the one loop correction to the wave function renormalization constant also vanishes.

The cancellation between $\frac{\partial k_0^{(0)}}{\partial m_0}$ and $k_0^{(1)}$ is not a coincidence. In fact it happens for all the two point functions k_X and $\bar{k}_X$ ($X \in \{S,\mu\}$, $\Gamma_X \in \{\mathbb{1},\gamma_\mu\}$). The reason is, that for arbitrary observables $\mathcal{O}$

$$\frac{\partial}{\partial m_0}\langle\mathcal{O}\rangle = -\frac{1}{2}\sum_x a^2\left(\langle\xi^\top(x)C\xi(x)\mathcal{O}\rangle - \langle\xi^\top(x)C\xi(x)\rangle\langle\mathcal{O}\rangle\right). \tag{5.40}$$

In case of the two point functions it means that only the diagram shown in fig. 5.3 contributes which is given by

$$\frac{\partial k_X^{(0)}(x_0,p_1)}{\partial m_0} = a\sum_{y_0} \mathrm{tr}[\breve{G}(x_0-y_0,p_1)\breve{G}(y_0,-p_1)\Gamma_X]\,. \tag{5.41}$$

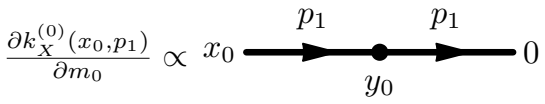

Figure 5.3: Contribution to the derivative of k_X with respect to the bare mass.

Multiplied with $m_c^{(1)}$ one obtains exactly $-k_X^{(1)}(x_0,p_1)$.

Due to these cancellations at $m_0 = m_c$ the renormalized two point functions are given to order g^2 by their tree-level values

$$(k_X)_R = k_X^{(0)}\Big|_{m_0=m_c^{(0)}} + O(g^4)\,. \tag{5.42}$$

In order to keep the physical volume fixed while taking the continuum limit it is necessary to stay at a constant value of some renormalized coupling. A convenient definition is

$$g_R^2 = Z_\psi^{-2}\frac{4a^2}{(T-2a)L}\left\langle \breve{\xi}_1^\top(T/2)C\breve{\xi}_1(0)\breve{\xi}_2^\top(T/2)C\breve{\xi}_2(0)\right\rangle\,. \tag{5.43}$$

The diagrams at order g^0 vanish due to time inversion symmetry and antiperiodicity in the temporal direction. At order g^2 one diagram contributes (see fig. 5.4).

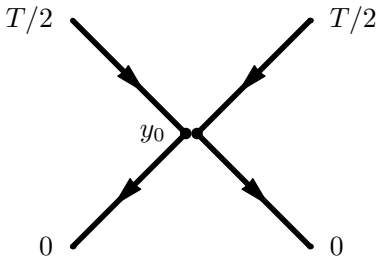

Figure 5.4: Tree-level contribution to g_R^2.

It is given by

$$\begin{aligned} g_R^{(0)\,2} &= \frac{4a}{T-2a}\sum_{x_0} a\,\mathrm{tr}\left[\breve{G}(T/2-x_0)\breve{G}(x_0)\right]^2 \\ &= \frac{4a}{T-2a}\sum_{x_0} a\,(h_+(T/2-x_0)h_+(x_0)+h_-(T/2-x_0)h_-(x_0))^2 \\ &= g^2\,. \end{aligned} \tag{5.44}$$

The possible 1-loop contributions are shown graphically in fig. 5.5.

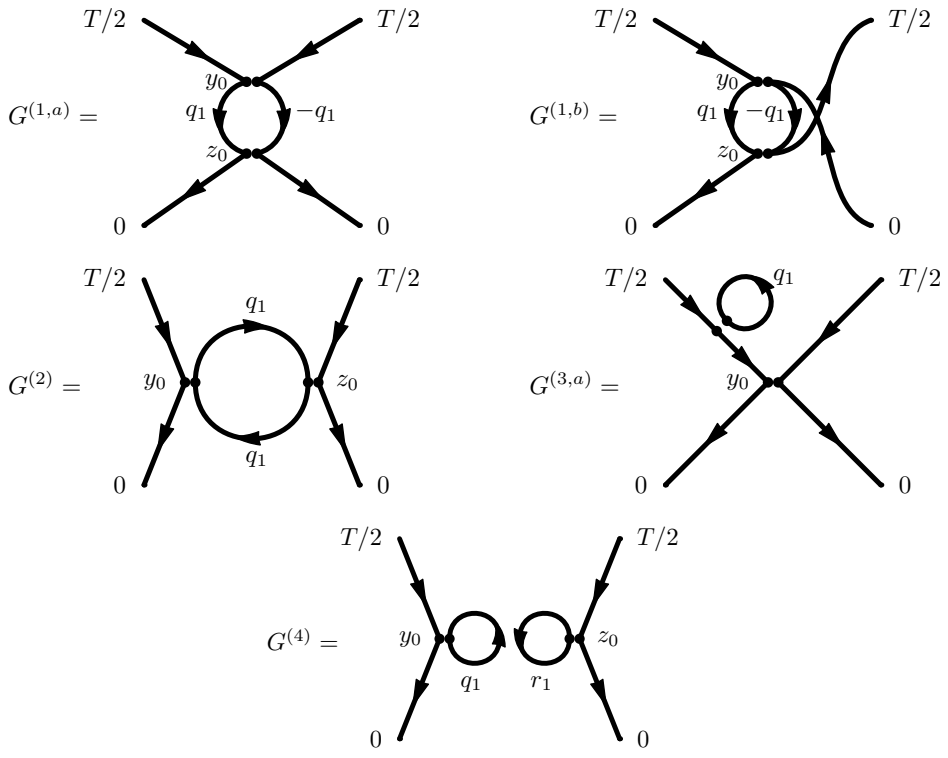

Figure 5.5: 1 loop contributions to g_R^2.

Again the contribution $G^{(4)}$ vanishes due to antiperiodicity and time reflection invariance. $G^{(1,a)}$ and $G^{(1,b)}$ have the same continuum limit. $G^{(1,a)}$

evaluates to

$$\begin{aligned} G^{(1,a)} &= \frac{4a^2}{(T-2a)L}\sum_{y_0,z_0,q_1} a^2\,\mathrm{tr}\left[\breve{G}(T/2-y_0)\breve{G}(y_0-z_0,q_1)\breve{G}(z_0)\right]^2 \\ &= \frac{4a^2}{(T-2a)L}\Big\{\sum_{y_0,q_1} a\Big(\frac{T}{16a}(h_+(y_0,q_1)^2+h_-(y_0,q_1)^2) \\ &\qquad +\frac{T-4a}{8a}h_+(y_0,q_1)h_-(y_0,q_1)\Big) \\ &\qquad +\frac{1}{2}\sum_{q_1} h_+(T/2,q_1)h_-(T/2,q_1)\Big\}. \end{aligned} \tag{5.45}$$

The remaining sums have to be performed numerically. Again the asymptotic cutoff dependence can be extracted (table C.6) for $L = T$ resulting in

$$\begin{aligned} G^{(1,a)} &= \frac{T}{T-2a}\Big(0.1548258837-\frac{1}{2\pi}\frac{a}{L}\log\Big(\frac{a}{L}\Big)-0.13124372\frac{a}{L}-0.50745\frac{a^2}{L^2} \\ &\qquad +0.296\frac{a^3}{L^3}+O(a^4)\Big), \end{aligned} \tag{5.46}$$

$$G^{(1,b)} = \frac{T}{T-2a}\left(0.1548258837-0.288307863\frac{a}{L}+0.12\frac{a^4}{L^4}+O(a^5)\right) \tag{5.47}$$

There is no divergence in these two diagrams. Wherever exact coefficients like $1/2\pi$ appear, they were seen numerically to at least 10 digits and then assumed to be exact.

The graph $G^{(2)}$ which is absent in the Thirring model contributes with

$$\begin{aligned} G^{(2)} &= \frac{4a^2}{(T-2a)L}(\mathcal{N}-2)\sum_{x_0,y_0,q_1} a^2\,\mathrm{tr}\left[\breve{G}(T/2-x_0)\breve{G}(x_0)\right] \\ &\qquad \times\mathrm{tr}\left[\breve{G}(x_0-y_0,q_1)\breve{G}(y_0,x_0,q_1)\right]\mathrm{tr}\left[\breve{G}(T/2-y_0)\breve{G}(y_0)\right]. \end{aligned} \tag{5.48}$$

The divergence is universal, whereas the lattice artifacts are given by (table C.6)

$$G^{(2)} = \frac{(\mathcal{N}-2)T}{T-2a}\left(\frac{\log(L/a)}{2\pi}-0.483524477+0.5451956\frac{a}{L}+0.5025\frac{a^2}{L^2}+O(a^3)\right) \tag{5.49}$$

Finally each of the four graphs similar to $G^{3,a}$ is given by

$$\begin{aligned} G^{(3,a)} &= -\frac{a^2}{(T-2a)L}(\mathcal{N}-1)\sum_{x_0,y_0,q_1}\mathrm{tr}\left[\breve{G}(T/2-x_0)\breve{G}(x_0-y_0)\breve{G}(y_0)\right] \\ &\qquad \mathrm{tr}\left[\breve{G}(T/2-y_0)\breve{G}(y_0)\right]\mathrm{tr}\left[\breve{G}(0,q_1)\right] \\ &= -\frac{1}{2}(\mathcal{N}-1)K. \end{aligned} \tag{5.50}$$

To calculate the renormalized coupling to 1-loop it is also necessary to evaluate

$$\frac{\partial}{\partial m_0}\, g_R^{(0)\,2}\Big|_{m_0=m_c^{(0)}} = 2a\,, \tag{5.51}$$

and therefore (like with the two point functions before) the diagrams $G^{(3)}$ are exactly canceled by

$$m_c^{(1)}\, \frac{\partial g_R^{(0)\,2}}{\partial m_0}\bigg|_{m_0=m_c^{(0)}} = 2a(\mathcal{N}-1)K = -4\mathrm{G}^{(3,a)}\,. \tag{5.52}$$

Chapter 6

Monte-Carlo Simulation

6.1 Algorithms

An important tool to carry out nonperturbative numerical calculations in quantum field theories is the Monte-Carlo simulation. The general ideas behind the method and many practical algorithms as well as error-estimation are covered in numerous textbooks (e.g. [64, 52, 8]).

In the Gross-Neveu model with auxiliary-field action (2.33) and with the fermions already integrated out, the typical lattice path integral to calculate is

$$\langle O \rangle = \frac{\int D\sigma \, O[\sigma] \, e^{-S[\sigma]}}{\int D\sigma \, e^{-S[\sigma]}} \,, \tag{6.1}$$

where $O[\sigma]$ is some arbitrary observable. A typical importance sampling Monte-Carlo algorithm provides a sequence of field configurations $\sigma^{(i)} = \left\{\sigma^{(i)}(x) | x \in \mathbb{Z}^2\right\}$ such that

$$\lim_{n\to\infty} \frac{1}{n} \sum_{i=1}^{n} O[\sigma^{(i)}] = \langle O \rangle \,. \tag{6.2}$$

In most cases this sequence is obtained from a Markov process. A configuration σ is followed by a configuration σ' with the transition probability $W(\sigma \to \sigma')$. The Monte-Carlo algorithm provides in some way the Markov-matrix W. The desired property (6.2) is fulfilled if the transition probabilities respect two criteria

1. stability
$$\sum_{\sigma} e^{-S[\sigma]} \, W(\sigma \to \sigma') = e^{-S[\sigma']} \tag{6.3}$$

2. ergodicity
$$W^n(\sigma \to \sigma') > 0 \qquad \forall \sigma, \sigma' \tag{6.4}$$
with some fixed number of transitions n.

Of course in order to be a proper probability W has to be non-negative and $\sum_{\sigma'} W(\sigma \to \sigma') = 1$. Often instead of the stability criterion the more strict detailed balance criterion is used (which implies stability)

$$e^{-S[\sigma]}\, W(\sigma \to \sigma') = e^{-S[\sigma']}\, W(\sigma' \to \sigma)\,. \tag{6.5}$$

In practice the number of configurations (i.e. the n in eq. 6.2) is limited to some finite value. This introduces statistical errors into the Monte-Carlo estimates. For all primary and derived observables that are calculated within this thesis the method introduced in [86] is used to estimate these errors precisely including autocorrelation effects.

The Gross-Neveu model has been used as a testground for fermion algorithms before. Among the tested methods were the Langevin algorithm [6], the pseudo-fermion algorithm [14] and the Kramers equation algorithm [5]. A variant of the chiral Gross-Neveu model has been studied with the hybrid Monte-Carlo method [36].

6.1.1 A global acceptance algorithm

The simplest algorithm that one can think of for the N flavor Gross Neveu model with Wilson fermions has the following three steps (it can be easily extended to the chiral Gross-Neveu model and to different formulations, e.g. staggered fermions):

1. An auxiliary field configuration is drawn from the "quenched" ensemble
$$P_{quenched}(\bar{\sigma}) \propto \exp\left[-\sum_x \frac{\bar{\sigma}^2(x)}{2g^2}\right] \tag{6.6}$$
2. A proposal is constructed according to
$$\sigma'(x) = \cos(\Phi)\,\sigma(x) + \sin(\Phi)\,\bar{\sigma}(x)\,, \tag{6.7}$$
where σ is the old configuration. Φ is a free parameter of the algorithm that should be tuned to minimize the autocorrelation times of the algorithm.
3. The proposal is accepted with the probability
$$P_{acc}(\sigma \to \sigma') = \min\left\{1, \frac{\det(D_W + m_0 + \sigma')^N}{\det(D_W + m_0 + \sigma)^N}\right\} \tag{6.8}$$

Hence the total probability to obtain a configuration σ' starting from a configuration σ is

$$\begin{aligned} W(\sigma \to \sigma') &= \exp\left[-\sum_x \frac{(\sigma'(x) - \cos(\Phi)\sigma(x))^2}{2g^2 \sin^2(\Phi)}\right] \\ &\times \min\left\{1, \frac{\det(D_W + m_0 + \sigma')^N}{\det(D_W + m_0 + \sigma)^N}\right\} \end{aligned} \tag{6.9}$$

otherwise the old configuration is kept. Clearly the algorithm is ergodic for $\Phi \neq n\pi, n \in \mathbb{N}$. It also satisfies detailed balance

$$\begin{aligned} \frac{W(\sigma \to \sigma')}{W(\sigma' \to \sigma)} &= \exp\left[-\sum_x \frac{\sigma'^2(x) - \sigma^2(x)}{2g^2}\right] \frac{\det(D_W + m_0 + \sigma')^N}{\det(D_W + m_0 + \sigma)^N} \\ &= \frac{\exp(-S[\sigma'])}{\exp(-S[\sigma])} . \end{aligned} \tag{6.10}$$

The most time consuming part is the calculation of the exact determinant which costs $O\left((2LT)^3\right)$ operations. Hence the algorithm is feasible only for relatively small lattices and basically only in two dimensional systems. For larger lattices one could replace the exact determinant by a stochastic estimate as has been done in [45].

The parameter Φ was introduced because without it ($\Phi = \pi/2$) the acceptance drops down rapidly when the coupling or the lattice size become larger. How the autocorrelation time depends on this parameter is shown in figure 6.1. When it is too small the autocorrelations are high due to a low acceptance. When it is too large the autocorrelations are high because the new configuration is dominated by the contribution of the old one. In between an optimal value can be found which however also depends on the other simulation parameters of the theory.

The main advantages of this algorithm are its simplicity and the fact that all even values of N are accessible. The Pfaffian that would occur for odd N instead of the determinant is unfortunately not always positive, therefore the Boltzman weight cannot be interpreted as a probability, which makes Monte-Carlo simulations with common methods impossible.

The main drawbacks are its high computational costs, and that for larger lattices the angle Φ has to be chosen very small in order to get any acceptance at all. For small lattices this algorithm provides an independent check for the results obtained with the more sophisticated Hybrid Monte-Carlo algorithm described in the next section.

6.1.2 Hybrid Monte-Carlo algorithm

The hybrid Monte-Carlo algorithm has been introduced by S. Duane, A.D. Kennedy, B.J. Pendelton and D. Roweth [23]. It foots partially on ideas developed in [66, 29].

In the following a variant of the algorithm is developed for the Gross-Neveu model with Wilson fermions. Subsequently variants of the algorithm for the chiral Gross-Neveu model and for the staggered discretization are proposed.

The partition function of the Gross-Neveu model is given by

$$Z = \int D\bar{\psi} D\psi D\sigma \; e^{-S^{aux}} \tag{6.11}$$

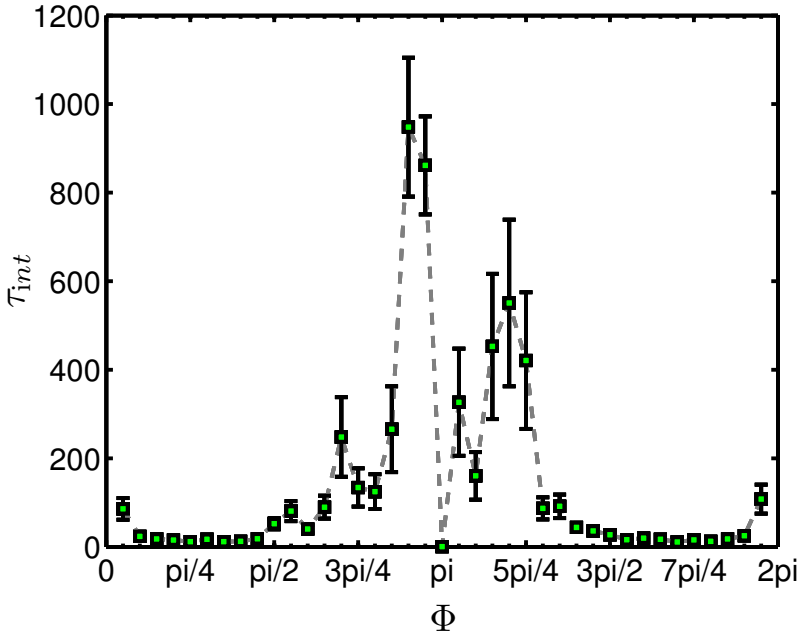

Figure 6.1: The integrated autocorrelation time of the observable $\langle\sigma\rangle$ is plotted for different values of the angle Φ. The simulations were done in the Thirring model with Wilson fermions on an 8×8 lattice with $g = 0.3$ and $m_0 = -0.0167$.

with the auxiliary field action action

$$S^{aux} = \bar{\psi}(D_W + m_0 + \sigma)\psi + \frac{\sigma^2}{2g^2}\,. \tag{6.12}$$

The fermion matrix $D := [D_W + m_0 + \sigma]$ is real if the γ-matrices are in the Majorana representation. Integrating out the Grassmann-valued fields yields

$$Z = \int D\sigma\, e^{-\frac{\sigma^2}{2g^2}} \det(D_W + m_0 + \sigma)^N\,. \tag{6.13}$$

Since the determinant can be written as the square of a real Pfaffian, it must be positive, hence $\det D = \det \sqrt{D^\top D}$. Therefore one can introduce N real pseudo-fermion fields $\phi^{(i)}$ to represent the determinant as

$$Z = \int D\sigma D\phi\, e^{-\frac{\sigma^2}{2g^2} - \sum_i \phi^{(i)\top}[DD^\top]^{-1}\phi^{(i)}}\,, \tag{6.14}$$

where the measure is given by

$$D\phi \propto \prod_{x,\alpha,i} d\phi^{(i)}_\alpha(x)\,. \tag{6.15}$$

In the next step the partition function is multiplied by a 1 in the form of a Gaussian integral and the larger system

$$Z = \int D\sigma D\phi Dp\, e^{-H} \tag{6.16}$$

is considered. The new field p plays the role of a conjugated momentum field to the auxiliary field σ and H is the Hamiltonian

$$H = \sum_x \frac{p^2}{2} + \sum_x \frac{\sigma^2}{2g^2} + \sum_i \phi^{(i)\top}[DD^\top]^{-1}\phi^{(i)}\,. \tag{6.17}$$

One update of the HMC-algorithm consists of the following steps

1. Generate momenta randomly from a probability distribution $\propto e^{-p^2/2}$
2. Draw Gaussian random numbers from a distribution $\propto e^{-\eta^2}$ and generate pseudo-fermion fields according to $\phi^{(i)} = D\eta$.
3. Calculate the evolution of the fields σ and p according to Hamilton's equations of motion from time t to time $t+\tau$. (This time has no physical meaning).
4. Take the resulting configuration as a proposal, which is accepted with the probability $P_{\text{acc}} = \min[1, \exp(-\Delta H)]$, where ΔH is the energy difference between the old and the new configuration (which would be zero if the integration was performed exactly).

The third step is the nontrivial one. The equations of motion for the σ-field read

$$\dot{\sigma}(x) = \frac{\partial H}{\partial p(x)} = p(x)\,. \tag{6.18}$$

The momenta evolve according to

$$\begin{aligned} \dot{p}(x) &= -\frac{\partial H}{\partial \sigma(x)} \\ &= -\frac{\sigma(x)}{g^2} - \frac{\partial}{\partial \sigma(x)} \sum_i \phi^{(i)\top}[DD^\top]^{-1}\phi^{(i)}\,. \end{aligned} \tag{6.19}$$

The identity

$$\begin{aligned} \frac{\partial\left([DD^\top]^{-1}[DD^\top]\right)}{\partial\sigma(x)} &= \left(\frac{\partial}{\partial\sigma(x)}[DD^\top]^{-1}\right)[DD^\top] + [DD^\top]^{-1}\left(\frac{\partial}{\partial\sigma(x)}[DD^\top]\right) \\ &= 0\,, \end{aligned} \tag{6.20}$$

can be used to write

$$\frac{\partial}{\partial\sigma(x)}\phi^\top[DD^\top]^{-1}\phi = -\left([DD^\top]^{-1}\phi\right)^\top\left(\frac{\partial}{\partial\sigma(x)}[DD^\top]\right)\left([DD^\top]^{-1}\phi\right). \quad (6.21)$$

The derivative in the middle is given by

$$\left[\frac{\partial}{\partial\sigma(x)}[DD^\top]\right]_{\alpha\beta}(y,z) = \delta_{y,x}D^\top_{\alpha\beta}(y,z) + D_{\alpha\beta}(y,z)\delta_{z,x} \quad (6.22)$$

Altogether the evolution of the momenta is given by

$$\begin{aligned}\dot{p}(x) &= -\frac{\sigma_x}{g^2} + 2\sum_i\sum_\alpha \varphi^{(i)}_\alpha(x)\left[D^\top\varphi^{(i)}\right]_\alpha(x) && (6.23)\\ &=: F(x)\,. && (6.24)\end{aligned}$$

with

$$\varphi^{(i)} = [DD^\top]^{-1}\phi^{(i)}\,. \quad (6.25)$$

The quantity F is the force that drives the system.

The integration of the equations of motion can be only done numerically. Detailed balance has been proven for the algorithm assuming that the numerical integration scheme is area preserving and reversible [23]. The simplest of such integration schemes is the leapfrog integrator. In this scheme the time interval $[t, t+\tau]$ is divided into N_{traj} pieces of length $\Delta\tau = \tau/N_{traj}$ and the integration is carried out according to the following scheme

- First a half step in the momenta:

$$p(x)^{[t+\Delta\tau/2]} = p(x)^{[t]} + \frac{\Delta\tau}{2}F(x)^{[t]} \quad (6.26)$$

- Then $N-1$ full steps according to the recursion

$$\begin{aligned}\sigma(x)^{[t+\Delta\tau]} &= \sigma(x)^{[t]} + \Delta\tau\, p(x)^{[t+\Delta\tau/2]} && (6.27)\\ p(x)^{[t+3\Delta\tau/2]} &= p(x)^{[t+\Delta\tau/2]} + \Delta\tau\, F(x)^{[t+\Delta\tau]} && (6.28)\end{aligned}$$

- At last a full step for σ is followed by a half step for p

$$\begin{aligned}\sigma(x)^{[t+\tau]} &= \sigma(x)^{[t+\tau-\Delta\tau]} + \Delta\tau\, p(x)^{[t+\tau-\Delta\tau/2]} && (6.29)\\ p(x)^{[t+\tau]} &= p(x)^{[t+\tau-\Delta\tau/2]} + \frac{\Delta\tau}{2}F(x)^{[t+\tau]}\,. && (6.30)\end{aligned}$$

The same scheme with the roles of p and σ interchanged is also possible. The symmetric structure of this integrator is responsible for the cancellation of the leading order discretization errors so that the error is of order $O\left(\Delta\tau^2 N_{traj}\right)$.

The most expensive part of the algorithm are the inversions in (6.25). At each step of the trajectory this sparse linear system of equations needs to be solved which in this work is accomplished with the conjugate gradient method [38, 73].

Chiral Gross-Neveu model

Hybrid Monte-Carlo works with the chiral Gross-Neveu model almost identically. The HMC-Hamiltonian in this case is given by

$$\begin{aligned} H &= \sum_x \frac{p_\sigma^2 + p_\Pi^2 + p_{A_0}^2 + p_{A_1}^2}{2} + \sum_x \frac{\sigma^2}{2g_0^2} + \sum_x \frac{\Pi^2}{2g_5^2} + \sum_x \frac{A_0^2 + A_1^2}{2g_V^2} \\ &\quad + \sum_i \phi_i^\dagger (DD^\dagger)^{-1} \phi_i \,, \end{aligned} \tag{6.31}$$

where $D = D_\mathrm{W} + m_0 + \sigma + i\gamma_5\Pi + \not{A}$ with the auxiliary fields Π, σ and A_μ and their conjugate momenta p_σ, p_Π and p_{A_μ}. The pseudo-fermions in this case are complex, because $\det D$ cannot be written as the square of a real Pfaffian anymore. Therefore only even values of N can be simulated. The equations of motion are

$$\dot{\sigma}(x) = p_\sigma(x) \tag{6.32}$$

$$\dot{\Pi}(x) = p_\Pi(x) \tag{6.33}$$

$$\dot{A}_\mu(x) = p_{A_\mu}(x) \tag{6.34}$$

$$\dot{p}_\sigma(x) = -\frac{\sigma(x)}{g_\mathrm{S}^2} + 2\mathrm{Re}\left(\varphi_\alpha^\dagger(x)[D^\dagger\varphi]_\alpha(x)\right) \tag{6.35}$$

$$\dot{p}_\Pi(x) = -\frac{\Pi(x)}{g_\mathrm{P}^2} + 2\mathrm{Re}\left(\varphi_\alpha^\dagger(x)[i\gamma_5 D^\dagger\varphi]_\alpha(x)\right) \tag{6.36}$$

$$\dot{p}_{A_\mu}(x) = -\frac{A_\mu(x)}{g_\mathrm{V}^2} + 2\mathrm{Re}\left(\varphi_\alpha^\dagger(x)[\gamma_\mu D^\dagger\varphi]_\alpha(x)\right) \tag{6.37}$$

with

$$\varphi = (DD^\dagger)^{-1}\phi \,. \tag{6.38}$$

Staggered fermions

For simulations of the chiral Gross-Neveu model with staggered action 3.74 the following equations of motion emerge

$$\dot{\sigma}(x) = p_\sigma(x) \tag{6.39}$$
$$\dot{\Pi}(x) = p_\Pi(x) \tag{6.40}$$
$$\dot{A}_\mu(x) = p_{A_\mu}(x) \tag{6.41}$$
$$\dot{p}_\sigma(x) = -\frac{\sigma(x)}{4g_S^2} + \frac{1}{4}\mathrm{Re}\left(\sum_\rho \varphi(x+\rho)[K^\dagger\varphi](x+\rho)\right) \tag{6.42}$$
$$\dot{p}_\Pi(x) = -\frac{\Pi(x)}{4g_P^2} + \frac{1}{4}\mathrm{Re}\left(\sum_{\rho,\xi} \varphi(x+\rho) i\sigma^{(2)}_{\rho_0\xi_0}\sigma^{(1)}_{\rho_1\xi_1}[K^\dagger\varphi](x+\xi)\right) \tag{6.43}$$
$$\dot{p}_{A_0}(x) = -\frac{A_0(x)}{4g_V^2} + \frac{1}{4}\mathrm{Re}\left(\sum_{\rho,\xi} \varphi(x+\rho)\sigma^{(1)}_{\rho_0\xi_0}\mathbb{1}_{\rho_1\xi_1}[K^\dagger\varphi](x+\xi)\right) \tag{6.44}$$
$$\dot{p}_{A_1}(x) = -\frac{A_1(x)}{4g_V^2} + \frac{1}{4}\mathrm{Re}\left(\sum_{\rho,\xi} \varphi(x+\rho)\sigma^{(3)}_{\rho_0\xi_0}\sigma^{(1)}_{\rho_1\xi_1}[K^\dagger\varphi](x+\xi)\right). \tag{6.45}$$

Where

$$\varphi = (KK^\dagger)^{-1}\phi\,. \tag{6.46}$$

6.2 Implementation and tests of the code

The implementation of a Hybrid-Monte-Carlo program for the Gross-Neveu models with Wilson and staggered fermions has been one of the main achievements of this thesis. The Wilson-fermion version in `C` with `MPI` for the Gross-Neveu model alone has got roughly 6000 lines of code. To guarantee that the whole software package does what it is supposed to do many tests were performed.

The Dirac operator

The key routine of every version of the code is a function that applies the Dirac operator D or $D^\top$ to a real or complex pseudo fermion field. The same routines were implemented independently in matlab in order to perform crosschecks. Since this routine is called in every iteration of the CG-solver, some care is necessary with regard to the optimization.

The CG-solver

The conjugate-gradient method (see e.g. [73] for a comprehensible introduction) is used to solve linear systems of the form

$$(DD^\top)x = b\,, \tag{6.47}$$

for x. That is equivalent to calculate the inverse applied to a given source $x = (DD^\top)^{-1}b$ which is necessary in every step of the leap-frog integrator. To test the solver the convergence rate was monitored and the expected behavior was found. The number of iterations needed to reach a certain relative precision was proportional to the square-root of the spectral condition number of $DD^\top$.

For the stopping criterion [4] was consulted.

Leap-frog integrator

Since the system to integrate is a Hamiltonian one, the energy is conserved. The difference ΔH has to decrease when the size of the integration steps is reduced. This is a good test for the integrator. Figure 6.2 shows the observed behavior which agrees well with the expectations thus indicating that the equations of motion were derived correctly and that the integrator works properly.

Observables

The implementation of the observables is not always straightforward. The current-current correlators with Noether-currents and Wilson fermions for instance are quite complex. To exclude the possibility of errors the routines were called with a vanishing auxiliary field, thus producing the free-theory results which can be compared with analytic calculations (like in figs. 6.3 and 6.4). Wherever one loop perturbative results were available, the Monte-Carlo results were compared with the bare perturbative ones on a small lattice and a series of small couplings. The last test probes not only the observable-routines but the whole Monte-Carlo code. Figures 6.5 - 6.8 show this comparison with bare perturbation theory for the Thirring model with Wilson fermions. The data shown there can be found in tabular form in the appendix C.3.

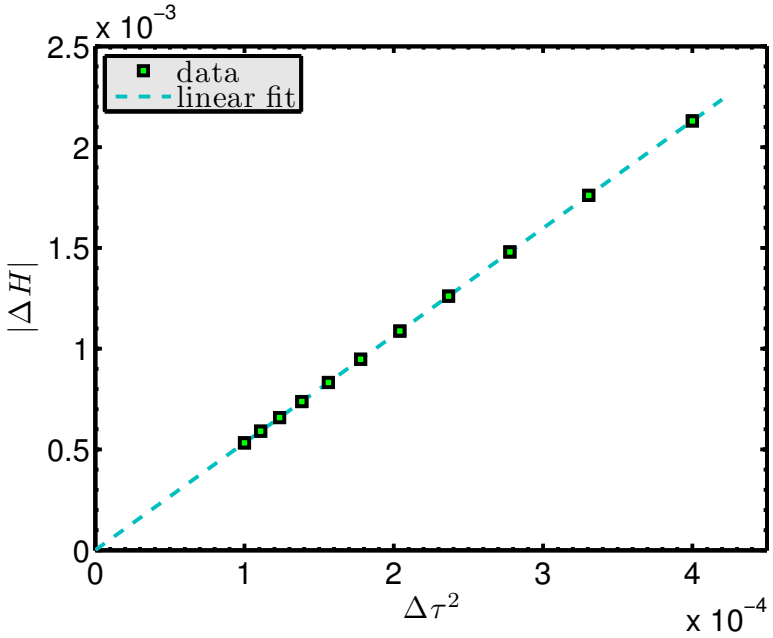

Figure 6.2: The same leapfrog integration has been performed with a fixed trajectory length $\tau = 1$ and different step-sizes $\Delta\tau = \tau/50 \ldots \tau/100$. As expected the integration error decreases linearly with $\Delta\tau^2$.

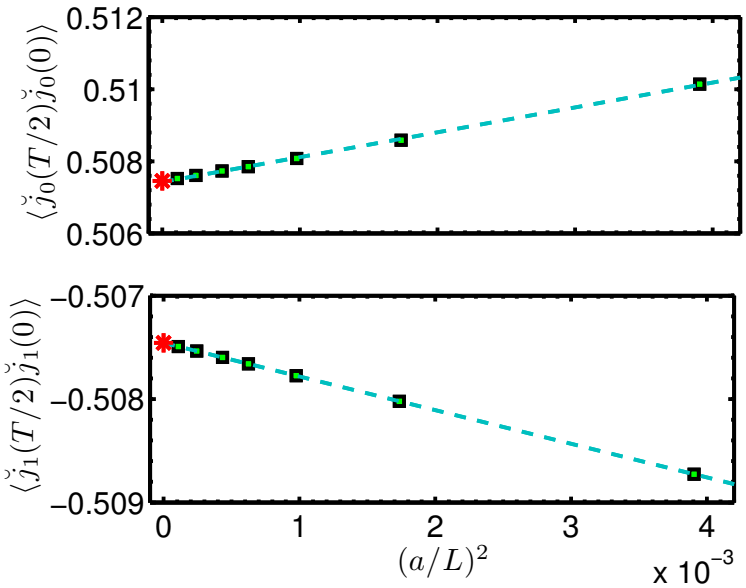

Figure 6.3: The plot shows the continuum extrapolation of the current-current correlators measured with Wilson-fermions in the free theory. Noether currents were used. The extrapolated continuum value is in perfect agreement with the analytic continuum prediction (asterisk).

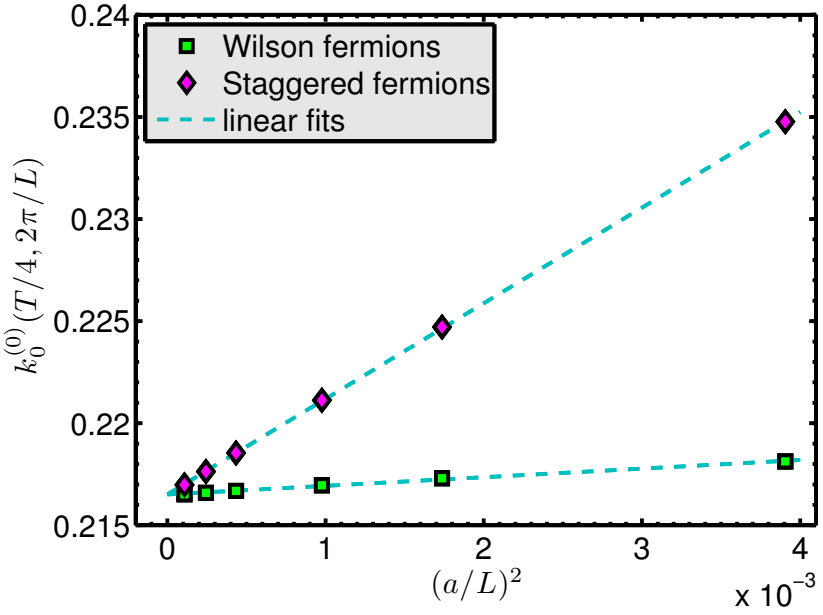

Figure 6.4: The correlator $k_0(T/4, 2\pi/L)$ was measured with vanishing auxiliary field on several lattices with Wilson and with staggered fermions. In both cases the data extrapolates to the common continuum value.

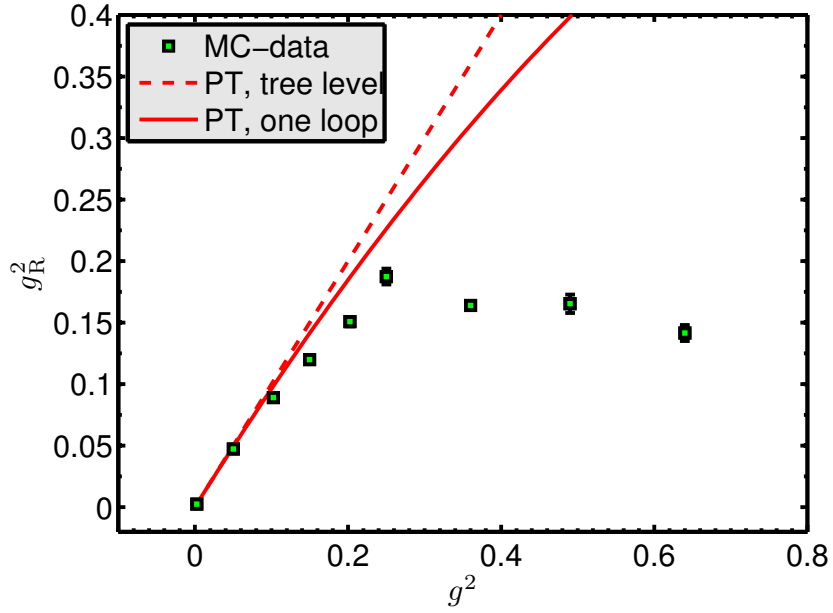

Figure 6.5: For small bare couplings g the Monte Carlo simulation reproduces the perturbative results for $Z_\psi^2 g_R$.

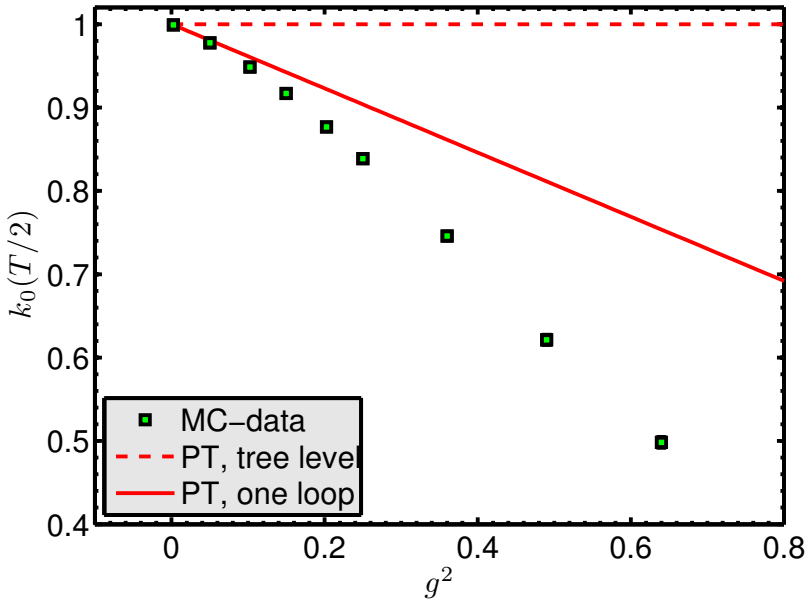

Figure 6.6: For small bare couplings g the Monte Carlo simulation reproduces the perturbative results for $k_0(T/2, 0)$.

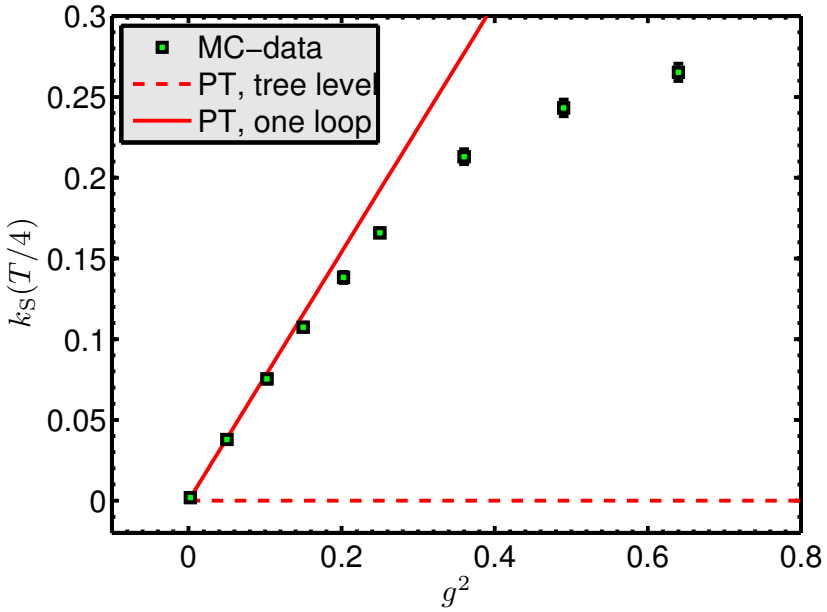

Figure 6.7: For small bare couplings g the Monte Carlo simulation reproduces the perturbative results for $k_S(T/4, 0)$.

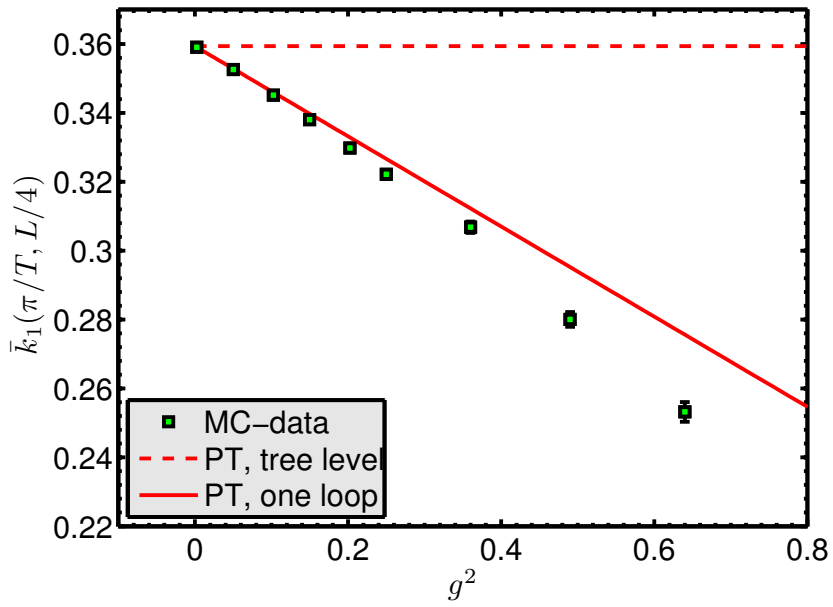

Figure 6.8: For small bare couplings g the Monte Carlo simulation reproduces the perturbative results for $\bar{k}_1(\pi/T, L/4)$.

Other tests of the code

Sometimes the expectation value of an observable is known. Such observables usually provide very nontrivial tests of the code. The following list of observables has been measured in every simulation of the Gross-Neveu model and their compatibility with the known values has been assured

$$\left\langle e^{-\Delta H} \right\rangle = 1 \tag{6.48}$$
$$k_S(T/2, p_1) = 0 \tag{6.49}$$
$$\mathrm{Re} k_1(x_0, p_1) = 0 \tag{6.50}$$
$$\mathrm{Re} \bar{k}_0(p_0, x_1) = 0 \tag{6.51}$$
$$\bar{k}_1(p_0, L/2) = 0 \tag{6.52}$$

Thermalization

Unless one does not start with an auxiliary field configuration for which the Dirac operator is nearly singular, there are no troubles with thermalization. Independent of the starting configuration compatible mean values are obtained for all observables when the first configurations are ignored (in 2d one can afford to discard the first few hundred). For the Gross-Neveu model there are two particularly convenient starting points. One is to start

from a "quenched" configuration (i.e. generate Gaussian auxiliary fields). The other is to start from a constant auxiliary field that has the large-N expectation value of σ. Figure 6.9 shows how two different starts lead to the same result.

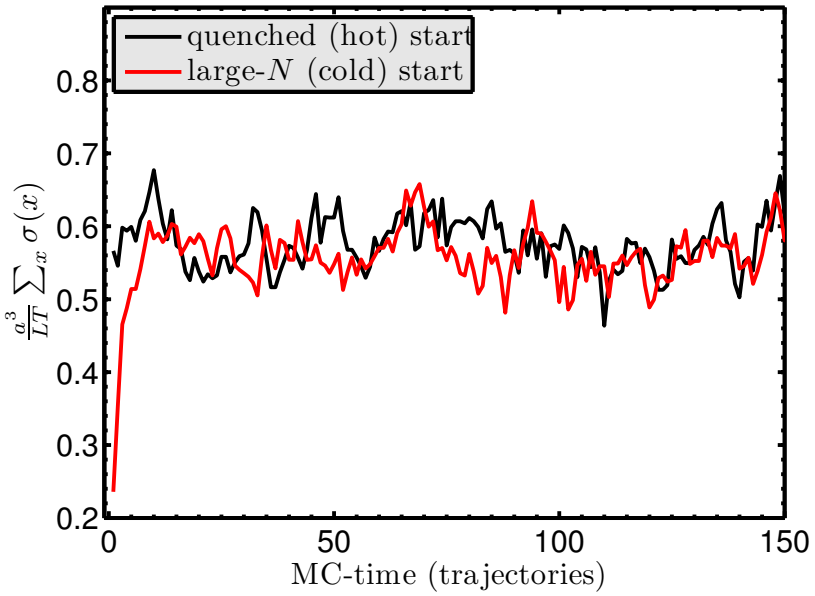

Figure 6.9: In the Thirring model the hot start is usually closer to the mean value, because the γ_5 symmetry is unbroken (in contrast to the situation at large-N).

Algorithmic troubles

Although the operator $DD^\top$ is positive definite it can happen that its lowest eigenvalue becomes extremely small, leading to a very bad conditioning number of $DD^\top$. This happens for instance in the Thirring model when the bare coupling is increased. When the leap-frog integrator runs into a region of configuration space where this happens, it fails to calculate the trajectory accurately and a high value of ΔH is obtained. In extreme cases the operator can become nearly singular, and the solver fails to converge at all. In these cases the reversibility of the integration scheme is violated and the corresponding runs are worthless. Figure 6.10 shows how with increasing g simulations become less and less feasible. Similar problems have been also observed in QCD simulations [41, 22]. The spikes become less severe when the integration step $\Delta\tau$ is reduced.

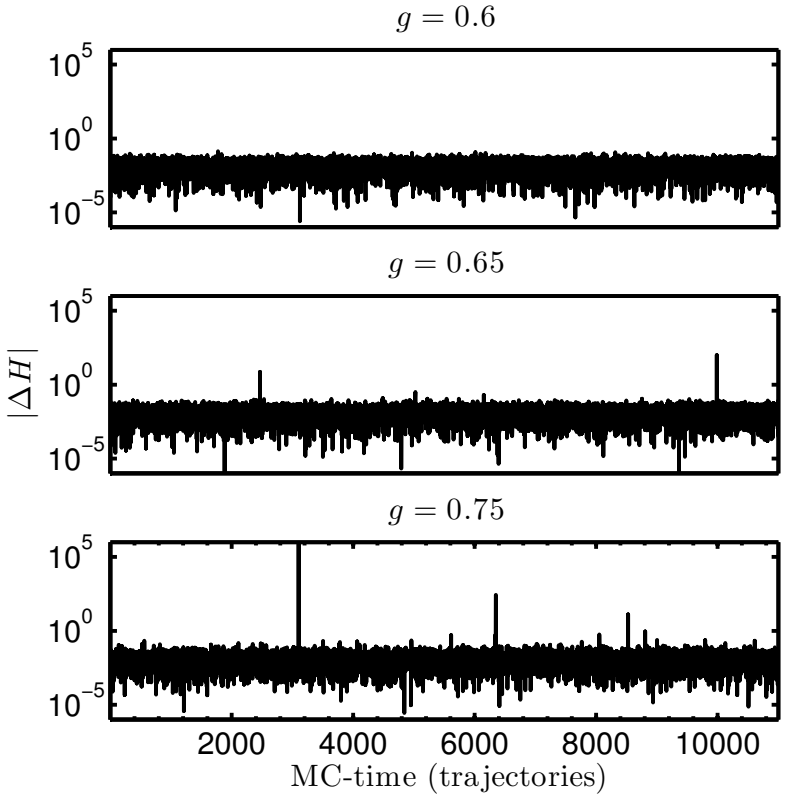

Figure 6.10: This figure shows how the energy difference between starting point and ending point of a trajectory develops spikes when the bare coupling is increased. It was generated in the Thirring model with Wilson fermions on a 8×8 lattice. The bare mass was set to the 1-loop perturbative value. The leap-frog integration step $\Delta\tau$ was kept constant.

In the Gross-Neveu models with $N > 1$ the HMC algorithm has got problems with ergodicity when the bare coupling is increased. In large-N the γ_5-symmetry is spontaneously broken even in finite volume. This cannot happen at finite N. Instead there are two preferred values around which k_S fluctuates. Due to tunnelings between these two positions the mean value should be 0. Unfortunately when the bare coupling is increased, the number of tunnelings per Monte-Carlo-time drops down. Eventually the algorithm is stuck in only one of the two minima throughout the whole run. The situation is visualized in figure 6.11 for the case of staggered fermions, where the γ_5-symmetry is realized already at finite lattice spacing. With Wilson fermions the situation is similar, but the consequences are more severe. The critical mass is defined by the vanishing of $k_S(T/4, 0)$. If the tunnelings happen rarely, the autocorrelation times of this observable are enormous and it cannot be estimated precisely enough. Although the

algorithm in principle stays ergodic, the enormous autocorrelation times of certain observables make meaningful simulations impossible.

Observables that are even under the γ_5-symmetry (like k_0 or the renormalized coupling) should not suffer under this lack of ergodicity. This should make staggered-simulations to some extent feasible in spite of the problem.

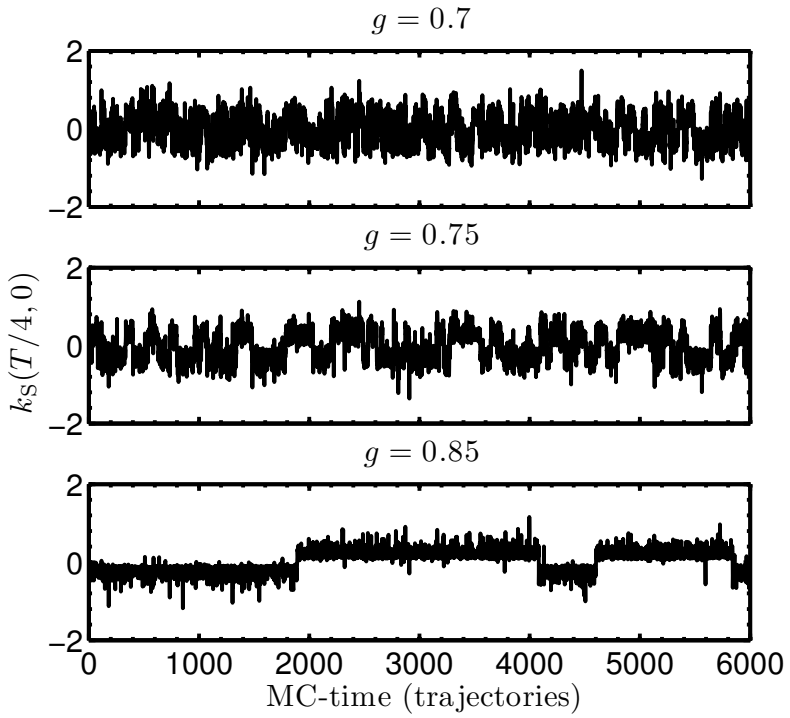

Figure 6.11: The figure shows how the HMC-algorithm looses ergodicity when the bare coupling is increased. These short runs were performed in the $N = 4$ Gross-Neveu model with staggered fermions. The plotted observable should average to zero for all values of g due to the γ_5 invariance that is preserved by the staggered discretization.

6.3 Simulations of the chiral Gross-Neveu model

To perform a continuum limit in the chiral Gross-Neveu model with Wilson fermions four parameters need to be tuned simultaneously. The couplings g_S and g_V control the lattice spacing and distinguish between different continuum limits of the chiral Gross-Neveu model, while the ratio g_S/g_P and the bare mass parameter m_0 are fixed by the enforcement of chiral symmetry. With staggered fermions the additive mass renormalization does not apply.

One of the negative results of this work has been that this tuning of four free parameters is not feasible in practice, at least not if one is interested in high precision results. The simulations that were performed in this model in the Schrödinger functional setup have only been used to test the code against bare perturbation theory [54, 53]. These few results are not presented in this thesis, instead the text continuous with the discussion of the $O(\mathcal{N})$ Gross-Neveu model which was found much more suitable for high precision calculations.

6.4 Simulations of the $N > 1$ Gross-Neveu model

With Wilson fermions Gross-Neveu models with an arbitrary value of N can be simulated. With staggered fermions only values of N are possible that are multiples of 4. Results are available for Wilson fermions.

At $N = 4$ the following bare quantities were measured

$$
\begin{aligned}
&k_S(T/4,0),\quad k_S(3T/4,0),\quad k_S(T/4,2\pi/L),\quad k_S(3T/4,2\pi/L),\\
&\bar{k}_S(\pi/T,L/4),\quad \bar{k}_S(\pi/T,3L/4),\\
&k_0(T/4,0),\quad k_0(T/2,0),\quad k_0(3T/4,0),\\
&k_0(T/4,2\pi/L),\quad k_0(T/2,2\pi/L),\quad k_0(3T/4,2\pi/L),\\
&\bar{k}_1(\pi/T,L/4),\quad \bar{k}_1(\pi/T,L/2),\quad \bar{k}_1(\pi/T,3L/4),\\
&Z_\psi^2 g_{\mathrm{R}}^2
\end{aligned}
$$

Symmetries, i.e. axis reversals and (anti)periodicity, imply that

$$
\begin{aligned}
k_S(T/4,p_1) &= -k_S(3T/4,p_1) && (6.53)\\
\bar{k}_S(p_0,L/4) &= \bar{k}_S(p_0,3L/4) && (6.54)\\
k_0(T/4,p_1) &= k_0(3T/4,p_1) && (6.55)\\
\bar{k}_1(p_0,L/4) &= -\bar{k}_1(p_0,3L/4)\,. && (6.56)
\end{aligned}
$$

These symmetries are not realized on each configuration individually but only in average. That the values are really compatible within the errors provides a further test of the simulation code. After this check, the data can be combined in order to increase statistics. The following renormalized

quantities were constructed

$$(k_S)_R(T/4,p_1) = \frac{k_S(T/4,p_1)-k_S(3T/4,p_1)}{2k_0(T/2,0)} \quad (6.57)$$

$$(\bar{k}_S)_R(\pi/T,L/4) = \frac{\bar{k}_S(\pi/T,L/4)+\bar{k}_S(\pi/T,3L/4)}{2k_0(T/2,0)} \quad (6.58)$$

$$(\bar{k}_S)_R(\pi/T,L/2) = \frac{\bar{k}_S(\pi/T,L/2)}{k_0(T/2,0)} \quad (6.59)$$

$$(k_0)_R(T/4,p_1) = \frac{k_0(T/4,p_1)+k_0(3T/4,p_1)}{2k_0(T/2,0)} \quad (6.60)$$

$$(\bar{k}_1)_R(\pi/T,L/4) = \frac{\bar{k}_1(\pi/T,L/4)-\bar{k}_1(\pi/T,3L/4)}{2k_0(T/2,0)} \quad (6.61)$$

$$g_R^2 \quad (6.62)$$

for $p_1 = 0$ and $p_1 = 2\pi/L$. Simulations were done at two different values of the renormalized coupling g_R as defined in 5.43. For each value simulations were carried out on a series of lattices with sizes $L \times T = 16 \times 16$, 24×24, 32×32, 40×40 and 48×48. For each lattice the bare mass m_0 has been tuned to its critical value, such that $k_S(T/4) = 0$ within statistical errors. A first guess is given by the perturbative value $m_0 = g_0^2 m_c^{(1)}$. An example for the tuning process is depicted in figure 6.12.

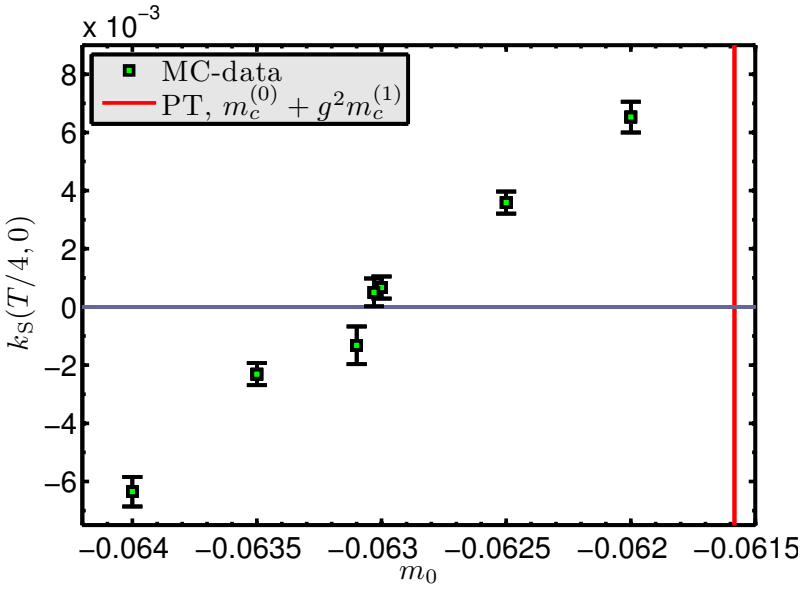

Figure 6.12: The tuning of the bare mass to its critical value. This example is associated with the Thirring-model on a 48×48 lattice.

To obtain the same value of g_R on every lattice (again up to statistical

errors), the bare coupling g needs to be adjusted properly. Again a first guess is given by perturbation theory. The β-function is known to 3-loops [55] and the first two coefficients are scheme independent[1]. To one loop the change in the bare coupling while going from a lattice of size L/a to a lattice of size L/a' is approximately given by

$$g'^2 = g^2 + \frac{L/a - L/a'}{L/a} \frac{N-2}{2\pi} g^4 . \tag{6.63}$$

In the appendices C.4.2 and C.4.1 all the runs required for the tuning are summarized in tabular form.

Once the values of m_0 and g are known for the series of lattices, the renormalized observables (6.57) on these lattices can be used to extrapolate to their continuum values. Several examples are shown in the figures 6.13 - 6.15.

The functional form of the extrapolations in asymptotically free theories is dictated by Symanzik's effective theory [78]. Since no order a improvement has been implemented, the expected leading cutoff effects with Wilson fermions are linear in a/L. However, all mass-dimension three operators with the symmetries of the Wilson action like $(\bar{\psi}\psi)^3$, $(\bar{\psi}\psi)(\bar{\psi}\partial\!\!\!/\psi)$ or $(\bar{\psi}\gamma_\mu\psi)(\bar{\psi}\gamma_\mu\psi)(\bar{\psi}\psi)$ are odd under the discrete γ_5 symmetry. Since this symmetry is realized up to lattice artifacts due to the normalization condition 5.28 these operators should not contribute to the linear cutoff effects in simulations at $m_0 = m_c$. Along the lines of argumentation presented in [28, 21] one can argue, that operators which are even under the γ_5 symmetry and for which one cannot find an order a term in the Symanzik expansion are automatically order a improved. The correlators k_μ and $\bar{k}_\mu$ as well as the current-current correlators $\check{f}_{\mu\nu}$ belong to this class, which explains the functional form of the extrapolations in the figures. Fits linear in a^2 have all acceptable χ^2-values. Quantities that are odd under the γ_5 symmetry vanish in the continuum limit with a rate proportional to a. For the extrapolations order a and also subleading cutoff-effects of order a^2 are considered.

A summary of the continuum results is given in table 6.3. As expected all continuum values of $(k_S)_R$ and $(\bar{k}_S)_R$ are compatible with zero, reflecting the fact, that the discrete chiral symmetry of the model is restored in the continuum limit.

[1] That is only the case if the renormalized couplings in the different schemes are connected perturbatively, i.e. $g_R = \sum_i c_i \tilde{g}_R^i$ and vice versa.

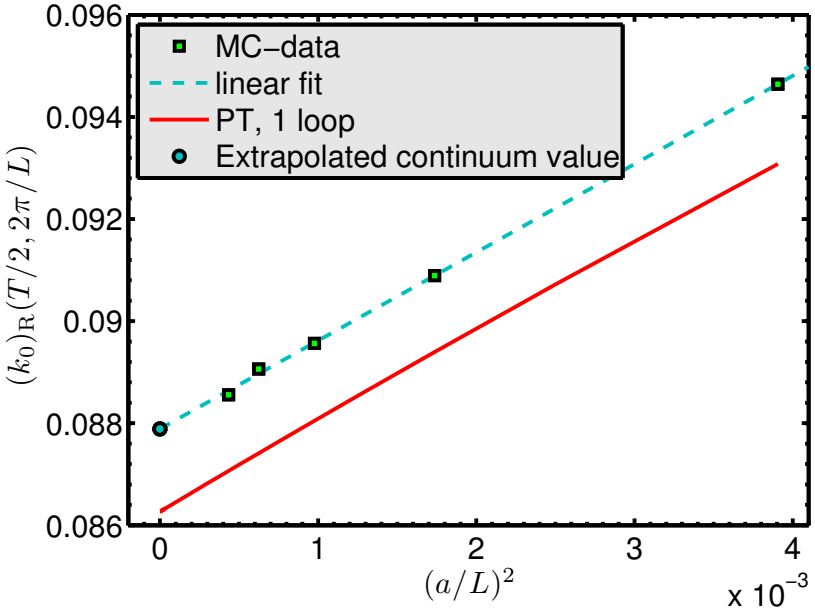

Figure 6.13: The quantity $(k_0)_R(T/2, 2\pi/L)$ at $g_R = 0.443$

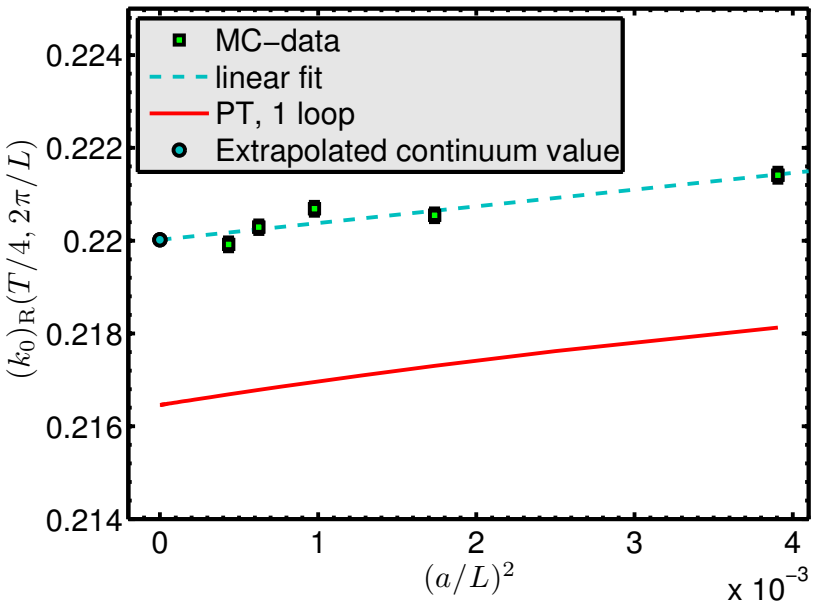

Figure 6.14: The quantity $(k_0)_R(T/4, 2\pi/L)$ at $g_R = 0.443$

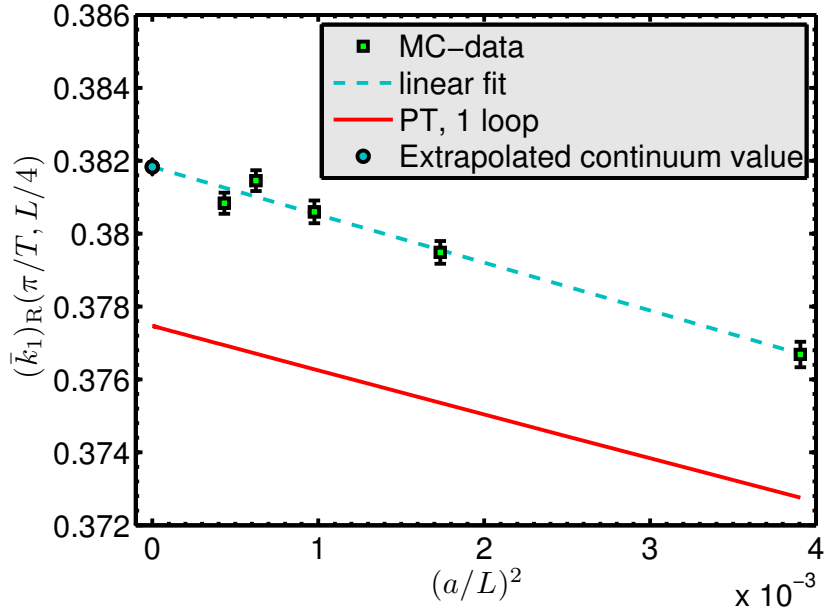

Figure 6.15: The quantity $(\bar{k}_1)_R(\pi/T, L/4)$ at $g_R = 0.443$

Doubling the number of lattice sites in each direction while the other parameters are kept fixed, allows it to measure the step-scaling function

$$\Sigma\left(g_R^2, L/a, 2\right) := g_R^2(2L, L/a)\,. \tag{6.64}$$

Its continuum limit is a universal quantity

$$\sigma\left(g_R^2, 2\right) := \lim_{a\to 0} \Sigma\left(g_R^2, L/a, 2\right)\,. \tag{6.65}$$

The extrapolation is shown in figure 6.16. Since the step-scaling function and the β function of a theory are related to each other, there also exists a relation between their expansion coefficients in perturbation theory [57]. If the expansions are

$$-\beta(g_R^2) = b_0 g_R^4 + b_1 g_R^6 + b_2 g_R^8 + \ldots \tag{6.66}$$

$$\sigma(g_R^2, s) = g_R^2 + \sigma_0(s) g_R^2 + \sigma_1(s) g_R^6 + \sigma_2(s) g_R^8 + \ldots\,, \tag{6.67}$$

then the coefficients σ_i can be obtained from the b_i. In [57] this relation has been worked out for the first three coefficients

$$\sigma_0 = b_0 \log s \tag{6.68}$$

$$\sigma_1 = b_0^2 (\log s)^2 + b_1 \log s \tag{6.69}$$

$$\sigma_2 = b_0^3 (\log s)^3 + \frac{5}{2} b_0 b_1 (\log s)^2 + b_2 \log s\,. \tag{6.70}$$

The first two coefficients of the β-function are scheme independent, hence the result from [55, 32]

$$b_0 = \frac{\mathcal{N}-2}{2\pi} \tag{6.71}$$

$$b_1 = -\frac{\mathcal{N}-2}{4\pi^2} \tag{6.72}$$

can be used to calculate the first two coefficients of the step-scaling function and compare them to the nonperturbative result, as is done in the figure.

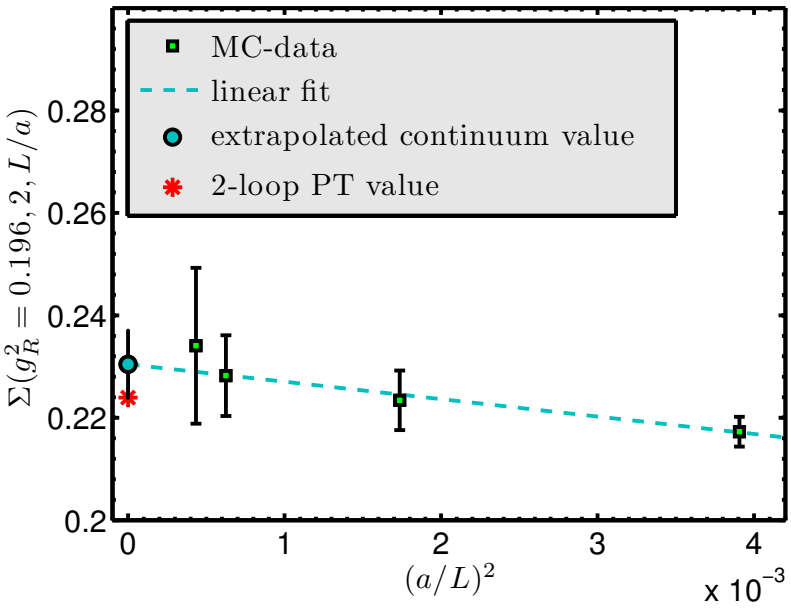

Figure 6.16: The continuum extrapolation of the step-scaling function at $g_R = 0.44$ and comparison with 2-loop perturbation theory.

6.5 Simulations of the massless Thirring model

Thirring model (i.e. the Gross-Neveu model with $N = 1$) the same quantities as in the Gross-Neveu model are measured and in addition the current-current correlators as defined in 2.52. The tuning of the bare parameters is simpler than in the previous case, because the β-function of the Thirring-model vanishes and hence the simulations on different lattices are performed at the same value of the bare coupling g. The two data-points presented below correspond to bare couplings $g = 0.4$ and 0.7 or renormalized couplings $g_R = 0.411$ and 0.779 (This is the finite renormalization that has been observed already in perturbation theory 5.3). The mass needs to

be tuned also in this model. There are two possibilities. The first is, to tune the bare mass parameter on every lattice separately. The second, to use the value of the finest lattice for all the lattices. The two methods differ only in their lattice artifacts (figure 6.17 shows a typical example). These artifacts are smaller with the first method, which however is much more demanding. Nevertheless the numbers quoted below in table 6.4 were all obtained with the first method.

Although the Thirring model is not asymptotically free, the same functional form of the lattice artifacts is assumed as in the $N > 1$ Gross-Neveu models. This is supported by perturbation theory. The χ^2-values of the fits are all acceptable.

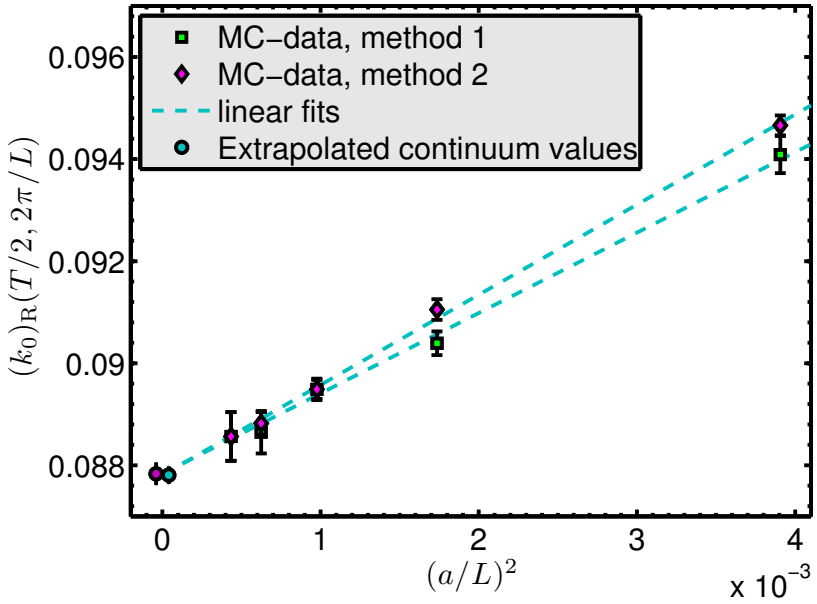

Figure 6.17: The figure shows continuum extrapolations for the quantity $(k_0)_R(T/2, 2\pi/L)$ with the two different methods of fixing m_c. The first method is to tune the bare mass to its critical value on each lattice separately. With the second method the value obtained on the finest lattice is used for all coarser lattices too.

In the Thirring model there exist detailed predictions for the current-current correlator. Using Noether-currents the quantities

$$\check{f}_{00}(T/2,0) = \left\langle \check{j}_0(0,0)\check{j}_0(T/2,0)\right\rangle \quad \textit{and} \quad \check{f}_{11}(T/2,0) = \left\langle \check{j}_1(0,0)\check{j}_1(T/2,0)\right\rangle$$

were measured (which is quite expensive if one avoids stochastic estimators) and compared to the predictions. The continuum extrapolations for

one of the points are shown in figures 6.18 and 6.19, while the comparison with the exact prediction is given in figure 6.20.

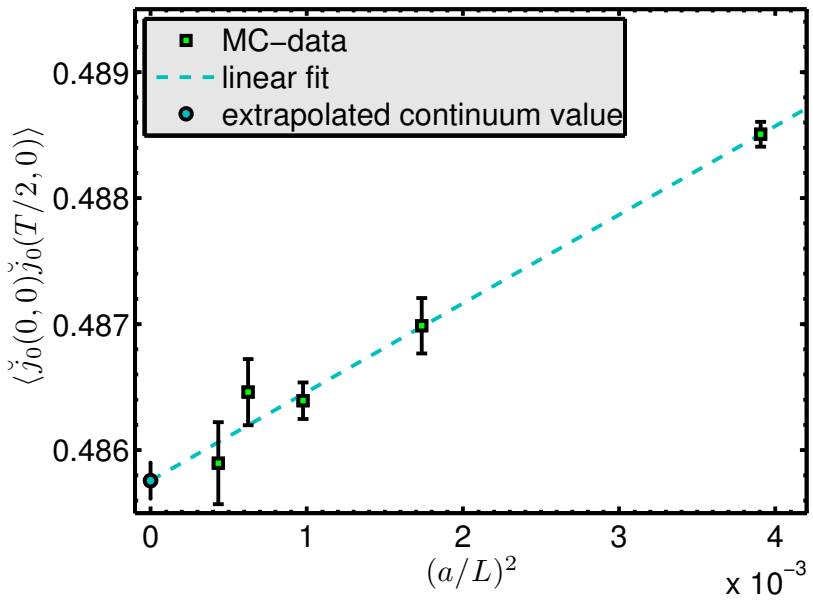

Figure 6.18: The continuum extrapolation of the correlator $\check{f}_{00}(T/2, 0)$.

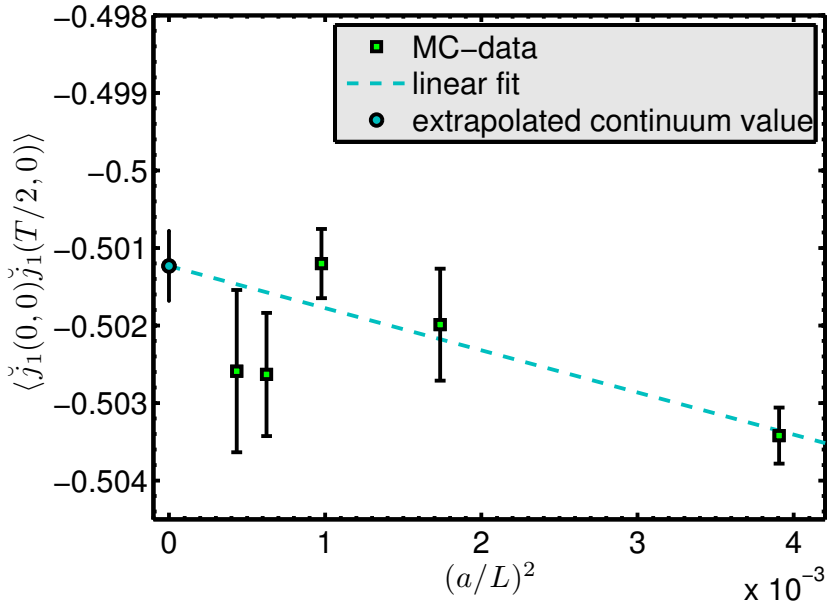

Figure 6.19: The continuum extrapolation of the correlator $\breve{f}_{11}(T/2,0)$.

6.6 Simulation results

In the following the main findings of the simulations with Wilson fermions are summarized. First the results of the tuning are presented and afterwards universal predictions for the $N = 4$ Gross-Neveu and the Thirring model are made.

6.6.1 Results of the tuning

The following tables show the nonperturbatively estimated values of the critical mass in the Thirring model and both the critical masses and the bare couplings for the $N = 4$ Gross-Neveu model. The complete list of simulations required to obtain these results can be found in the appendices C.4.2 and C.4.1.

g	L/a	m_c
0.4	16	-0.06295 ± 0.00008
0.4	24	-0.06298 ± 0.00011
0.4	32	-0.06301 ± 0.00018
0.4	40	-0.06301 ± 0.00093
0.4	48	-0.06303 ± 0.00047
0.7	16	-0.203 ± 0.011
0.7	24	-0.2031 ± 0.0022
0.7	32	-0.2033 ± 0.0016
0.7	40	-0.2041 ± 0.0046
0.7	48	-0.2043 ± 0.0076

Table 6.1: Critical masses in the Thirring model with Wilson fermions.

g_R	g	L/a	m_c
0.442	0.430 ± 0.002	16	-0.5085 ± 0.0027
	0.420 ± 0.002	24	-0.4846 ± 0.0056
	0.415 ± 0.002	32	-0.473 ± 0.015
	0.405 ± 0.002	40	-0.450 ± 0.029
	0.400 ± 0.002	48	-0.439 ± 0.066

Table 6.2: Critical masses and the tuning of the bare coupling in the $N = 4$ Gross-Neveu model with Wilson fermions.

The errors on m_c require some explanation. The tuning is such that $k_S(T/4, 0) = 0$ within its statistical error Δk_S. The quoted error Δm_c on m_c is determined by

$$k_S|_{m_0=m_c+\Delta m_c} \approx k_S|_{m_0=m_c} + \Delta m_c \left.\frac{\partial k_S}{\partial m_0}\right|_{m_0=m_c} \stackrel{!}{=} k_S|_{m_0=m_c} + \Delta k_S \tag{6.73}$$

hence

$$\Delta m_c = \Delta k_S \left(\left.\frac{\partial k_S}{\partial m_0}\right|_{m_0=m_c} \right)^{-1} . \tag{6.74}$$

For the derivative the tree level perturbative value is used. For the errors on g the tree level value of the derivative $\frac{\partial g_R}{\partial g} = 1$ was used.

6.6.2 Universal predictions

Continuum extrapolated universal quantities in the asymptotically free $N = 4$ Gross-Neveu model are presented in table 6.3, while table 6.4 shows the results for the massless Thirring (i.e. the $N = 1$ Gross-Neveu) model. The

step scaling function has been measured only in the first model, the current-current correlators only in the second one. The values obtained for these correlators are compared to the analytic continuum solution in figure 6.20.

The actual simulation results that enter the extrapolations and the corresponding plots can be found in the appendix C.5.

g_R	Observable	continuum value	
0.442	$(k_S)_R(T/4, 2\pi/L)$	0.0012	± 0.0011
	$(\bar{k}_S)_R(\pi/T, L/4)$	0.0058	± 0.0057
	$(\bar{k}_S)_R(\pi/T, L/2)$	0.0036	± 0.0043
	$(k_0)_R(T/4, 0)$	1.00421	± 0.00034
	$(k_0)_R(T/4, 2\pi/L)$	0.22002	± 0.00011
	$(k_0)_R(T/2, 2\pi/L)$	0.087889	± 0.000050
	$(\bar{k}_1)_R(\pi/T, L/4)$	0.38183	± 0.00021
	$\sigma(g_R^2, 2)$	0.2295	± 0.0071

Table 6.3: Universal predictions for the $N = 4$ Gross-Neveu model.

g	Observable	continuum value	
0.4	$(k_S)_R(T/4, 2\pi/L)$	0.00063	± 0.00020
	$(\bar{k}_S)_R(\pi/T, L/4)$	−0.00051	± 0.00094
	$(\bar{k}_S)_R(\pi/T, L/2)$	0.00008	± 0.00072
	$(k_0)_R(T/4, 0)$	1.000288	± 0.000097
	$(k_0)_R(T/4, 2\pi/L)$	0.216768	± 0.000026
	$(k_0)_R(T/2, 2\pi/L)$	0.086382	± 0.000027
	$(\bar{k}_1)_R(\pi/T, L/4)$	0.377783	± 0.000055
	$\check{f}_{00}(T/2, 0)$	0.48576	± 0.00014
	$\check{f}_{11}(T/2, 0)$	−0.45144	± 0.00045
0.7	$(k_S)_R(T/4, 2\pi/L)$	0.0031	± 0.0026
	$(\bar{k}_S)_R(\pi/T, L/4)$	0.012	± 0.013
	$(\bar{k}_S)_R(\pi/T, L/2)$	0.007	± 0.010
	$(k_0)_R(T/4, 0)$	1.0043	± 0.0013
	$(k_0)_R(T/4, 2\pi/L)$	0.21974	± 0.00041
	$(k_0)_R(T/2, 2\pi/L)$	0.08784	± 0.00022
	$(\bar{k}_1)_R(\pi/T, L/4)$	0.38180	± 0.00078
	$\check{f}_{00}(T/2, 0)$	0.43326	± 0.00096
	$\check{f}_{11}(T/2, 0)$	−0.4803	± 0.0030

Table 6.4: Universal predictions for the massless Thirring model.

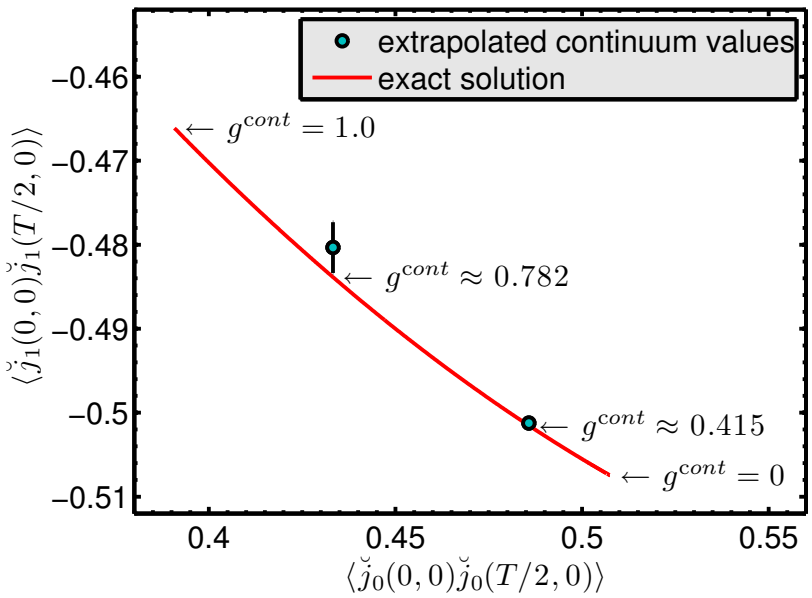

Figure 6.20: The plot shows the universal curve $\breve{f}_{00}(T/2,0)$ versus $\breve{f}_{11}(T/2,0)$. The values depend on the coupling g^{cont} of the continuum theory. The analytic solution is plotted between $g^{cont} = 0$ and $g^{cont} = 1$. The two datapoints obtained from Monte-Carlo simulations correspond to $g = 0.4$ and $g = 0.7$.

Chapter 7

Summary and discussion

In the first part of this work the Gross-Neveu models and different possibilities of their discretization were introduced. It has been shown in the limit of an infinite number of flavors that all the considered discretizations, i.e. with Wilson, with staggered and with overlap fermions, reproduce the same continuum result. The quantity that was compared in this study is a finite volume observable similar to the Lüscher-Weisz-Wolff-coupling. It is closely related to the dynamically acquired fermion mass.

The main part of the thesis was concerned with the perturbative and nonperturbative renormalization of the Gross-Neveu model with an arbitrary number of flavors. A finite volume position-space renormalization scheme was set up carefully and tested in lattice perturbation theory with Wilson fermions at one loop. It has been shown that the renormalized coupling in this scheme exhibits the well known universal divergence at one loop for all Gross-Neveu-models with $N > 1$. The $N = 1$ model, which is equivalent to the Thirring model, plays a special role. It has got a vanishing β-function and needs only a finite coupling renormalization.

On the non-perturbative side, simulation codes for the Monte-Carlo simulations of the Gross-Neveu and chiral Gross-Neveu models with staggered and with Wilson fermions were developed and tested. The Monte-Carlo method that was mainly employed was a Gross-Neveu version of the Hybrid-Monte-Carlo algorithm. It is well suited for simulations of these models in small and intermediate volumes, but becomes less effective - and in the end even useless, when the volumes get too large. The situation is similar to massless QCD in the Schrödinger functional setup, where simulations are feasible only when the temporal direction is "short" enough.

The model with a continous chiral symmetry seems to have more in common with massless QCD, but unfortunately has turned out to be unfavorable when it comes to high precision Monte Carlo simulations. The reason lies in its high number of free parameters in the action. With Wilson fermions a simultaneous adjustment of four parameters would be neces-

sary in order to take a controlled chiral continuum limit. Therefore the main attention in this thesis was put on the $O(2N)$ symmetric model, for which the nonperturbative renormalization procedure has been carried out for the Wilson case in the $N = 1$ (Thirring) and in the $N = 4$ Gross-Neveu model. It has been shown that the employed position space renormalization scheme is very well suited for high precision computations. For both values of N plenty of universal finite volume observables were calculated quite accurately. These can be compared with results obtained in different schemes in the future. In addition in the exactly solvable Thirring model recent analytical results for the current-current correlator in finite volume were confirmed by the Monte-Carlo simulations.

There are several interesting paths that one could pursuit in the future. All expansions (i.e. large N as well as perturbation theory) could be extended to the next orders. Especially interesting would be to investigate whether the different discretizations still lead to the same continuum results when the first $1/N$ correction is taken into account. Insights on the question how - if at all - the $O(2N)$ symmetry is restored in the continuum limit of the Gross-Neveu model with staggered fermions could be gained.

A different research direction concerns the applied algorithms. The widely used HMC algorithm has certain problems with the Gross-Neveu models when the bare coupling gets too large. Almost every improvement that one could get here would carry over to QCD simulations. A possible improvement that however is restricted to the Gross-Neveu model, would be to test different factorizations of the four fermion term. Auxiliary fields of the Ising-type could prove advantageous for the Thirring model. When no significant progress in algorithms can be made, there is still the possibility to switch to the *massive* Gross-Neveu models which should be much easier to simulate. Controlled extrapolations to zero mass would require major efforts on both the simulation and the theory side.

The maybe most interesting and most straightforward task would be to try to reproduce the obtained results with different fermion actions. With ordinary staggered fermions one should be able to reproduce the $N = 4$ numbers, while the $N = 1$ model would require a rooting-procedure. With the available tools this investigation seems to be within reach.

Bibliography

[1] S. Aoki. New phase structure for lattice QCD with Wilson fermions. *Phys. Rev.*, D30:2653, 1984.

[2] S. Aoki. Unquenched QCD simulation results. *Nucl. Phys. Proc. Suppl.*, 94:3–18, 2001.

[3] S. Aoki and K. Higashijima. The recovery of the chiral symmetry in lattice Gross-Neveu model. *Prog. Theor. Phys.*, 76:521, 1986.

[4] R. Barrett, M. Berry, T. F. Chan, J. Demmel, J. Donato, J. Dongarra, V. Eijkhout, R. Pozo, C. Romine, and H. V. der Vorst. *Templates for the Solution of Linear Systems: Building Blocks for Iterative Methods, 2nd Edition*. SIAM, Philadelphia, PA, 1994.

[5] M. Beccaria, G. Curci, and L. Galli. The Kramers equation simulation algorithm. 2. an application to the Gross-Neveu model. *Phys. Rev.*, D49: 2590–2596, 1994.

[6] L. Belanger, R. Lacaze, M. A., N. Attig, B. Petersson, and M. Wolff. Simulating the Gross-Neveu model with the Langevin algorithm: A comparison of analytical and numerical results. *Nucl. Phys.*, B340: 245–279, 1990.

[7] B. Berg and P. Weisz. Exact S matrix of the chiral invariant SU(N) Thirring model. *Nucl. Phys.*, B146:205, 1978.

[8] K. Binder and D. Heermann. *Monte Carlo Simulation in Statistical Physics. An Introduction*. Springer, 2002.

[9] J.-P. Blaizot, R. Mendez-Galain, and N. Wschebor. The Gross-Neveu model at finite temperature at next to leading order in the 1/N expansion. ((T)). *Ann. Phys.*, 307:209–271, 2003.

[10] M. Bochicchio, L. Maiani, G. Martinelli, G. C. Rossi, and M. Testa. Chiral symmetry on the lattice with Wilson fermions. *Nucl. Phys.*, B262:331, 1985.

[11] A. Bode, P. Weisz, and U. Wolff. Two loop computation of the Schrödinger functional in lattice QCD. *Nucl. Phys.*, B576:517–539, 2000.

[12] B. Bunk, M. Della Morte, K. Jansen, and F. Knechtli. The locality problem for two tastes of staggered fermions. *Nucl. Phys. Proc. Suppl.*, 140:782–784, 2005.

[13] D. K. Campbell and A. R. Bishop. Soliton excitations in polyacetylene and relativistic field theory models. *Nucl. Phys.*, B200:297, 1982.

[14] M. Campostrini, G. Curci, and P. Rossi. The Gross-Neveu model and the pseudofermion algorithm. *Nucl. Phys.*, B314:467–518, 1989.

[15] Y. Cohen, S. Elitzur, and E. Rabinovici. A Monte Carlo study of the Gross-Neveu model. *Nucl. Phys.*, B220:102–118, 1983.

[16] S. R. Coleman. Quantum sine-Gordon equation as the massive Thirring model. *Phys. Rev.*, D11:2088, 1975.

[17] M. Creutz. *QUARKS, GLUONS AND LATTICES*. Cambridge, Uk: Univ. Pr., 1983.

[18] R. F. Dashen and Y. Frishman. Thirring model with U(N) symmetry - scale invariant only for fixed values of a coupling constant. *Phys. Lett.*, B46:439–442, 1973.

[19] R. F. Dashen, B. Hasslacher, and A. Neveu. Semiclassical bound states in an asymptotically free theory. *Phys. Rev.*, D12:2443, 1975.

[20] C. T. H. Davies, G. P. Lepage, F. Niedermayer, and D. Toussaint. The quenched continuum limit. *Nucl. Phys. Proc. Suppl.*, 140:261–263, 2005.

[21] M. Della Morte and M. Luz. Cutoff effects of Wilson fermions in the absence of spontaneous chiral symmetry breaking. *Phys. Lett.*, B632: 663–666, 2006.

[22] M. Della Morte, R. Hoffmann, F. Knechtli, and U. Wolff. Impact of large cutoff-effects on algorithms for improved Wilson fermions. *Comput. Phys. Commun.*, 165:49–58, 2005.

[23] S. Duane, A. D. Kennedy, B. J. Pendleton, and D. Roweth. Hybrid Monte Carlo. *Phys. Lett.*, B195:216–222, 1987.

[24] J. Feinberg. All about the static fermion bags in the Gross-Neveu model. *Annals Phys.*, 309:166–231, 2004.

[25] P. Forgacs, F. Niedermayer, and P. Weisz. The exact mass gap of the Gross-Neveu model. 1. The thermodynamic Bethe ansatz. *Nucl. Phys.*, B367:123–143, 1991.

[26] P. Forgacs, F. Niedermayer, and P. Weisz. The exact mass gap of the Gross-Neveu model. 2. The 1/N expansion. *Nucl. Phys.*, B367:144–157, 1991.

[27] P. Forgacs, S. Naik, and F. Niedermayer. The exact mass gap of the chiral Gross-Neveu model. *Phys. Lett.*, B283:282–286, 1992.

[28] R. Frezzotti and G. C. Rossi. Chirally improving Wilson fermions. i: O(a) improvement. *JHEP*, 08:007, 2004.

[29] F. Fucito, E. Marinari, G. Parisi, and C. Rebbi. A proposal for Monte Carlo simulations of fermionic systems. *Nucl. Phys.*, B180:369, 1981.

[30] K. Fujikawa. On the evaluation of chiral anomaly in gauge theories with gamma(5) couplings. *Phys. Rev.*, D29:285, 1984.

[31] P. H. Ginsparg and K. G. Wilson. A remnant of chiral symmetry on the lattice. *Phys. Rev.*, D25:2649, 1982.

[32] J. A. Gracey. Three loop calculations in the O(N) Gross-Neveu model. *Nucl. Phys.*, B341:403–418, 1990.

[33] D. J. Gross and A. Neveu. Dynamical symmetry breaking in asymptotically free field theories. *Phys. Rev.*, D10:3235, 1974.

[34] Y. K. Ha. Boson formulation of fermion field theories. *Phys. Rev.*, D29: 1744–1756, 1984.

[35] S. Hands, A. Kocic, and J. B. Kogut. The four Fermi model in three-dimensions at nonzero density and temperature. *Nucl. Phys.*, B390: 355–378, 1993.

[36] S. J. Hands, J. B. Kogut, and C. G. Strouthos. The (2+1)-dimensional Gross-Neveu model with a U(1) chiral symmetry at non-zero temperature. *Phys. Lett.*, B515:407–413, 2001.

[37] P. Hasenfratz, S. Hauswirth, K. Holland, T. Jorg, F. Niedermayer, and U. Wenger. The construction of generalized Dirac operators on the lattice. *Int. J. Mod. Phys.*, C12:691–708, 2001.

[38] M. R. Hestenes and E. Stiefel. Methods of conjugate gradients for solving linear systems. *J. Research Nat. Bur. Standards*, 49:409–436, 1952.

[39] A. Irving, C. McNeile, and C. Michael, editors. *XXIIIrd International Symposium on Lattice Field Theory*, 2005. PoS.

[40] T. Jolicoeur, A. Morel, and B. Petersson. Continuum symmetries of lattice models with staggered fermions. *Nucl. Phys.*, B274:225, 1986.

[41] B. Joo et al. Instability in the molecular dynamics step of hybrid Monte Carlo in dynamical fermion lattice QCD simulations. *Phys. Rev.*, D62: 114501, 2000.

[42] D. B. Kaplan. A method for simulating chiral fermions on the lattice. *Phys. Lett.*, B288:342–347, 1992.

[43] M. Karowski and H. J. Thun. Complete S matrix of the O(2N) Gross-Neveu model. *Nucl. Phys.*, B190:61, 1981.

[44] H. Kluberg-Stern, A. Morel, O. Napoly, and B. Petersson. Flavors of lagrangian susskind fermions. *Nucl. Phys.*, B220:447, 1983.

[45] F. Knechtli and U. Wolff. Dynamical fermions as a global correction. *Nucl. Phys.*, B663:3–32, 2003.

[46] F. Knechtli, T. Korzec, B. Leder, and U. Wolff. Universality in the Gross-Neveu model. *Nucl. Phys. Proc. Suppl.*, 140:785–787, 2005.

[47] R. Koberle, V. Kurak, and J. A. Swieca. Scattering theory and 1/N expansion in the chiral Gross- Neveu model. *Phys. Rev.*, D20:897, 1979.

[48] J. B. Kogut. An introduction to lattice gauge theory and spin systems. *Rev. Mod. Phys.*, 51:659, 1979.

[49] T. Korzec and U. Wolff. Gross-Neveu model as a laboratory for fermion discretization. *PoS*, LAT2006:218, 2006.

[50] T. Korzec, F. Knechtli, U. Wolff, and B. Leder. Monte-Carlo simulation of the chiral Gross-Neveu model. *PoS*, LAT2005:267, 2006.

[51] J. M. Kosterlitz and D. J. Thouless. Ordering, metastability and phase transitions in two- dimensional systems. *J. Phys.*, C6:1181–1203, 1973.

[52] D. P. Landau. *A Guide to Monte Carlo Simulations in Statistical Physics*. Cambridge University Press, 2000.

[53] B. Leder. PhD thesis, in preparation. 2006.

[54] B. Leder and T. Korzec. Perturbative renormalisation of the chiral Gross-Neveu model. *PoS*, LAT2005:266, 2006.

[55] C. Luperini and P. Rossi. Three loop beta function(s) and effective potential in the Gross-Neveu model. *Ann. Phys.*, 212:371–401, 1991.

[56] M. Lüscher. Exact chiral symmetry on the lattice and the Ginsparg-Wilson relation. *Phys. Lett.*, B428:342–345, 1998.

[57] M. Lüscher, P. Weisz, and U. Wolff. A numerical method to compute the running coupling in asymptotically free theories. *Nucl. Phys.*, B359: 221–243, 1991.

[58] M. Lüscher, R. Narayanan, P. Weisz, and U. Wolff. The schrödinger functional: A renormalizable probe for nonabelian gauge theories. *Nucl. Phys.*, B384:168–228, 1992.

[59] M. Lüscher, R. Sommer, U. Wolff, and P. Weisz. Computation of the running coupling in the SU(2) yang-mills theory. *Nucl. Phys.*, B389: 247–264, 1993.

[60] I. Montvay and G. Münster. *Quantum fields on a lattice*. Cambridge, UK: Univ. Pr., 1994.

[61] E. Moreno and F. A. Schaposnik. On the issues of symmetries in the Gross-Neveu model. *Int. J. Mod. Phys.*, A4:2827–2835, 1989.

[62] K.-i. Nagai and K. Jansen. Two-dimensional lattice Gross-Neveu model with Wilson twisted mass fermions. *Phys. Lett.*, B633:325–330, 2006.

[63] H. Neuberger. Exactly massless quarks on the lattice. *Phys. Lett.*, B417: 141–144, 1998.

[64] M. Newman and G. Barkema. *Monte Carlo Methods in Statistical Physics*. Clarendon Press, 1999.

[65] H. B. Nielsen and M. Ninomiya. Absence of neutrinos on a lattice. 1. proof by homotopy theory. *Nucl. Phys.*, B185:20, 1981.

[66] J. Polonyi and H. W. Wyld. Microcanonical simulation of fermionic systems. *Phys. Rev. Lett.*, 51:2257, 1983.

[67] H. J. Rothe. Lattice gauge theories: An introduction. *World Sci. Lect. Notes Phys.*, 74:1–605, 2005.

[68] O. Schnetz, M. Thies, and K. Urlichs. Full phase diagram of the massive Gross-Neveu model. *ANNALS PHYS.*, 321:2604, 2006. URL `http://www.citebase.org/abstract?id=oai:arXiv.org:hep-th/0511206`.

[69] J. S. Schwinger. Gauge invariance and mass. ii. *Phys. Rev.*, 128:2425–2429, 1962.

[70] H. S. Sharatchandra, H. J. Thun, and P. Weisz. Susskind fermions on a Euclidean lattice. *Nucl. Phys.*, B192:205, 1981.

[71] S. R. Sharpe. Rooted staggered fermions: good, bad, or ugly? *PoS*, LAT2006, 2006.

[72] B. Sheikholeslami and R. Wohlert. Improved continuum limit lattice action for QCD with Wilson fermions. *Nucl. Phys.*, B259:572, 1985.

[73] J. Shewchuk. An introduction to the conjugate gradient method without the agonizing pain. 1994.

[74] S. Sint. On the schrödinger functional in QCD. *Nucl. Phys.*, B421: 135–158, 1994.

[75] J. Smit. Introduction to quantum fields on a lattice: A robust mate. *Cambridge Lect. Notes Phys.*, 15:1–271, 2002.

[76] e. . Stone, M. *Bosonization*. Singapore: World Scientific, 1994.

[77] L. Susskind. Lattice fermions. *Phys. Rev.*, D16:3031–3039, 1977.

[78] K. Symanzik. Continuum limit and improved action in lattice theories. 1. principles and phi**4 theory. *Nucl. Phys.*, B226:187, 1983.

[79] M. Thies. From relativistic quantum fields to condensed matter and back again: Updating the Gross-Neveu phase diagram. *J.PHYS.A*, 39:12707, 2006. URL `http://www.citebase.org/abstract?id=oai:arXiv.org:hep-th/0601049`.

[80] W. E. Thirring. A soluble relativistic field theory. *Annals Phys.*, 3: 91–112, 1958.

[81] W. Wetzel. Two loop beta function for the Gross-Neveu model. *Phys. Lett.*, B153:297, 1985.

[82] K. G. Wilson. *QUARKS AND STRINGS ON A LATTICE*. Plenum Press, New York, 1977. New Phenomena In Subnuclear Physics. Part A. Proceedings of the First Half of the 1975 International School of Subnuclear Physics, Erice, Sicily, July 11 - August 1, 1975, ed. A. Zichichi, p. 69, CLNS-321.

[83] E. Witten. Some properties of the (psi-bar psi)**2 model in two- dimensions. *Nucl. Phys.*, B142:285, 1978.

[84] U. Wolff. Discrete GN model on the lattice. *Internal Notes*, 2006.

[85] U. Wolff. The phase diagram of the infinite N Gross-Neveu model at finite temperature and chemical potential. *Phys. Lett.*, B157:303–308, 1985.

[86] U. Wolff. Monte Carlo errors with less errors. *Comput. Phys. Commun.*, 156:143–153, 2004.

[87] A. B. Zamolodchikov and A. B. Zamolodchikov. Relativistic factorized S matrix in two-dimensions having O(N) isotopic symmetry. *Nucl. Phys.*, B133:525, 1978.

[88] J. Zinn-Justin. Quantum field theory and critical phenomena. *Int. Ser. Monogr. Phys.*, 113:1–1054, 2002.

Appendix A

Conventions

A.1 Lattice Notation

In the following the lattice notation used throughout the thesis is introduced.

On a d-dimensional lattice with lattice spacing a a vector of length a that is parallel to the axis μ is denoted by $\hat{\mu}$. The lowest order approximations to the partial derivative ∂_μ are given by either the forward derivative[1]

$$\partial_\mu f(x) \coloneqq \frac{f(x+\hat{\mu}) - f(x)}{a}\,, \tag{A.1}$$

or the backward derivative

$$\partial^*_\mu f(x) \coloneqq \frac{f(x) - f(x-\hat{\mu})}{a}\,. \tag{A.2}$$

With these one can define the symmetric lattice derivative and the second lattice derivative

$$\tilde{\partial}_\mu f(x) \coloneqq \frac{\partial_\mu + \partial^*_\mu}{2} f(x) \tag{A.3}$$

$$\Delta_\mu f(x) \coloneqq \partial^*_\mu \partial_\mu f(x) = \frac{[\partial_\mu - \partial^*_\mu]}{a} f(x)\,. \tag{A.4}$$

Einstein's summation convention does not apply in the last line. There is no exact Leibniz rule on the lattice, but one can derive the related expressions

$$\partial_\mu[f(x)g(x)] = [\partial_\mu f(x)]g(x) + f(x)[\partial_\mu g(x)] + a[\partial_\mu f(x)][\partial_\mu g(x)] \tag{A.5}$$

$$\partial^*_\mu[f(x)g(x)] = [\partial^*_\mu f(x)]g(x) + f(x)[\partial^*_\mu g(x)] - a[\partial^*_\mu f(x)][\partial^*_\mu g(x)] \tag{A.6}$$

$$\begin{aligned}\tilde{\partial}_\mu[f(x)g(x)] &= [\tilde{\partial}_\mu f(x)]g(x) + f(x)[\tilde{\partial}_\mu g(x)] \\ &\quad + a[\tilde{\partial}_\mu f(x)][\partial_\mu g(x)] - a[\partial^*_\mu f(x)][\tilde{\partial}_\mu g(x)]\,.\end{aligned} \tag{A.7}$$

[1] It is common to use the same symbol as in the continuum to keep the notation simple.

And similarly

$$\begin{aligned}\Delta_\mu[f(x)g(x)] &= [\Delta_\mu f(x)]g(x) + f(x)[\Delta_\mu g(x)] \\ &\quad +[\partial_\mu f(x)][\partial^*_\mu g(x)] + [\partial^*_\mu f(x)][\partial_\mu g(x)] \\ &\quad +a^2[\Delta_\mu f(x)][\Delta_\mu g(x)]\,. \end{aligned} \tag{A.8}$$

The following shortcuts are frequently used

$$\mathring{p}_\mu := \frac{1}{a}\sin(ap_\mu) \tag{A.9}$$

$$\hat{p} := \frac{2}{a}\sin\left(\frac{a}{2}p_\mu\right). \tag{A.10}$$

These are essentially the lattice difference operators in momentum space (see appendix A.6 for the conventions concerning Fourier transformation). More precisely

$$\tilde{\partial}_\mu e^{-ipx} = -i\mathring{p}_\mu e^{-ipx} \tag{A.11}$$

$$\partial^*_\mu\partial_\mu e^{-ipx} = \hat{p}^2 e^{-ipx} \tag{A.12}$$

A.2 Traces

In this work many matrices in different spaces occur. When a trace of a matrix is taken, it is not always clear in which space this is meant. These are the notational conventions:

$$\mathrm{T}r\,M = \sum_{\alpha,i,x} M_{\alpha i,\alpha i}(x,x) \qquad \textit{spacetime, Dirac, flavor} \tag{A.13}$$

$$\mathrm{t}r\,M = \sum_{\alpha} M_{\alpha,\alpha} \qquad \textit{spin} \tag{A.14}$$

$$\mathrm{t}r^f\,M = \sum_{i} M_{i,i} \qquad \textit{flavor} \tag{A.15}$$

$$\mathrm{t}r^{s,f}\,M = \sum_{\alpha,i} M_{\alpha i,\alpha i} \qquad \textit{spin, flavor} \tag{A.16}$$

A.3 Pauli matrices

The Pauli matrices are a set of 2×2 complex hermitian and unitary matrices

$$\begin{aligned}\sigma^{(1)} &= \begin{pmatrix} 0 & 1 \\ 1 & 0 \end{pmatrix} \\ \sigma^{(2)} &= \begin{pmatrix} 0 & -i \\ i & 0 \end{pmatrix} \\ \sigma^{(3)} &= \begin{pmatrix} 1 & 0 \\ 0 & -1 \end{pmatrix}. \end{aligned} \tag{A.17}$$

A.4 Clifford algebra

There is some freedom in the choice of the γ-matrices. Throughout the whole work a "Majorana" representation is incorporated, in which the matrices γ_μ are real, symmetric and orthogonal:

$$\gamma_0 = \sigma^{(3)} = \begin{pmatrix} 1 & 0 \\ 0 & -1 \end{pmatrix}$$
$$\gamma_1 = \sigma^{(1)} = \begin{pmatrix} 0 & 1 \\ 1 & 0 \end{pmatrix}. \tag{A.18}$$

They fulfill the Clifford algebra

$$\{\gamma_\mu, \gamma_\nu\} = 2\delta_{\mu\nu}\,. \tag{A.19}$$

The matrix γ_5 is given by

$$\gamma_5 = i\gamma_0\gamma_1 = -\sigma^{(2)} = \begin{pmatrix} 0 & i \\ -i & 0 \end{pmatrix}. \tag{A.20}$$

It is purely imaginary, hermitian, unitary and anticommutes with γ_0 and γ_1.

A.5 The $SU(N)$

The special unitary group plays an important role in the models studied in this thesis. This appendix fixes the conventions.

The generators of the Lie algebra $su(N)$

$$\lambda^{(k)}, \qquad k = 1 \ldots N^2 - 1 \tag{A.21}$$

are chosen to be hermitian and traceless $N \times N$ matrices normalized such that

$$\mathrm{tr}^f\left[\lambda^{(k)}\lambda^{(l)}\right] = 2\delta_{k,l}. \tag{A.22}$$

They satisfy the Lie-algebra

$$\left[\lambda^{(a)}, \lambda^{(b)}\right] = i\, f^{(a,b,c)}\lambda^{(c)} \tag{A.23}$$

with $f^{(a,b,c)}$ being the antisymmetric and real structure-constants of $SU(N)$. An arbitrary element of $SU(N)$ can be represented by

$$U = \exp\left(\sum_{k=1}^{N^2-1} i\,\lambda^{(k)}\omega^{(k)}\right), \qquad \omega^{(k)} \in \mathbb{R}\,. \tag{A.24}$$

Together with the matrix

$$\lambda^{(0)} = \sqrt{\frac{2}{N}}\mathbb{1} \tag{A.25}$$

the generators form an complete (orthogonal) basis in the space of $N \times N$ matrices, i.e each such matrix X can be written as

$$X = \sum_{k=0}^{N^2-1} X_k \lambda^{(k)} \tag{A.26}$$

with

$$X_k = \frac{1}{2} tr^f \left[X \lambda^k \right] . \tag{A.27}$$

An useful example is given by

$$\begin{aligned} X_{ij}^{kl} &= 2\delta_{il}\delta_{jk} \\ &= \sum_{k=0}^{N^2-1} \lambda_{ij}^{(k)} \lambda_{kl}^{(k)} \\ &= \sum_{k=1}^{N^2-1} \lambda_{ij}^{(k)} \lambda_{kl}^{(k)} + \frac{2}{N}\delta_{ij}\delta_{kl} . \end{aligned} \tag{A.28}$$

It makes it possible to write

$$\sum_{i,j} \bar{\psi}_i \psi_j \bar{\psi}_j \psi_i = \bar{\psi}\lambda^{(k)}\psi\bar{\psi}\lambda^{(k)}\psi + \frac{1}{n}\bar{\psi}\psi\bar{\psi}\psi . \tag{A.29}$$

A.6 Fourier transformations

In the definition of Fourier transformations there is always some freedom concerning the normalization. In this work the following conventions are exercised:

Continuum

Square integrable functions $f : \mathbb{R} \to \mathbb{R}$ have a Fourier transformed

$$\tilde{f}(p) = \int_{-\infty}^{+\infty} dx\, e^{-ipx} f(x) . \tag{A.30}$$

The inverse transformation is given by

$$f(x) = \int_{-\infty}^{\infty} \frac{dp}{2\pi}\, e^{ipx} \tilde{f}(p) . \tag{A.31}$$

Finite volume

If the function is defined only in a finite volume $f : [0, L] \to \mathbb{R}$, the boundary conditions need to be specified. With generalized periodic boundaries $f(x + L) = e^{i\theta} f(x)$ the Fourier transform and its inverse are given by

$$\tilde{f}(p) = \int_0^L dx\, e^{-ipx} f(x) \tag{A.32}$$

$$f(x) = \frac{1}{L} \sum_p e^{ipx} \tilde{f}(p)\,, \tag{A.33}$$

where the momentum summation ranges over the momenta $p = \frac{2\pi n+\theta}{L}, n \in \mathbb{N}$.

Infinite lattice

If the function is defined only on the points $x = na,\ n \in \mathbb{N}$ with some lattice spacing a the transformations take the form

$$\tilde{f}(p) = a \sum_x e^{-ipx} f(x) \tag{A.34}$$

$$f(x) = \int_{-\pi/a}^{+\pi/a} \frac{dp}{2\pi}\, e^{ipx} \tilde{f}(p)\,. \tag{A.35}$$

Finite lattice

On a finite lattice $x = 0, a, \ldots L - a$ the form of the transformation again depends on the choice of the boundary conditions. With generalized periodic boundaries they are

$$\tilde{f}(p) = a \sum_x e^{-ipx} f(x) \tag{A.36}$$

$$f(x) = \frac{1}{L} \sum_p e^{ipx} \tilde{f}(p)\,, \tag{A.37}$$

with momenta summed over $p = \frac{2\pi n+\theta}{L}, n = 0 \ldots L/a - 1$.

Two dimensions

Fourier transformation can be easily generalized to two (or more) dimensions. In this thesis we call $\tilde{f}(p_0, p_1)$ the full two dimensional transformation, while the variants in which the transformation is performed only along one

of the directions are called $\check{f}(x_0, p_1)$ and $\hat{f}(p_0, x_1)$. When the spatial momentum is zero, sometimes the abbreviation $\check{f}(x_0) \equiv \check{f}(x_0, 0)$ is used.

Often the fields to apply the Fourier transform on will be fermion fields with mass-dimension 1/2, i.e. $[\psi] = [a^{-1/2}]$. The transformed fields then have

$$[\psi] = [a^{-1/2}] \tag{A.38}$$
$$\left[\tilde{\psi}\right] = [a^{3/2}] \tag{A.39}$$
$$\left[\check{\psi}\right] = \left[\hat{\psi}\right] = [a^{1/2}]\,. \tag{A.40}$$

Correspondingly bilinears like the current $j_\mu = \bar{\psi}\gamma_\mu\psi$ or the propagator have

$$[j_\mu] = [a^{-1}] \tag{A.41}$$
$$\left[\tilde{j}_\mu\right] = [a] \tag{A.42}$$
$$\left[\check{j}_\mu\right] = \left[\hat{j}_\mu\right] = [1]\,. \tag{A.43}$$

The Fourier transformations are based on the identities

$$\delta^2(x) := \frac{1}{TL}\sum_p e^{ipx} = \frac{1}{a^2}\delta_{x_0,0}\delta_{x_1,0} \tag{A.44}$$
$$\delta^2(p) := a^2\sum_x e^{-ipx} = TL\delta_{p_0,0}\delta_{p_1,0}\,. \tag{A.45}$$

Appendix B

Additional Calculations

B.1 Noether currents with Wilson fermions

To derive the Noether current of the $U(N)_{\mathrm{V}}$ symmetry with Wilson fermions the following identities are useful

$$\partial^*_\mu f(x+\hat{\mu}) = \partial_\mu f(x) \tag{B.1}$$
$$\partial_\mu f(x-\hat{\mu}) = \partial^*_\mu f(x)\,. \tag{B.2}$$

Assuming an infinite lattice or periodic boundary conditions one also has

$$\sum_x f(x)\partial^*_\mu g(x) = \sum_x f(x+\hat{\mu})\partial_\mu g(x) \tag{B.3}$$
$$\sum_x f(x)\partial_\mu g(x) = \sum_x f(x-\hat{\mu})\partial^*_\mu g(x)\,. \tag{B.4}$$

In infinitesimal form the $U(N)_{\mathrm{V}}$ transformations read

$$\psi \rightarrow \psi + i\epsilon\lambda^{(a)}\psi \tag{B.5}$$
$$\bar{\psi} \rightarrow \bar{\psi} - i\epsilon\bar{\psi}\lambda^{(a)} \tag{B.6}$$

With $\lambda^{(a)}$ being the traceless, hermitian generators of the $SU(N)$ group or the unit matrix. The action is not invariant under *local* transformations ($\epsilon \rightarrow \epsilon(x)$), the change is

$$\begin{aligned}\delta S^{(a)} &= i\sum_x \left(\bar{\psi}(x)\lambda^{(a)} D_W[\epsilon(x)\psi(x)] - \epsilon(x)\bar{\psi}(x)\lambda^{(a)} D_W\psi(x)\right) \\ &= i\sum_x j^{(a)}_\mu(x)\partial_\mu\epsilon(x)\end{aligned} \tag{B.7}$$

with the Noether current

$$\begin{aligned} j_\mu^{(a)}(x) &:= \frac{1}{2}\bar{\psi}(x)\lambda^{(a)}\gamma_\mu[1+a\partial_\mu]\psi(x) \\ &+ \frac{r}{2}\bar{\psi}(x)\lambda^{(a)}[-1-a\partial_\mu^*-a^2\Delta_\mu]\psi(x) \\ &+ \frac{1}{2}\bar{\psi}(x+\hat{\mu})\lambda^{(a)}\gamma_\mu[1-a\partial_\mu^*]\psi(x+\hat{\mu}) \\ &+ \frac{r}{2}\bar{\psi}(x+\hat{\mu})\lambda^{(a)}[1-a\partial_\mu+a^2\Delta_\mu]\psi(x+\hat{\mu}) \end{aligned} \tag{B.8}$$

which simplifies nicely to

$$\begin{aligned} j_\mu^{(a)}(x) &= \frac{1}{2}\left(\bar{\psi}(x)\lambda^{(a)}\gamma_\mu\psi(x+\hat{\mu})+\bar{\psi}(x+\hat{\mu})\lambda^{(a)}\gamma_\mu\psi(x)\right) \\ &- \frac{r}{2}\left(\bar{\psi}(x)\lambda^{(a)}\psi(x+\hat{\mu})-\bar{\psi}(x+\hat{\mu})\lambda^{(a)}\psi(x)\right). \end{aligned} \tag{B.9}$$

The flavor singlet current ($\lambda^{(0)} \propto \mathbb{1}$) is simply denoted by j_μ. It is easy to see (assuming that $\bar{\psi}$ and ψ satisfy the lattice-Dirac-equation) that this current is indeed conserved

$$\partial_\mu^* j_\mu(x) = \bar{\psi}D_W\psi - \bar{\psi}\overleftarrow{D}_W\psi = 0\,. \tag{B.10}$$

B.2 Fierz transformations

The hermitian matrices $\mathbb{1}, \gamma_1, \gamma_2$ and γ_5 form a basis in the space of complex 2×2 matrices. One possible realization is:

$$\begin{aligned} \Omega^{(1)} &:= \mathbb{1} = \begin{pmatrix} 1 & 0 \\ 0 & 1 \end{pmatrix} \qquad \Omega^{(2)} := \gamma_1 = \begin{pmatrix} 1 & 0 \\ 0 & -1 \end{pmatrix} \\ \Omega^{(3)} &:= \gamma_2 = \begin{pmatrix} 0 & 1 \\ 1 & 0 \end{pmatrix} \qquad \Omega^{(4)} := \gamma_5 = \begin{pmatrix} 0 & i \\ -i & 0 \end{pmatrix} \end{aligned} \tag{B.11}$$

Any 2×2 matrix Γ can be written as

$$\Gamma = \frac{1}{2}\sum_A \Omega^{(A)}\, tr(\Omega^{(A)}\Gamma) \tag{B.12}$$

The basis matrices fulfill the following orthogonality relation

$$tr(\Omega^{(A)}\Omega^{(B)}) = 2\delta_{A,B} \tag{B.13}$$

Now for arbitrary matrices $\Lambda^{(1)}$ and $\Lambda^{(2)}$, matrices $\Gamma^{(jk)}$ can be defined in the following way

$$\Gamma_{il}^{(jk)} := \Lambda_{ij}^{(1)}\Lambda_{kl}^{(2)} \tag{B.14}$$

Expanding such a matrix according to (B.12) one gets

$$\begin{aligned}
\Gamma^{(jk)}_{il} &= \frac{1}{2}\sum_A \Omega^{(A)}_{il}\, tr(\Omega^{(A)}\Gamma^{(jk)}) \\
&= \frac{1}{2}\sum_A \Omega^{(A)}_{il} \sum_n \left[\Omega^{(A)}\Gamma^{(jk)}\right]_{nn} \\
&= \frac{1}{2}\sum_{A,n,m} \Omega^{(A)}_{il}\,\Omega^{(A)}_{nm}\Gamma^{(jk)}_{mn} \\
&= \frac{1}{2}\sum_{A,n,m} \Omega^{(A)}_{il}\,\Omega^{(A)}_{nm}\Lambda^{(1)}_{mj}\Lambda^{(2)}_{kn} \\
&= \frac{1}{2}\sum_A \Omega^{(A)}_{il}\left[\Lambda^{(2)}\Omega^{(A)}\Lambda^{(1)}\right]_{kj} \qquad \text{(B.15)}
\end{aligned}$$

This identity can be used to prove the following *Fierz-transformation*: Let $\psi_i, \quad i = 1\ldots 4$ be anticommuting two-spinors. Then

$$\begin{aligned}
(\bar\psi_1\Lambda^{(1)}\psi_2)(\bar\psi_3\Lambda^{(2)}\psi_4) &= -\bar\psi_{1a}\bar\psi_{3b}\Lambda^{(1)}_{ac}\Lambda^{(2)}_{bd}\psi_{2c}\psi_{4d} \\
&= -\frac{1}{2}\sum_A (\bar\psi_1\Omega^{(A)}\psi_4)(\bar\psi_3\Lambda^{(2)}\Omega^{(A)}\Lambda^{(1)}\psi_2) \qquad \text{(B.16)}
\end{aligned}$$

Some Fierz-transformations that are important when discussing four-fermion interactions are

$$\begin{aligned}
\bar\psi_i\psi_i\bar\psi_j\psi_j &= -\frac{1}{2}\left(\bar\psi_i\psi_j\bar\psi_j\psi_i + \bar\psi_i\gamma_5\psi_j\bar\psi_j\gamma_5\psi_i + \bar\psi_i\gamma_\mu\psi_j\bar\psi_j\gamma_\mu\psi_i\right) \\
\bar\psi_i\gamma_5\psi_i\bar\psi_j\gamma_5\psi_j &= -\frac{1}{2}\left(\bar\psi_i\psi_j\bar\psi_j\psi_i + \bar\psi_i\gamma_5\psi_j\bar\psi_j\gamma_5\psi_i - \bar\psi_i\gamma_\mu\psi_j\bar\psi_j\gamma_\mu\psi_i\right) \\
\bar\psi_i\gamma_\mu\psi_i\bar\psi_j\gamma_\mu\psi_j &= -\left(\bar\psi_i\psi_j\bar\psi_j\psi_i - \bar\psi_i\gamma_5\psi_j\bar\psi_j\gamma_5\psi_i\right). \qquad \text{(B.17)}
\end{aligned}$$

Using the identity B.16 and solving a simple linear system of equations one can write this in terms of the basis of interaction terms defined in 2.22

$$\mathcal{L}^{SS'} = -\frac{2+N}{N}\mathcal{L}^{SS} - \mathcal{L}^{PP} - \mathcal{L}^{VV} \qquad \text{(B.18)}$$

$$\mathcal{L}^{PP'} = -\mathcal{L}^{SS} - \frac{2+N}{N}\mathcal{L}^{PP} + \mathcal{L}^{VV} \qquad \text{(B.19)}$$

$$\mathcal{L}^{VV'} = -2\mathcal{L}^{SS} + 2\mathcal{L}^{PP} - \frac{2}{N}\mathcal{L}^{VV}. \qquad \text{(B.20)}$$

B.3 Fujikawa Jacobian

Here the anomalous Jacobian of an axial $U(1)$ transformation in the chiral Gross-Neveu model is derived à là Fujikawa [30]. The transformation under

discussion is

$$\begin{aligned} \psi(x) &\rightarrow e^{-\gamma_5\phi(x)}\psi(x) \\ \bar{\psi}(x) &\rightarrow \bar{\psi}(x)e^{-\gamma_5\phi(x)}\,, \end{aligned} \tag{B.21}$$

or in its infinitesimal form

$$\begin{aligned} \psi(x) &\rightarrow (1-\gamma_5\delta\phi(x))\psi(x) \\ \bar{\psi}(x) &\rightarrow \bar{\psi}(x)(1-\gamma_5\delta\phi(x))\,. \end{aligned} \tag{B.22}$$

The associated Jacobian is

$$J_F = \det(1-\gamma_5\delta\phi(x))^{-1} = \exp[-\mathrm{T}r\,\log(1-\gamma_5\delta\phi(x))] \tag{B.23}$$

For infinitesimal $\delta\phi$ its enough to keep the first term of the expansion of the logarithm

$$J_F = \exp[\mathrm{T}r(\gamma_5\delta\phi)] \tag{B.24}$$

The trace can be evaluated in the basis of orthonormal eigenfunctions of the Hermitian operator ($\not{D} = \not{\partial} + i\not{A} + i\not{B}$)

$$\not{D}\varphi_n = \lambda_n\varphi_n\,, \tag{B.25}$$

where φ_n has got N flavor and two Dirac components. The (continuous) index n labels the eigenfunction. This leads to

$$J_F = \exp\left[i\sum_n \int d^2x\ \mathrm{tr}^{s,f}(\varphi_n^\dagger(x)\gamma_5\delta\phi(x)\varphi_n(x))\right] \tag{B.26}$$

This expression is ill-defined (like $\infty\cdot 0$). To make sense out of it, one may introduce a regulator function f with $f(0) = 1$ which drops exponentially for large arguments

$$J_F = \lim_{\Lambda\to\infty} \exp\left[\sum_n \int d^2x\ \mathrm{tr}^{s,f}\left(\varphi_n^\dagger(x)\gamma_5\delta\phi f\left(\frac{\lambda_n^2}{\Lambda^2}\right)\varphi_n(x)\right)\right]. \tag{B.27}$$

In this expression λ_n^2 can be replaced by $\not{D}^2$, because the operator stands in front of φ_n. The trace is independent of the basis it is evaluated in, in particular one can switch to the plane wave basis for the spatial part

$$J_F = \lim_{\Lambda\to\infty} \exp\left[i\int \frac{d^2x\,d^2p}{(2\pi)^2}\, e^{-ipx}\delta\phi(x)\,\mathrm{tr}^{s,f}\left(\gamma_5 f\left(\frac{\not{D}^2}{\Lambda^2}\right)\right)e^{ipx}\right]. \tag{B.28}$$

Using

$$f\left(\frac{\not{D}^2}{\Lambda^2}\right)e^{ipx} = e^{ipx} f\left(\frac{(i\not{p}+\not{D})^2}{\Lambda^2}\right) \tag{B.29}$$

the two exponentials cancel each other. In the limit $\Lambda \to \infty$ only the high momentum part of the p-integral contributes, so one is allowed to keep just the first terms of the expansion

$$f\left(\frac{(i\not{p} + \not{D})^2}{\Lambda^2}\right) = f\left(\frac{-p^2}{\Lambda^2}\right) + f'\left(\frac{-p^2}{\Lambda^2}\right)\left(\frac{2i\not{p}\not{D} + \not{D}^2}{\Lambda^2}\right) + \dots \tag{B.30}$$

Some terms vanish due to the spin or flavor trace ($\mathrm{tr}^s\gamma_5 = 0, \quad \mathrm{tr}^f\lambda^i = 0$), and one ends up with

$$J_F = \lim_{\Lambda\to\infty} \exp\left[N \int d^2x\, \delta\phi(x) \mathrm{tr}^s(2\gamma_5 \not{\partial}\not{B}) \int \frac{d^2p}{(2\pi)^2} \frac{f'\left(\frac{-p^2}{\Lambda^2}\right)}{\Lambda^2}\right]. \tag{B.31}$$

The momentum integration can be performed in polar coordinates

$$\begin{aligned} & \int_0^\infty \frac{d\rho}{2\pi}\, \rho \frac{f'\left(\frac{-\rho^2}{\Lambda^2}\right)}{\Lambda^2} \\ = & -\int_0^\infty \frac{d\rho}{4\pi}\, f'(\rho) \\ = & \frac{1}{4\pi}\,. \end{aligned} \tag{B.32}$$

Hence the Jacobian of the infinitesimal transformation reads

$$\begin{aligned} J_F &= \exp\left[\frac{N}{4\pi} \int d^2x\, \delta\phi(x) \mathrm{tr}^s(2\gamma_5 \not{\partial}\not{B})\right] \\ &= \exp\left[\frac{N}{4\pi} \int d^2x\, 4i\delta\phi(x)\left(\partial_0^2\phi(x) + \partial_1^2\phi(x)\right)\right] \\ &= \exp\left[-i\frac{N}{\pi} \int d^2x\, \partial_\mu\delta\phi(x)\partial_\mu\phi(x)\right]. \end{aligned} \tag{B.33}$$

In the last step it was assumed that either ϕ or $\partial_\mu\delta\phi$ vanish for $x_\mu \to \pm\infty$ Finite transformations can be built up from the infinitesimal ones, but as B changes after each infinitesimal step, an additional factor of $\frac{1}{2}$ arises. The Jacobian of the finite transformation finally is given by

$$J_F = \exp\left[-i\frac{N}{2\pi} \int d^2x\, \partial_\mu\phi(x)\partial_\mu\phi(x)\right]. \tag{B.34}$$

B.4 Continuum limit of the chiral Gross-Neveu model

Aoki and Higashijima [3] derived in the large-N approximation, how the ratio of the couplings g_S/g_P and the bare mass m_0 have to be scaled to obtain a chirally symmetric continuum limit of the chiral Gross-Neveu model with Wilson fermions. In this appendix the calculation is repeated and partially extended to the model with an additional vector-vector interaction.

B.4.1 Continuum model

The action of the model is ($\lambda_S = N g_{\mathbb{N}}^2$, $\lambda_V = N g_V^2$)

$$S = \iint d^2x \left\{ \bar{\psi} \not{\partial} \psi - \frac{\lambda_S}{2N} \left[(\bar{\psi}\psi)^2 - (\bar{\psi}\gamma_5\psi)^2 \right] - \frac{\lambda_V}{2N} \bar{\psi}\gamma_\mu\psi\bar{\psi}\gamma_\mu\psi \right\} \tag{B.35}$$

After introduction of auxiliary fields to eliminate the four-fermion terms the effective potential in leading order of the large-N expansion is

$$V_{eff} = \frac{\sigma^2 + \Pi^2}{2\lambda_S} + \frac{A_\mu A_\mu}{2\lambda_V} - \iint_{-\infty}^{+\infty} \frac{d^2k}{(2\pi)^2} \log\left(\sigma^2 + \Pi^2 + [k_\mu - iA_\mu]^2\right) \tag{B.36}$$

It has a rotational symmetry in the σ-Π-plane. It is convenient t introduce the radial variable $\rho^2 = \sigma^2 + \Pi^2$. The extrema of the effective potential are given by the simultaneous solution of the gap-equations

$$\frac{\rho}{\lambda_S} - \iint_{-\infty}^{+\infty} \frac{d^2k}{(2\pi)^2} \frac{2\rho}{\rho^2 + (k_\mu - iA_\mu)^2} = 0 \tag{B.37}$$

$$\frac{A_\mu}{\lambda_V} + \iint_{-\infty}^{+\infty} \frac{d^2k}{(2\pi)^2} \frac{2A_\mu}{\rho^2 + (k_\mu - iA_\mu)^2} = 0 \tag{B.38}$$

The second equation has got only the trivial solution $A_\mu = 0$ which when inserted into the first equation leads to the gap-equation of the Gross-Neveu model with discrete chiral symmetry. The nontrivial solution is

$$\rho = \sqrt{\frac{M^2}{e^{2\pi/\lambda_S} - 1}} \xrightarrow{M\to\infty,\lambda_S\to 0} M \exp\left(-\frac{\pi}{\lambda_S}\right) =: \Lambda\,. \tag{B.39}$$

Here M is a spherical momentum-cutoff and the scale parameter Λ (dynamically generated mass) was defined, which is held fixed while the cutoff is removed. The effective potential for $A_\mu = 0$ can now be expressed in terms of physical quantities and in the $M \to \infty$ limit is given by

$$V_{eff}(\sigma^2 + \Pi^2) - V_{eff}(0) = (\sigma^2 + \Pi^2) \log\left(\frac{\sigma^2 + \Pi^2}{e\Lambda^2}\right). \tag{B.40}$$

B.4.2 Lattice model with Wilson fermions

The goal is to reproduce result (B.40) with a model defined by the lattice action

$$S = \sum_x \Big[\bar\psi(D_W + m_0)\psi - \frac{\lambda_S}{2N}(\bar\psi\psi)^2 - \frac{\lambda_P}{2N}(\bar\psi i\gamma_5\psi)^2 - \frac{\lambda_V}{2N}\bar\psi\gamma_\mu\psi\bar\psi\gamma_\mu\psi\Big], \tag{B.41}$$

where D_W is the Wilson Dirac operator. To obtain the correct continuum limit the bare mass parameter m_0 and the couplings will have to be tuned in a special way.

After introduction of auxiliary fields the effective potential in leading order of the large-N expansion is

$$\begin{aligned} V_{eff} &= \frac{\sigma^2}{2\lambda_S} + \frac{\Pi^2}{2\lambda_P} + \frac{A_\mu A_\mu}{2\lambda_V} \\ &- \iint_{-\pi/a}^{+\pi/a} \frac{d^2k}{(2\pi)^2} \log\Bigg[\underbrace{(\sigma+m_0)^2 + \Pi^2 - [i\mathring{k}_\mu + A_\mu]^2 + \left(\frac{2r}{a} - \sum_\mu \frac{r}{a}\cos(k_\mu a)\right)^2}_{=:\Delta} \\ &\qquad + \underbrace{2(\sigma+m_0)\left(\frac{2r}{a} - \sum_\mu \frac{r}{a}\cos(k_\mu a)\right)}_{=:\epsilon}\Bigg]. \end{aligned} \tag{B.42}$$

As in the continuum one can deduce from the gap-equations that the minimum of the effective potential is found at $A_\mu = 0$. To extract the σ and Π dependence, the $a \to 0$ limit of the integral

$$\iint_{-\pi/a}^{+\pi/a} \frac{d^2k}{(2\pi)^2}\log(\Delta+\epsilon) = \iint_{-\pi/a}^{+\pi/a} \frac{d^2k}{(2\pi)^2}\left(\log(\Delta) + \log\left(1+\frac{\epsilon}{\Delta}\right)\right) = \sum_n I_n \tag{B.43}$$

is investigated, where

$$I_0 = \iint_{-\pi/a}^{+\pi/a} \frac{d^2k}{(2\pi)^2}\log(\Delta) \tag{B.44}$$

$$I_n = -\frac{(-1)^n}{n}\iint_{-\pi/a}^{+\pi/a} \frac{d^2k}{(2\pi)^2}\frac{\epsilon^n}{\Delta^n} \tag{B.45}$$

$$\xrightarrow{a\to 0} \quad -\frac{(-1)^n}{n}[2(\sigma+m_0)r]^n a^{n-2}\iint_{-\pi}^{+\pi}\frac{d^2k}{(2\pi)^2}\frac{\left(\sum_\mu(1-\cos(k_\mu))\right)^n}{\left(\sum_\mu \sin^2(k_\mu) + (2r - \sum_\mu r\cos(k_\mu))^2\right)^n}.$$

Hence only I_0, I_1 and I_2 have a non-vanishing (i.e. constant or divergent) continuum limit. The finite integrals can be evaluated numerically (for $r = 1$) and one finds

$$I_1 = \frac{2(\sigma+m_0)r}{a} C_1 \qquad C_1 \approx 0.3849001795 \tag{B.46}$$

$$I_2 = -2r^2(\sigma + m_0)^2 C_2 \qquad C_2 \approx 0.1548258837 \tag{B.47}$$

C_1 is identical to the previously defined constant K_0. The divergent integral is

$$\begin{aligned} I_0 &= \iint_{-\pi/a}^{+\pi/a} \frac{d^2k}{(2\pi)^2} \log\left((\sigma + m_0)^2 + \Pi^2 - [i\mathring{k}_\mu + A_\mu]^2 + \left(\frac{2r}{a} - \sum_\mu \frac{r}{a} \cos(k_\mu a) \right)^2 \right) \\ &= \int_0^{(\sigma+m_0)^2+\Pi^2} d\rho \iint_{-\pi/a}^{+\pi/a} \frac{d^2k}{(2\pi)^2} \left(-[i\mathring{k}_\mu + A_\mu]^2 + \left(\frac{2r}{a} - \sum_\mu \frac{r}{a} \cos(k_\mu a) \right)^2 + \rho \right)^{-1} \\ &+ \iint_{-\pi/a}^{+\pi/a} \frac{d^2k}{(2\pi)^2} \log\left(-[i\mathring{k}_\mu + A_\mu]^2 + \left(\frac{2r}{a} - \sum_\mu \frac{r}{a} \cos(k_\mu a) \right)^2 \right) \end{aligned}$$

With $A_\mu = 0$ the last line amounts to a (infinite) shift of V_{eff} and can be neglected. In the limit $a \to 0$ one finds[1]

$$\begin{aligned} I_0 &\overset{a\to 0}{=} \int_0^{(\sigma+m_0)^2+\Pi^2} d\rho \left[\iint_{-\pi/a}^{+\pi/a} \tfrac{d^2k}{(2\pi)^2} \left(k_\mu k_\mu + \rho \right)^{-1} + C_0 \right], \qquad C_0 \approx 0.0209351 \\ &= \int_0^{(\sigma+m_0)^2+\Pi^2} d\rho \left[\tfrac{1}{4\pi} \log\left[\tfrac{1}{\rho a^2} \right] + \hat{C}_0 \right], \qquad \hat{C}_0 \approx 0.2245732\,. \end{aligned}$$

Now the continuum limit can be studied. With $\tilde{\sigma} = \sigma + m_0$ the effective potential is

$$\begin{aligned} V_{eff}(\tilde{\sigma}, \Pi, A_\mu = 0) &- V_{eff}(0,0,0) = \\ &\frac{1}{4\pi}(\tilde{\sigma}^2 + \Pi^2) \log\left(\frac{\tilde{\sigma}^2 + \Pi^2}{e} \right) \\ &+ \tilde{\sigma}^2 \left(\frac{1}{2\lambda_S} + 2r^2 C_2 - \hat{C}_0 + \frac{1}{4\pi} \log(a^2) \right) \\ &+ \Pi^2 \left(\frac{1}{2\lambda_P} - \hat{C}_0 + \frac{1}{4\pi} \log(a^2) \right) \\ &- \tilde{\sigma} \left(\frac{m_0}{\lambda_S} + \frac{2r}{a} C_1 \right) \end{aligned} \tag{B.48}$$

[1] There is a slight disagreement between the C_0 value quoted in [3] and the one obtained here. This has however no impact on the flow of argumentation.

This agrees exactly with (B.40) when

$$\Lambda a := \exp\left[-4r^2\pi C_2 + 2\pi\hat{C}_0 - \frac{\pi}{\lambda_S}\right] \tag{B.49}$$

is defined and the a dependence of the bare couplings is chosen as follows

$$\frac{1}{2\lambda_S} = \hat{C}_0 - 2r^2 C_2 + \frac{1}{4\pi}\log\left(\frac{1}{\Lambda^2 a^2}\right) \tag{B.50}$$

$$\frac{1}{2\lambda_P} = \hat{C}_0 + \frac{1}{4\pi}\log\left(\frac{1}{\Lambda^2 a^2}\right) \tag{B.51}$$

$$\frac{m_0}{\lambda_S} = -\frac{2r}{a}C_1\,. \tag{B.52}$$

The authors in [3] conclude that in order to obtain a renormalized effective potential that exhibits the desired symmetry from the continuum limit of the Wilson discretization, it is necessary to properly tune the bare mass parameter *and* the ratio of the two couplings.

B.5 Free propagators for the Gross-Neveu model

With Wilson fermions the free propagator in momentum space (r = 1) is given by

$$\tilde{G}(p) = \frac{-i\mathring{\not{p}} + M(p)}{\mathring{p}^2 + M(p)^2} \tag{B.53}$$

and

$$M(p) = m_0 + \frac{a}{2}\hat{p}^2\,. \tag{B.54}$$

When the half Fourier transformed propagators

$$\breve{G}(t, p_1) = \frac{1}{T}\sum_{p_0} e^{ip_0 t}\tilde{G}(p) \quad \text{and} \quad \hat{G}(p_0, x_1) = \frac{1}{L}\sum_{p_1} e^{ip_1 x_1}\tilde{G}(p) \tag{B.55}$$

are needed, the sums can be performed by complex integration techniques as has been worked out in [84]. In the following this calculation is reviewed. One can rewrite

$$\breve{G}(t, p_1) = (-i\mathring{p}_1\gamma_1 + 1 + M_1)f(t) - P_+ f(t+a) - P_- f(t-a)\,, \tag{B.56}$$

where $P_\pm = \frac{1}{2}(\mathbb{1} \pm \gamma_0)$, $M_1 = m_0 + \frac{a}{2}\hat{p}_1^2$ and

$$f(t) = \frac{1}{T}\sum_{p_0} e^{ip_0 t}\frac{1}{\mathring{p}^2 + M^2}\,. \tag{B.57}$$

From here on lattice units $a = 1$ are used. The T allowed values for p_0 have all the property that $(e^{ip_0})^T = u$, The phase u depends on the boundary-conditions in the temporal direction, for instance $u = 1$ for periodic and

$u = -1$ for antiperiodic b.c. In terms of the variables $z = e^{ip_0}$ equation (B.57) reads

$$\begin{aligned} f(t) &= \frac{1}{T} \sum_{\{z_i | z_i^T = u\}} \frac{z_i^t}{1 + \mathring{p}_1^2 + (1+M_1)^2 - (1+M_1)(z_i + z_i^{-1})} \\ &= \frac{1}{T} \sum_{\{z_i | z_i^T = u\}} \oint_\gamma \frac{dz}{2\pi i} \frac{1}{z - z_i} \frac{z^t}{1 + \mathring{p}_1^2 + (1+M_1)^2 - (1+M_1)(z + z^{-1})} \end{aligned} \tag{B.58}$$

The second line holds if the integration contour γ contains all the poles at $z = z_i$ but not the other two poles of the integrand which are located at

$$z = e^{\pm\alpha} \quad with \quad \alpha = \mathrm{a}cosh\left[\frac{1}{2}\left(1 + M_1 + \frac{1 + \mathring{p}_1^2}{1 + M_1}\right)\right]. \tag{B.59}$$

The situation is sketched in figure B.1.

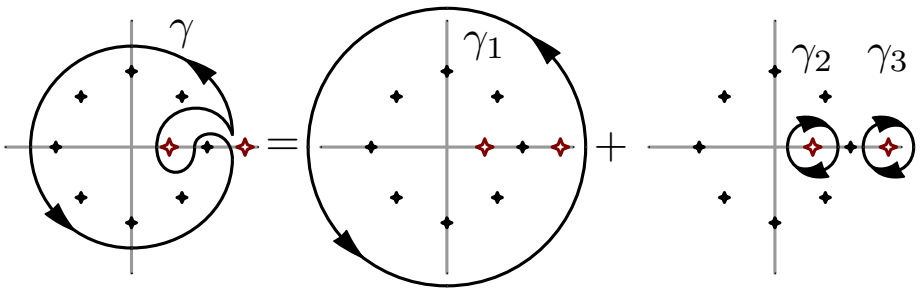

Figure B.1: A draft of the integration contours. The Black symbols denote the poles at $z = z_i = e^{ip_0}$. The two red symbols indicate the poles at $z = e^{\pm\alpha}$.

The identity

$$\prod_{\{z_i | z_i^T = u\}} (z - z_i) = z^T - u \tag{B.60}$$

is obvious if one realizes that both the left and the righthand side are polynomials in z of degree T with the same zeros in $z = z_i$. Differentiation of the logarithm of this identity leads to the expression

$$\frac{1}{T} \sum_{\{z_i | z_i^T = u\}} \frac{1}{z - z_i} = \frac{z^{T-1}}{z^T - u}, \tag{B.61}$$

which can be used to get rid of the summation in (B.58)

$$\begin{aligned} f(t) &= \oint_\gamma \frac{dz}{2\pi i} \frac{z^{T-1}}{z^T - u} \frac{z^t}{1 + \mathring{p}_1^2 + (1+M_1)^2 - (1+M_1)(z + z^{-1})} \\ &= -\frac{1}{1+M_1} \oint_\gamma \frac{dz}{2\pi i} \frac{z^{T-1}}{z^T - u} \frac{z^{t-1}}{(z^{-1} - e^{\alpha})(z^{-1} - e^{-\alpha})}. \end{aligned} \tag{B.62}$$

The integral can be rewritten as $\oint_\gamma = \oint_{\gamma_1} + \oint_{\gamma_2} + \oint_{\gamma_3}$ (figure B.1) and the last two terms can be easily calculated. The result is

$$\begin{aligned} & -\frac{1}{1+M_1} \oint_{\gamma_2+\gamma_3} \frac{dz}{2\pi i} \frac{z^{T-1}}{z^T-u} \frac{z^{t-1}}{(z^{-1}-e^{\alpha})(z^{-1}-e^{-\alpha})} \\ = & \frac{1}{1+M_1} \frac{\sinh(\alpha t) - u\sinh(\alpha(T+t))}{\sinh(\alpha)(1+u^2-2u\cosh(\alpha T))} . \end{aligned} \tag{B.63}$$

To evaluate the first term it is useful to perform a change of variables $z \to z^{-1}$ which leads to

$$f(t) = \frac{-1}{1+M_1} \oint_{\gamma_1'} \frac{dz}{2\pi i} \frac{1}{1-uz^T} \frac{z^{-t}}{(z-e^{\alpha})(z-e^{-\alpha})} . \tag{B.64}$$

The new integrand has got a pole in the origin. The contour γ_1' is shown in figure B.2. One minus sign arises, because the orientation of the contour is changed.

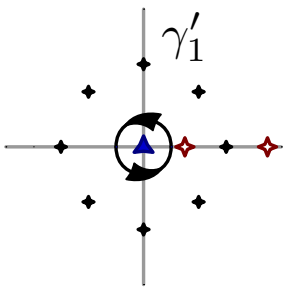

Figure B.2: The contour after change of variables. The radius of γ_1 can always be chosen large enough, such that γ_1' contains only the pole at the origin.

If it is assumed, that $0 \le t \le T$ and the first factor is written as a geometric series

$$\frac{1}{1-uz^T} = \sum_{n=0}^{\infty} (uz^T)^n , \tag{B.65}$$

then only the first term contributes to the integral, because for all other terms the integrand is analytic in 0. This non vanishing term gives (residue theorem)

$$\begin{aligned} & \frac{-1}{1+M_1} \oint_{\gamma_1'} \frac{dz}{2\pi i} \frac{z^{-t}}{(z-e^{\alpha})(z-e^{-\alpha})} \\ = & \frac{-1}{1+M_1} \frac{1}{(t-1)!} \frac{d^{t-1}}{dz^{t-1}} \frac{1}{(z-e^{\alpha})(z-e^{-\alpha})}\Big|_{z=0} \\ = & \frac{-1}{1+M_1} \frac{\sinh(\alpha t)}{\sinh(\alpha)} . \end{aligned} \tag{B.66}$$

and hence for $u = -1$ the whole integral has the value

$$f(t) = \frac{-1}{2(1+M_1)\sinh(\alpha)} \frac{\sinh(\alpha(t-T/2))}{\cosh(\alpha T/2)}\,. \tag{B.67}$$

A similar calculation yields the result

$$\hat{G}(p_0, x_1) = (-i\mathring{p}_0\gamma_0 + 1 + M_0)g(x_1) - Q_+ g(x_1+a) - Q_g(x_1-a)\,, \tag{B.68}$$

with the projectors $Q_\pm = \frac{1}{2}(\mathbb{1} \pm \gamma_1)$, $M_0 = m_0 + \frac{a}{2}\hat{p}_0^2$ and

$$g(x_1)\frac{1}{e^{2\bar{\alpha}}-1}\frac{\cosh(\bar{\alpha}(x_1 - L/2))}{\sinh(\bar{\alpha}L/2)}\,. \tag{B.69}$$

The angle $\bar{\alpha}$ is given in this case by

$$\bar{\alpha} = \mathrm{a}cosh\left(\frac{1}{2}\left(1 + M_0 + \frac{1+\mathring{p}_0^2}{1+M_0}\right)\right). \tag{B.70}$$

B.6 Feynman rules for the Gross-Neveu model

The following rules can be used to carry out perturbative calculations

Vertices

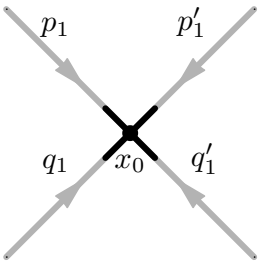

$$\propto \frac{a}{L^3}\frac{g^2}{8}\sum_{x_0}\sum_{i\neq j=1}^{N}\delta_{p_1+p_1'+q_1+q_1',0}$$

Loops

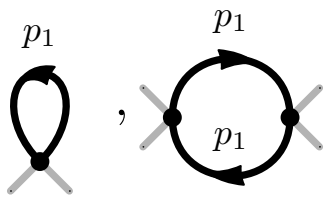

$$\propto \sum_{p_1}$$

Propagators

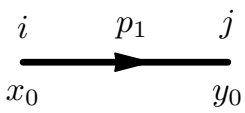

$$\propto L\delta_{i,j}\breve{G}(x_0 - y_0, p_1)C^{-1}$$

Traces

The vertices are often drawn like here in order to be able to read off the spin-traces from the graph (one for each closed path).

In addition there is a global factor for each graph depending on its symmetries. For instance this symmetry factor is 32 for the graph

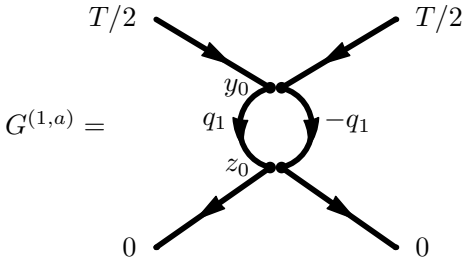

which appears at one loop in the calculation of the renormalized coupling. There are 8 equivalent possibilities to connect a vertex to one of the external legs and 4 possibilities to connect the second vertex to the first.

Appendix C

Tables and figures

C.1 Large-N calculation

C.1.1 Determination of m_c with Wilson fermions in infinite volume

Table C.1: Determination of m_c for different values of λ. Last column gives the value of σa

λ	$m_c a$	σa
1/0.379	-1.9987 ± 0.0001	0.237338
2.5	-1.8974 ± 0.0001	0.215810
2.4	-1.8240 ± 0.0001	0.200566
2.3963	-1.8213 ± 0.0001	0.200006
2.35	-1.7872 ± 0.0001	0.193038
2.3	-1.7503 ± 0.0001	0.185574
2.25	-1.7133 ± 0.0001	0.178175
2.2	-1.6763 ± 0.0001	0.170843
2.1	-1.6021 ± 0.0001	0.156386
2.0	-1.5276 ± 0.0001	0.142219
1.93615	-1.4798 ± 0.0001	0.133334
1.9	-1.4528 ± 0.0001	0.128363
1/0.55	-1.3914 ± 0.0001	0.117277
1.8	-1.3777 ± 0.0001	0.114846
1.7	-1.3025 ± 0.0001	0.101703
1.6	-1.2269 ± 0.0001	0.088974
1.5	-1.1512 ± 0.0001	0.076711
1.4146	-1.0863 ± 0.0001	0.066658
1.4	-1.0752 ± 0.0001	0.064981
1.35	-1.0371 ± 0.0001	0.059338

λ	$m_c a$	σa
1.3	-0.9990 ± 0.0001	0.053858
1.2	-0.9226 ± 0.0001	0.043432
1.1654	-0.8962 ± 0.0001	0.040006
1.15	-0.8844 ± 0.0001	0.038513
1.12	-0.8614 ± 0.0001	0.035662
1.1	-0.8461 ± 0.0001	0.033805
1.0	-0.7694 ± 0.0001	0.025057
0.9	-0.6926 ± 0.0001	0.017192
0.8	-0.6158 ± 0.0001	0.010302
0.7	-0.5388 ± 0.0001	0.005769
0.6	-0.4619 ± 0.0001	0.003801
0.5	-0.3849 ± 0.0001	0.002797
0.4	-0.3079 ± 0.0001	0.002146
0.3	-0.2309 ± 0.0001	0.001651
0.2	-0.1540 ± 0.0001	0.001225
0.1	-0.0770 ± 0.0001	0.000799

C.1.2 Determination of m_c with Wilson fermions on finite lattices

Table C.2: σL and the critical mass on a lattice of size $L/a = 10$

L/a	λ	$m_c L$	σL
10	1/0.379	-20.1850 ± 0.0001	1.999125
10	2.5	-19.1600 ± 0.0001	1.639663
10	2.4	-18.4206 ± 0.0001	1.335336
10	2.3963	-18.3224 ± 0.0001	1.322370
10	2.35	-18.0488 ± 0.0001	1.134679
10	2.3	-17.7007 ± 0.0001	0.984005
10	2.25	-17.3497 ± 0.0001	0.780739

Table C.3: σL and the critical mass on a lattice of size $L/a = 15$

L/a	λ	$m_c L$	σL
15	1/0.379	-30.1263 ± 0.0001	3.471764
15	2.5	-28.5980 ± 0.0001	3.089845
15	2.4	-27.4923 ± 0.0001	2.808505
15	2.3	-26.3839 ± 0.0001	2.517972
15	2.2	-25.2386 ± 0.0001	2.193847
15	2.1	-24.1568 ± 0.0001	1.882670
15	2.0	-23.0372 ± 0.0001	1.510891
15	1.93615	-22.3212 ± 0.0001	1.232806
15	1.9	-21.9199 ± 0.0001	1.053294

Table C.4: σL and the critical mass on a lattice of size $L/a = 30$

L/a	λ	$m_c L$	σL
30	1.9	-43.6044 ± 0.0001	3.732101
30	1.8	-41.3586 ± 0.0001	3.277247
30	1.7	-39.1064 ± 0.0001	2.808455
30	1.6	-36.8482 ± 0.0001	2.311215
30	1.5	-34.5708 ± 0.0001	1.741338
30	1.4146	-32.6466 ± 0.0001	1.159186
30	1.4	-32.3150 ± 0.0001	1.032007
30	1.35	-31.1785 ± 0.0001	0.384112

Table C.5: σL and the critical mass on a lattice of size $L/a = 50$

L/a	λ	$m_c L$	σL
50	1.5	-57.5700 ± 0.0001	3.717587
50	1.4	-53.7759 ± 0.0001	3.047038
50	1.35	-51.8589 ± 0.0001	2.690031
50	1.3	-49.9730 ± 0.0001	2.338642
50	1.2	-46.1601 ± 0.0001	1.509388
50	1.1654	-44.8420 ± 0.0001	1.145079
50	1.15	-44.2542 ± 0.0001	0.947965
50	1.12	-43.1086 ± 0.0001	0.358987

C.2 Extrapolation of Feynman diagrams

In order to determine the divergent and constant parts as well as the leading lattice artifacts of the Feynman diagrams that appear in chapter 5 the method introduced in [11] is used. The numerical data for symmetric lattices ($L = T$) is summarized in the following table.

Table C.6: Numerical values of Feynman diagrams.

L/a	K	$G^{(1,a)}$	$G^{(1,b)}$	$G^{(2)}$
8	0.3849637865895783	0.2298343597207694	0.1583872750455539	−0.1022118885195386
12	0.3849132211857289	0.2081829253684071	0.1569623397996175	−0.0469422067050661
16	0.3849043760344421	0.1969036821526046	0.1563514166997595	−0.0071028547075562
20	0.3849019132423367	0.1898563057100314	0.1560121537578140	0.0241972825165530
24	0.3849010197069316	0.1849883439095381	0.1557963333136479	0.0500373799185231
28	0.3849006343927452	0.1814026188787538	0.1556469618311666	0.0720727371380454
32	0.3849004466727558	0.1786400743322099	0.1555374451960517	0.0912988660557221
36	0.3849003465138255	0.1764398139704745	0.1554537091013827	0.1083625207141112
40	0.3849002891750112	0.1746419093006225	0.1553876082320195	0.1237083266004640
44	0.3849002544533024	0.1731425401301390	0.1553341017880862	0.1376554654759437
48	0.3849002324407436	0.1718712040186634	0.1552899030806659	0.1504410352987446
52	0.3849002179426058	0.1707782495343347	0.1552527775767456	0.1622461078440929
56	0.3849002080807132	0.1698276432235740	0.1552211530535415	0.1732121741081298
60	0.3849002011846234	0.1689925662791922	0.1551938911327478	0.1834519492937751
64	0.3849001962456875	0.1682526241713508	0.1551701472857271	0.1930567149146248
68	0.3849001926336857	0.1675920172779433	0.1551492817630012	0.2021014525149336
72	0.3849001899429323	0.1669983060277626	0.1551308010714163	0.2106485226231333
76	0.3849001879053339	0.1664615559497586	0.1551143184367326	0.2187503581749208
80	0.3849001863395556	0.1659737324419248	0.1550995264345465	0.2264514737843273
84	0.3849001851203680	0.1655282638118162	0.1550861776333516	0.2337899897573454
88	0.3849001841596562	0.1651197202285761	0.1550740706406510	0.2407988052924960
92	0.3849001833943677	0.1647435741034502	0.1550630398705609	0.2475065137047902
96	0.3849001827786852	0.1643960186931634	0.1550529479245799	0.2539381250128774
100	0.3849001822788471	0.1640738290031905	0.1550436798384109	0.2601156426743187
104	0.3849001818696555	0.1637742538711525	0.1550351386826288	0.2660585284934644
108	0.3849001815320814	0.1634949313395410	0.1550272421596317	0.2717840807974473
112	0.3849001812515965	0.1632338216357682	0.1550199199431306	0.2773077446361066
116	0.3849001810169975	0.1629891536129915	0.1550131115774692	0.2826433681826760
120	0.3849001808195647	0.1627593815878580	0.1550067648051209	0.2878034161786333
124	0.3849001806524512	0.1625431502854925	0.1550008342220787	0.2927991487915709
128	0.3849001805102378	0.1623392661623292	0.1549952801901281	0.2976407724130694
132	0.3849001803886019	0.1621466737878089	0.1549900679498877	0.3023375675253717
136	0.3849001802840720	0.1619644362695143	0.1549851668924578	0.3068979977067856
140	0.3849001801938409	0.1617917189334832	0.1549805499579102	0.3113298030217510

L/a	K	$G^{(1,a)}$	$G^{(1,b)}$	$G^{(2)}$
144	0.3849001801156248	0.1616277756428411	0.1549761931353850	0.3156400804112385
148	0.3849001800475532	0.1614719372682560	0.1549720750453989	0.3198353531979294
152	0.3849001799880878	0.1613236019239589	0.1549681765890477	0.3239216314312225
156	0.3849001799359555	0.1611822266605668	0.1549644806518498	0.3279044644859943
160	0.3849001798900977	0.1610473203662766	0.1549609718522189	0.3317889870802681
164	0.3849001798496291	0.1609184376754857	0.1549576363281127	0.3355799596761668
168	0.3849001798138072	0.1607951737211701	0.1549544615533951	0.3392818040701833
172	0.3849001797820068	0.1606771595973374	0.1549514361807667	0.3428986348421982
176	0.3849001797536977	0.1605640584213863	0.1549485499066673	0.3464342872327146
180	0.3849001797284300	0.1604555619055922	0.1549457933535983	0.3498923419211330
184	0.3849001797058200	0.1603513873621102	0.1549431579682934	0.3532761471143236
188	0.3849001796855387	0.1602512750787849	0.1549406359336060	0.3565888382839998
192	0.3849001796673044	0.1601549860129185	0.1549382200902334	0.3598333558508374
196	0.3849001796508743	0.1600622997588917	0.1549359038698085	0.3630124610670519
200	0.3849001796360383	0.1599730127522302	0.1549336812346240	0.3661287503097012
204	0.3849001796226144	0.1598869366785075	0.1549315466247778	0.3691846679745322
208	0.3849001796104441	0.1598038970602922	0.1549294949127613	0.3721825181346207
212	0.3849001795993897	0.1597237319991441	0.1549275213616269	0.3751244751000689
216	0.3849001795893307	0.1596462910531481	0.1549256215881369	0.3780125929961695
220	0.3849001795801609	0.1595714342331990	0.1549237915314582	0.3808488144795666
224	0.3849001795717890	0.1594990311035208	0.1549220274228890	0.3836349786732082
228	0.3849001795641313	0.1594289599740083	0.1549203257609361	0.3863728284069940
232	0.3849001795571172	0.1593611071735880	0.1549186832874092	0.3890640168373470
236	0.3849001795506822	0.1592953663951520	0.1549170969669459	0.3917101135053601
240	0.3849001795447710	0.1592316381041280	0.1549155639684016	0.3943126098907342
244	0.3849001795393313	0.1591698290034039	0.1549140816474170	0.3968729245123842
248	0.3849001795343205	0.1591098515483755	0.1549126475322633	0.3993924076195072
252	0.3849001795296972	0.1590516235069489	0.1549112593088319	0.4018723455108075
256	0.3849001795254273	0.1589950675593721	0.1549099148091251	0.4043139645116645
260	0.3849001795214784	0.1589401109340132	0.1549086119993725	0.4067184346587868
264	0.3849001795178212	0.1588866850751668	0.1549073489702122	0.4090868730900059
268	0.3849001795144316	0.1588347253397373	0.1549061239270532	0.4114203471982697
272	0.3849001795112854	0.1587841707198832	0.1549049351812874	0.4137198775399626
276	0.3849001795083622	0.1587349635890519	0.1549037811434124	0.4159864405447494
280	0.3849001795056439	0.1586870494690734	0.1549026603155806	0.4182209710220439
284	0.3849001795031121	0.1586403768164097	0.1549015712842412	0.4204243645006757
288	0.3849001795007527	0.1585948968256382	0.1549005127153662	0.4225974794002169
292	0.3849001794985523	0.1585505632486585	0.1548994833482614	0.4247411390584732
296	0.3849001794964973	0.1585073322279715	0.1548984819914695	0.4268561336146806
300	0.3849001794945761	0.1584651621430771	0.1548975075165177	0.4289432217800434
304	0.3849001794927791	0.1584240134685297	0.1548965588556237	0.4310031324806277
308	0.3849001794910967	0.1583838486427165	0.1548956349964751	0.4330365663981233
312	0.3849001794895200	0.1583446319464593	0.1548947349789352	0.4350441974149208
316	0.3849001794880413	0.1583063293905498	0.1548938578915940	0.4370266739641157
320	0.3849001794866529	0.1582689086115008	0.1548930028696735	0.4389846202950297
324	0.3849001794853490	0.1582323387746787	0.1548921690899999	0.4409186376644540

L/a	K	$G^{(1,a)}$	$G^{(1,b)}$	$G^{(2)}$
328	0.3849001794841225	0.1581965904844580	0.1548913557716765	0.4428293054540544
332	0.3849001794829688	0.1581616357005502	0.1548905621699032	0.4447171822180471
336	0.3849001794818832	0.1581274476602394	0.1548897875765237	0.4465828066741286
340	0.3849001794808598	0.1580940008058247	0.1548890313172532	0.4484266986263273
344	0.3849001794798949	0.1580612707170889	0.1548882927476997	0.4502493598500755
348	0.3849001794789847	0.1580292340481857	0.1548875712550739	0.4520512749112307
352	0.3849001794781255	0.1579978684688038	0.1548868662537740	0.4538329119462834
356	0.3849001794773130	0.1579671526090669	0.1548861771847117	0.4555947233989380
360	0.3849001794765455	0.1579370660080780	0.1548855035135203	0.4573371467132322
364	0.3849001794758193	0.1579075890657640	0.1548848447306029	0.4590606049904358
368	0.3849001794751322	0.1578787029976654	0.1548842003472924	0.4607655076115106
372	0.3849001794744816	0.1578503897926844	0.1548835698962616	0.4624522508220454
376	0.3849001794738644	0.1578226321733650	0.1548829529308723	0.4641212182910514
380	0.3849001794732791	0.1577954135586423	0.1548823490233474	0.4657727816359654
384	0.3849001794727246	0.1577687180288423	0.1548817577626158	0.4674073009256907
388	0.3849001794721978	0.1577425302927652	0.1548811787564137	0.4690251251513732
392	0.3849001794716969	0.1577168356567515	0.1548806116271623	0.4706265926821939
396	0.3849001794712222	0.1576916199955724	0.1548800560129626	0.4722120316823489
400	0.3849001794707698	0.1576668697249859	0.1548795115670336	0.4737817605308984
404	0.3849001794703397	0.1576425717758634	0.1548789779561804	0.4753360881940466
408	0.3849001794699307	0.1576187135698480	0.1548784548594992	0.4768753146064292
412	0.3849001794695416	0.1575952829964054	0.1548779419695629	0.4783997310096660
416	0.3849001794691697	0.1575722683909919	0.1548774389905796	0.4799096202869749
420	0.3849001794688166	0.1575496585146702	0.1548769456382209	0.4814052572845732
424	0.3849001794684784	0.1575274425346645	0.1548764616384954	0.4828869091136809
428	0.3849001794681575	0.1575056100060702	0.1548759867276273	0.4843548354304648
432	0.3849001794678500	0.1574841508545090	0.1548755206524240	0.4858092887218501
436	0.3849001794675562	0.1574630553597187	0.1548750631687109	0.4872505145577736
440	0.3849001794672769	0.1574423141400119	0.1548746140404955	0.4886787518501617
444	0.3849001794670093	0.1574219181375633	0.1548741730417301	0.4900942330872618
448	0.3849001794667539	0.1574018586044275	0.1548737399527343	0.4914971845561838
452	0.3849001794665093	0.1573821270893270	0.1548733145642927	0.4928878265766794
456	0.3849001794662757	0.1573627154250817	0.1548728966702410	0.4942663736976924
460	0.3849001794660512	0.1573436157166667	0.1548724860762168	0.4956330348942125
464	0.3849001794658356	0.1573248203299008	0.1548720825922199	0.4969880137766369
468	0.3849001794656308	0.1573063218807018	0.1548716860349695	0.4983315087510255
472	0.3849001794654341	0.1572881132247741	0.1548712962273278	0.4996637132101110
476	0.3849001794652460	0.1572701874479911	0.1548709129989906	0.5009848156967972
480	0.3849001794650649	0.1572525378570516	0.1548705361840858	0.5022950000622726
484	0.3849001794648915	0.1572351579706832	0.1548701656238126	0.5035944456231778
488	0.3849001794647248	0.1572180415112911	0.1548698011629653	0.5048833273122347
492	0.3849001794645652	0.1572011823969201	0.1548694426525900	0.5061618158131939
496	0.3849001794644114	0.1571845747336243	0.1548690899484524	0.5074300777043376
500	0.3849001794642646	0.1571682128082563	0.1548687429099251	0.5086882755837780
504	0.3849001794641232	0.1571520910814764	0.1548684014017069	0.5099365682027001
508	0.3849001794639866	0.1571362041812243	0.1548680652931792	0.5111751105737875
512	0.3849001794638562	0.1571205468963054	0.1548677344568464	0.5124040541013907

C.3 Comparison of simulations with bare perturbation theory

To test the code Monte-Carlo results were compared with bare perturbation theory for small bare couplings. The following tables summarize the data.

Table C.7: Monte-Carlo results for some bare observables in the Thirring model with Wilson fermions. The bare mass was set to the tree level critical mass value $m_0 = 0$.

g	$k_S(T/4,0)$	$k_0(T/2,0)$	$\bar{k}_1(\pi/T, L/4)$	$Z_\psi^2 g_R^2$
0.050	0.001906(45)	0.999090(26)	0.359035(9)	0.002493(6)
0.224	0.037920(63)	0.977670(51)	0.352584(18)	0.04727(23)
0.320	0.07535(10)	0.948509(87)	0.345136(31)	0.08897(39)
0.387	0.10741(12)	0.916982(99)	0.338011(34)	0.11987(31)
0.450	0.1382(35)	0.8768(30)	0.32983(94)	0.1507(37)
0.500	0.16588(22)	0.83863(20)	0.322186(67)	0.1874(64)
0.600	0.2130(46)	0.7459(52)	0.3068(16)	0.16384(43)
0.700	0.2432(52)	0.6213(62)	0.2801(21)	0.1653(75)
0.800	0.2652(53)	0.4984(65)	0.2532(29)	0.1415(65)

Table C.8: Monte-Carlo results for some bare observables in the $N = 4$ Gross-Neveu model with Wilson fermions. The bare mass was set to the tree level critical mass value $m_0 = 0$.

g	$k_S(T/4,0)$	$k_0(T/2,0)$	$\bar{k}_1(\pi/T, L/4)$	$Z_\psi^2 g_R^2$
0.032	0.00580(49)	0.99673(27)	0.358315(87)	0.001026(32)
0.045	0.01068(13)	0.994379(74)	0.357487(26)	0.001986(14)
0.050	0.01350(12)	0.992983(70)	0.357042(2)	0.002431(29)
0.063	0.021125(28)	0.988696(21)	0.355683(6)	0.003723(60)
0.224	0.20581(29)	0.76538(27)	0.308461(94)	0.02220(12)
0.320	0.26298(19)	0.49518(20)	0.255589(91)	0.014616(74)
0.387	0.24920(15)	0.33118(16)	0.215592(42)	0.007764(41)
0.450	0.21668(16)	0.22043(15)	0.18037(11)	0.003834(21)
0.500	0.18792(17)	0.15840(14)	0.15502(11)	0.002099(12)
0.600	0.136895(85)	0.083868(53)	0.114006(61)	0.000635(4)
0.700	0.099057(62)	0.046181(30)	0.084083(47)	0.000202(1)
0.800	0.072586(39)	0.026674(15)	0.062842(31)	0.000007(1)

C.4 Tuning of parameters in MC simulations

The tuning of the bare parameters which is necessary to satisfy the renormalization conditions is summarized in the following tables. The lines with m_0 closest to m_c are highlighted by a "→" while the runs where one of the problems described in section 6.2 appeared are marked with a "×".

C.4.1 $N = 4$ Gross-Neveu model

Table C.9: $\frac{L}{a} \times \frac{T}{a} = 48 \times 48$

	g	m_0	$k_S(T/4, 0)$	$k_0(T/2, 0)$	$Z_\psi^2 \bar{g}_R^2$	$\bar{g}_R^2$
	0.40	−0.4100	0.3289(37)	0.5509(46)	0.0560(27)	0.1845(82)
	0.40	−0.4200	0.2918(42)	0.7116(61)	0.0929(42)	0.1835(75)
	0.40	−0.4310	0.1810(61)	0.9029(50)	0.1575(89)	0.193(10)
	0.40	−0.4380	0.0182(43)	0.9749(14)	0.1890(42)	0.1988(42)
	0.40	−0.43889	0.0052(22)	0.97778(69)	0.1859(22)	0.1945(22)
	0.40	−0.4389	0.0035(22)	0.97849(70)	0.1879(22)	0.1963(22)
→	0.40	−0.4390	0.0021(22)	0.97925(68)	0.1869(23)	0.1950(23)
	0.40	−0.4400	−0.0226(43)	0.9805(12)	0.1844(37)	0.1918(37)
	0.40	−0.4412	−0.0468(90)	0.9798(32)	0.207(12)	0.216(12)
	0.40	−0.4420	−0.0622(42)	0.9746(14)	0.1939(41)	0.2041(41)
	0.40	−0.4500	−0.2331(81)	0.8852(62)	0.181(10)	0.231(12)
×	0.70	−1.3100	0.1430(11)	0.05050(58)	0.001293(64)	0.507(19)
×	0.70	−1.3200	0.1597(12)	0.06450(73)	0.00225(11)	0.541(21)
×	0.70	−1.3300	0.1763(16)	0.0797(10)	0.00406(23)	0.640(28)
×	0.70	−1.3430	0.2107(20)	0.1162(18)	0.00883(60)	0.654(34)
×	0.70	−1.3444	0.2129(21)	0.1225(18)	0.00962(59)	0.641(30)
×	0.70	−1.3450	0.2131(20)	0.1224(17)	0.00960(67)	0.641(38)
×	0.70	−1.3600	0.2596(32)	0.2074(45)	0.0380(37)	0.883(61)
×	0.70	−1.3650	−0.2554(68)	0.1531(64)	0.0435(56)	1.86(15)
×	0.70	−1.3660	−0.2363(60)	0.142(14)	0.045(11)	2.21(31)
×	0.70	−1.3670	−0.2358(52)	0.1341(59)	0.0421(57)	2.34(18)
×	0.70	−1.3700	−0.2093(48)	0.1010(42)	0.0225(28)	2.21(18)

Table C.10: $\frac{L}{a} \times \frac{T}{a} = 40 \times 40$

	g	m_0	$k_S(T/4,0)$	$k_0(T/2,0)$	$Z_\psi^2 \bar{g}_R^2$	$\bar{g}_R^2$
	0.40	−0.4395	−0.0039(21)	0.98134(65)	0.1886(23)	0.1959(22)
	0.40	−0.4400	−0.0037(84)	0.9820(30)	0.2010(95)	0.2084(92)
	0.40	−0.4450	−0.1083(87)	0.9730(34)	0.1904(86)	0.2011(88)
	0.405	−0.4450	0.0984(19)	0.9504(10)	0.1709(20)	0.1892(20)
	0.405	−0.4500	0.0066(21)	0.97877(71)	0.1847(21)	0.1928(21)
→	0.405	−0.45022	−0.0044(21)	0.97914(71)	0.1863(22)	0.1943(22)
	0.405	−0.45031	−0.0007(22)	0.97881(70)	0.1870(21)	0.1952(21)
	0.405	−0.4510	−0.0144(22)	0.98025(69)	0.1886(22)	0.1963(22)
	0.405	−0.4600	−0.1802(20)	0.9298(13)	0.1773(20)	0.2051(22)
	0.59	−0.9380	0.3113(29)	0.3314(48)	0.0455(32)	0.415(24)
	0.59	−0.9500	0.3178(17)	0.4590(34)	0.0997(30)	0.473(11)

Table C.11: $\frac{L}{a} \times \frac{T}{a} = 32 \times 32$

	g	m_0	$k_S(T/4,0)$	$k_0(T/2,0)$	$Z_\psi^2 \bar{g}_R^2$	$\bar{g}_R^2$
	0.41	−0.4450	0.1960(15)	0.8699(13)	0.1366(16)	0.1805(19)
	0.41	−0.4500	0.1503(16)	0.9146(11)	0.1543(18)	0.1844(19)
	0.41	−0.4530	0.1172(18)	0.9388(11)	0.1639(18)	0.1859(19)
→	0.415	−0.4733	−0.0001(22)	0.97803(74)	0.1886(20)	0.1971(20)
	0.415	−0.47343	−0.0054(20)	0.97936(71)	0.1906(21)	0.1987(21)
	0.415	−0.4735	−0.0077(21)	0.98074(73)	0.1928(21)	0.2005(21)
	0.42	−0.4500	0.30286(85)	0.6617(14)	0.07966(97)	0.1819(19)
	0.42	−0.4700	0.1879(16)	0.8777(14)	0.1481(17)	0.1923(21)
	0.42	−0.4791	0.0784(20)	0.9558(10)	0.1847(21)	0.2021(22)
	0.42	−0.4842	0.0101(23)	0.97610(82)	0.1947(23)	0.2044(23)
→	0.42	−0.48491	−0.0018(23)	0.97712(76)	0.1978(23)	0.2071(23)
	0.42	−0.5020	−0.2431(19)	0.8817(16)	0.1741(20)	0.2239(24)
	0.42	−0.5027	−0.2454(18)	0.8767(16)	0.1729(20)	0.2250(24)

Table C.12: $\frac{L}{a} \times \frac{T}{a} = 24 \times 24$

	g	m_0	$k_S(T/4,0)$	$k_0(T/2,0)$	$Z_\psi^2 \bar{g}_R^2$	$\bar{g}_R^2$
→	0.42	−0.4846	0.0009(20)	0.98018(73)	0.1873(20)	0.1950(20)
	0.42	−0.48477	0.0020(21)	0.98043(73)	0.1896(21)	0.1972(21)
	0.42	−0.4880	−0.0329(20)	0.98341(71)	0.1921(21)	0.1986(20)
	0.42	−0.4909	−0.0624(20)	0.98254(71)	0.1911(21)	0.1980(21)
	0.425	−0.4890	0.0754(20)	0.9571(10)	0.1784(21)	0.1947(21)
	0.425	−0.4909	0.0555(20)	0.96453(93)	0.1848(21)	0.1986(21)
	0.425	−0.4920	0.0474(20)	0.96783(88)	0.1821(20)	0.1944(20)
→	0.425	−0.49669	−0.0007(20)	0.97912(76)	0.1953(21)	0.2037(21)
	0.425	−0.49708	−0.0039(21)	0.98043(76)	0.1945(22)	0.2024(22)
	0.425	−0.49844	−0.0208(21)	0.98197(75)	0.1965(21)	0.2038(21)

Table C.13: $\frac{L}{a} \times \frac{T}{a} = 16 \times 16$

	g	m_0	$k_S(T/4,0)$	$k_0(T/2,0)$	$Z_\psi^2 \bar{g}_R^2$	$\bar{g}_R^2$
	0.42	−0.4700	0.0821(15)	0.95026(96)	0.1589(16)	0.1760(17)
	0.42	−0.4750	0.0527(16)	0.96515(88)	0.1695(17)	0.1820(17)
→	0.43	−0.5085	0.0011(19)	0.98211(82)	0.1865(20)	0.1934(19)
	0.43	−0.5100	−0.0115(20)	0.98372(80)	0.1879(20)	0.1942(19)
→	0.432	−0.5120	0.0027(19)	0.98151(85)	0.1897(19)	0.1969(19)
	0.432	−0.5122	0.0045(19)	0.98069(84)	0.1875(20)	0.1949(20)
	0.432	−0.5132	−0.0020(19)	0.98105(82)	0.1857(19)	0.1929(19)

C.4.2 Thirring model

Table C.14: $\frac{L}{a} \times \frac{T}{a} = 48 \times 48$

	g	m_0	$k_S(T/4,0)$	$k_0(T/2,0)$	$Z_\psi^2 \bar{g}_R^2$	$\bar{g}_R^2$
	0.4	−0.060	0.01893(51)	0.99016(64)	0.1630(39)	0.1662(38)
	0.4	−0.062	0.00653(53)	0.99632(76)	0.1661(42)	0.1673(41)
	0.4	−0.0625	0.00359(38)	0.99784(52)	0.1678(29)	0.1685(28)
	0.4	−0.063	0.00067(38)	0.99814(52)	0.1686(28)	0.1692(27)
→	0.4	−0.06303	0.00050(48)	0.99808(18)	0.16896(69)	0.16961(67)
	0.4	−0.0631	−0.00132(65)	0.99777(25)	0.16671(93)	0.16746(90)
	0.4	−0.0635	−0.00231(38)	0.99832(54)	0.1673(28)	0.1679(27)
	0.4	−0.064	−0.00635(51)	0.99838(76)	0.1685(39)	0.1690(38)
	0.7	−0.1900	0.184(14)	0.888(14)	0.413(28)	0.523(31)
	0.7	−0.2000	0.057(20)	0.9674(88)	0.572(50)	0.611(47)
	0.7	−0.2035	0.013(24)	0.9717(97)	0.488(37)	0.517(33)
	0.7	−0.2040	0.023(20)	0.978(13)	0.528(47)	0.552(40)
×	0.7	−0.2042	−0.0074(27)	0.9782(13)	0.5637(72)	0.5891(65)
×	0.7	−0.20424	−0.0108(77)	0.9758(37)	0.564(18)	0.592(16)
	0.7	−0.20424	−0.012(11)	0.9859(49)	0.624(29)	0.642(25)
→	0.7	−0.20425	−0.0043(84)	0.9803(36)	0.593(20)	0.617(18)
	0.7	−0.20425	−0.005(10)	0.9794(45)	0.559(21)	0.582(18)
	0.7	−0.20426	−0.004(10)	0.9843(48)	0.587(29)	0.606(27)
	0.7	−0.2045	−0.024(28)	0.967(11)	0.597(70)	0.638(66)
	0.7	−0.2200	−0.217(15)	0.889(12)	0.475(38)	0.601(40)
	0.7	−0.2400	−0.342(11)	0.619(16)	0.281(42)	0.732(93)
	0.7	−0.2600	−0.3517(81)	0.3689(86)	0.1034(93)	0.760(56)
	0.7	−0.2800	−0.3114(60)	0.2218(70)	0.0414(46)	0.842(64)
	0.7	−0.3000	−0.2460(51)	0.1229(41)	0.0149(18)	0.987(93)
	0.8	0.1000	0.01496(18)	0.000610(9)	0.00000024(2)	0.642(38)
×	0.8	0.0000	0.03700(48)	0.003488(58)	0.000009(1)	0.749(47)
×	0.8	−0.0040	0.03968(53)	0.004002(77)	0.000012(1)	0.757(53)
×	0.8	−0.0070	0.04082(55)	0.004228(82)	0.000014(1)	0.762(53)
×	0.8	−0.0100	0.04078(47)	0.004209(85)	0.000013(1)	0.725(37)
×	0.8	−0.0606	0.06655(82)	0.01106(19)	0.000091(6)	0.746(39)
×	0.8	−0.0616	0.0700(11)	0.01171(25)	0.000116(14)	0.843(84)
×	0.8	−0.0626	0.06896(99)	0.01203(25)	0.000119(9)	0.821(46)
×	0.8	−0.2463	0.308(11)	0.707(16)	0.426(32)	0.854(50)
×	0.8	−0.2473	0.304(13)	0.706(14)	0.382(31)	0.767(53)
×	0.8	−0.2630	0.076(24)	0.920(18)	0.614(59)	0.726(57)
×	0.8	−0.2730	−0.005(25)	0.950(11)	0.630(53)	0.698(50)
	0.8	−0.2830	−0.145(31)	0.903(21)	0.723(85)	0.886(85)
×	0.8	−0.3000	−0.317(14)	0.703(22)	0.523(58)	1.056(89)
	0.8	−0.4000	−0.1493(37)	0.0400(14)	0.00285(31)	1.78(13)
×	0.8	−0.5000	−0.03186(88)	0.001608(69)	0.000012(2)	4.61(57)

Table C.15: $\frac{L}{a} \times \frac{T}{a} = 40 \times 40$

	g	m_0	$k_S(T/4,0)$	$k_0(T/2,0)$	$Z_\psi^2 \bar{g}_R^2$	$\bar{g}_R^2$
	0.39	−0.0584	0.00726(24)	0.99666(56)	0.1577(38)	0.1587(37)
	0.39	−0.0585	0.00646(32)	0.99606(56)	0.1528(38)	0.1540(36)
	0.39	−0.0586	0.00788(33)	0.99654(58)	0.1607(42)	0.1618(41)
	0.4	−0.060	0.01683(36)	0.99264(60)	0.1686(40)	0.1711(39)
	0.4	−0.062	0.00478(40)	0.99698(58)	0.1663(39)	0.1673(37)
	0.4	−0.0625	0.00251(32)	0.99706(58)	0.1649(37)	0.1659(36)
	0.4	−0.063	0.00032(40)	0.99834(60)	0.1662(40)	0.1668(38)
→	0.4	−0.063006	−0.00030(46)	0.99818(18)	0.16813(67)	0.16874(64)
	0.4	−0.06302	−0.00072(46)	0.99846(18)	0.16857(66)	0.16909(64)
	0.4	−0.0631	−0.00132(65)	0.99777(25)	0.16671(93)	0.16746(90)
	0.4	−0.0635	−0.00233(38)	0.99886(58)	0.1645(38)	0.1649(37)
	0.4	−0.064	−0.00401(37)	0.99996(62)	0.1749(43)	0.1749(41)
	0.402	−0.061	0.01368(36)	0.99392(60)	0.1687(38)	0.1708(37)
	0.402	−0.062	0.00962(41)	0.99646(60)	0.1749(43)	0.1762(42)
	0.405	−0.062	0.01492(47)	0.99668(62)	0.1737(43)	0.1759(42)
	0.405	−0.063	0.00857(45)	0.99668(62)	0.1723(40)	0.1734(39)
	0.41	−0.0647	0.00987(50)	0.99402(64)	0.1753(42)	0.1774(41)
	0.42	−0.0644	0.02743(42)	0.98616(48)	0.1814(29)	0.1865(28)
	0.70	−0.2000	0.051(26)	0.963(12)	0.556(51)	0.600(47)
	0.70	−0.2038	−0.015(16)	0.9728(70)	0.510(30)	0.539(27)
	0.70	−0.2039	−0.0001(31)	0.9804(14)	0.5681(69)	0.5910(62)
	0.70	−0.2040	0.045(26)	0.983(11)	0.559(58)	0.577(52)
	0.70	−0.2040	−0.005(19)	0.9784(72)	0.577(35)	0.603(32)
→	0.70	−0.2041	−0.0018(64)	0.9742(32)	0.571(15)	0.602(13)
×	0.70	−0.2042	0.000(16)	0.9702(71)	0.539(29)	0.573(26)
	0.70	−0.2042	−0.0058(67)	0.9824(32)	0.594(15)	0.616(13)
	0.70	−0.20425	−0.0066(33)	0.9806(15)	0.5694(81)	0.5922(74)
	0.70	−0.2048	−0.016(10)	0.9775(45)	0.531(22)	0.555(20)
	0.70	−0.2050	0.007(23)	0.971(11)	0.559(39)	0.593(35)
	0.70	−0.2050	−0.031(10)	0.9814(45)	0.569(24)	0.590(22)
	0.70	−0.2052	−0.0229(96)	0.9764(51)	0.569(30)	0.596(27)
	0.70	−0.2030	0.017(23)	0.958(10)	0.496(43)	0.541(41)
	0.70	−0.2500	−0.3689(51)	0.5971(77)	0.264(13)	0.742(29)
×	0.80	−0.0100	0.06595(86)	0.01135(22)	0.000100(10)	0.776(65)
×	0.80	−0.0040	0.06346(86)	0.01042(24)	0.000086(10)	0.795(73)
	0.80	−0.0070	0.06503(88)	0.01088(21)	0.000081(5)	0.681(35)
×	0.80	−0.2453	0.271(12)	0.734(16)	0.463(33)	0.860(46)
×	0.80	−0.2463	0.251(11)	0.743(15)	0.464(39)	0.842(51)
×	0.80	−0.2473	0.249(13)	0.749(17)	0.482(37)	0.861(48)

Table C.16: $\frac{L}{a} \times \frac{T}{a} = 32 \times 32$

	g	m_0	$k_S(T/4,0)$	$k_0(T/2,0)$	$Z_\psi^2 \bar{g}_R^2$	$\bar{g}_R^2$
	0.39	−0.0595	0.00368(94)	0.99794(39)	0.1602(12)	0.1608(12)
	0.39	−0.06	−0.00074(94)	0.99861(39)	0.1608(13)	0.1613(12)
	0.39	−0.062	−0.0174(14)	1.00021(54)	0.1591(19)	0.1590(18)
	0.39	−0.063	−0.0239(14)	0.99967(55)	0.1574(18)	0.1575(17)
	0.398	−0.062	0.0053(14)	0.99784(58)	0.1681(21)	0.1689(20)
	0.398	−0.0623	0.00152(51)	0.99835(22)	0.16718(74)	0.16773(71)
→	0.398	−0.0624	−0.00024(51)	0.99802(21)	0.16543(72)	0.16609(69)
	0.398	−0.0625	−0.00182(62)	0.99866(26)	0.16690(88)	0.16735(85)
	0.398	−0.063	−0.0049(14)	0.99765(58)	0.1640(20)	0.1648(19)
	0.40	−0.0625	0.00270(87)	0.99762(37)	0.1681(13)	0.1689(12)
	0.40	−0.0629	0.00133(51)	0.99787(21)	0.16882(74)	0.16954(71)
→	0.40	−0.06301	0.00003(36)	0.99806(15)	0.16773(52)	0.16838(50)
	0.40	−0.0632	−0.00228(37)	0.99858(15)	0.16995(53)	0.17043(51)
	0.40	−0.0636	−0.0046(10)	0.99843(42)	0.1679(14)	0.1685(13)
	0.40	−0.0641	−0.003953(93)	0.99978(26)	0.1707(19)	0.1708(18)
	0.40	−0.0642	−0.004758(90)	0.99980(26)	0.1701(17)	0.1702(17)
	0.405	−0.062	0.01209(30)	0.99420(58)	0.1732(39)	0.1752(38)
	0.405	−0.063	0.00761(30)	0.99550(59)	0.1715(38)	0.1731(37)
	0.405	−0.064	0.00218(27)	0.99784(60)	0.1775(41)	0.1783(39)
	0.405	−0.0643	0.00226(11)	0.99800(26)	0.1750(18)	0.1757(18)
	0.70	−0.2030	−0.0052(98)	0.9791(44)	0.576(20)	0.601(18)
	0.70	−0.2032	0.0113(87)	0.9739(44)	0.551(19)	0.581(17)
	0.70	−0.20325	0.0148(55)	0.9839(31)	0.576(16)	0.595(14)
→	0.70	−0.20328	0.0022(26)	0.9780(13)	0.5649(68)	0.5905(62)
	0.70	−0.20329	0.0035(30)	0.9802(15)	0.5746(76)	0.5981(70)
×	0.70	−0.2033	−0.0075(66)	0.9814(32)	0.622(34)	0.646(33)
	0.70	−0.2034	−0.0095(83)	0.9826(38)	0.570(18)	0.590(17)
	0.70	−0.2040	−0.0161(97)	0.9879(47)	0.568(23)	0.582(21)
	0.70	−0.2042	−0.0063(94)	0.9848(51)	0.588(29)	0.606(26)
×	0.70	−0.20425	−0.0050(33)	0.9829(16)	0.5872(82)	0.6078(74)
	0.70	−0.2044	−0.014(11)	0.9812(49)	0.545(19)	0.566(17)
×	0.80	−0.0040	0.1040(13)	0.02839(51)	0.000546(37)	0.677(36)
×	0.80	−0.0070	0.1083(13)	0.03026(52)	0.000647(54)	0.707(48)
×	0.80	−0.0100	0.1083(13)	0.03087(49)	0.000621(40)	0.652(35)
×	0.80	−0.2463	0.215(12)	0.824(13)	0.537(39)	0.790(48)

Table C.17: $\frac{L}{a} \times \frac{T}{a} = 24 \times 24$

g	m_0	$k_S(T/4,0)$	$k_0(T/2,0)$	$Z_\psi^2 \bar{g}_R^2$	$\bar{g}_R^2$
0.40	−0.0629	0.00046(35)	0.99844(27)	0.1698(14)	0.1703(14)
→ 0.40	−0.06298	0.00017(35)	0.99821(26)	0.1684(14)	0.1690(13)
→ 0.70	−0.20314	0.0013(34)	0.9866(18)	0.5979(91)	0.6142(82)
0.70	−0.20425	−0.0049(32)	0.9807(16)	0.5718(78)	0.5945(71)

Table C.18: $\frac{L}{a} \times \frac{T}{a} = 16 \times 16$

g	m_0	$k_S(T/4,0)$	$k_0(T/2,0)$	$Z_\psi^2 \bar{g}_R^2$	$\bar{g}_R^2$
0.39	−0.059	0.00347(25)	0.99766(14)	0.15984(36)	0.16059(35)
0.39	−0.0594	0.00184(25)	0.99831(14)	0.16011(36)	0.16065(35)
0.39	−0.05985	0.00041(39)	0.99857(21)	0.16058(57)	0.16104(55)
→ 0.39	−0.0599	−0.00022(25)	0.99856(14)	0.16106(36)	0.16153(35)
0.39	−0.0608	−0.00387(28)	0.99959(15)	0.16123(38)	0.16137(37)
0.39	−0.061	−0.00459(28)	1.00009(15)	0.16229(38)	0.16226(37)
0.40	−0.061	0.00876(58)	0.99612(33)	0.16750(86)	0.16880(83)
0.40	−0.0629	0.00047(26)	0.99792(14)	0.16897(39)	0.16967(37)
→ 0.40	−0.06295	−0.00015(26)	0.99819(14)	0.16904(39)	0.16965(37)
0.40	−0.063	−0.00045(58)	0.99922(32)	0.16936(87)	0.16962(84)
0.40	−0.065	−0.00951(58)	1.00055(32)	0.16974(86)	0.16956(82)
0.70	−0.2010	0.0054(60)	0.9871(35)	0.584(15)	0.599(13)
0.70	−0.2020	0.0161(60)	0.9764(33)	0.548(13)	0.575(12)
0.70	−0.2021	0.00480(60)	0.98094(37)	0.576(18)	0.5991(16)
0.70	−0.2025	0.00412(60)	0.98160(37)	0.5797(18)	0.6016(16)
→ 0.70	−0.2030	−0.0051(56)	0.9841(34)	0.591(15)	0.610(14)
0.70	−0.20425	−0.0058(29)	0.9819(17)	0.5711(75)	0.5923(69)

C.5 Continuum extrapolations of the lattice data

The data that enters the continuum extrapolations is compiled in the following tables and plots. The values of m_0 and g that belong to a value of L/a can be found in tables 6.1 and 6.2.

C.5.1 $N = 4$ Gross-Neveu model at $g_R = 0.442$

Table C.19: Quantities that vanish in the continuum limit

L/a	$(k_S)_R(T/4, 2\pi/L)$	$(\bar{k}_S)_R(\pi/T, L/4)$	$(\bar{k}_S)_R(\pi/T, L/2)$
16	0.00263(23)	0.0008(12)	0.00081(93)
24	0.00104(25)	0.0011(13)	0.00092(99)
32	−0.00005(28)	−0.0018(15)	−0.0016(11)
40	−0.00014(27)	−0.0016(14)	−0.0012(11)
48	0.00054(28)	0.0031(15)	0.0021(11)

Table C.20: Quantities that do not vanish in the continuum limit

L/a	$(k_0)_R(T/4, 0)$	$(k_0)_R(T/4, 2\pi/L)$	$(k_0)_R(T/2, 2\pi/L)$	$(\bar{k}_1)_R(\pi/T, L/4)$	$\sigma(g_R^2, 2)$
16	1.00445(61)	0.22141(16)	0.094644(63)	0.37669(35)	0.2173(29)
24	1.00386(52)	0.22055(15)	0.090892(67)	0.37949(31)	0.2234(58)
32	1.00535(49)	0.22069(15)	0.089563(69)	0.38060(31)	–
40	1.00405(45)	0.22029(15)	0.089061(71)	0.38145(29)	0.2282(79)
48	1.00389(44)	0.21992(15)	0.088558(76)	0.38084(29)	0.234(15)

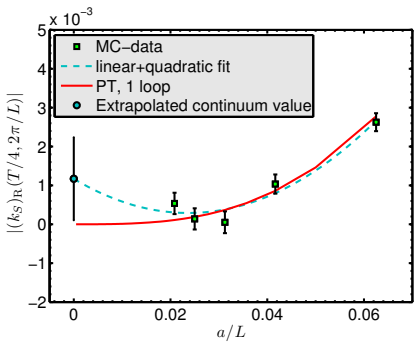

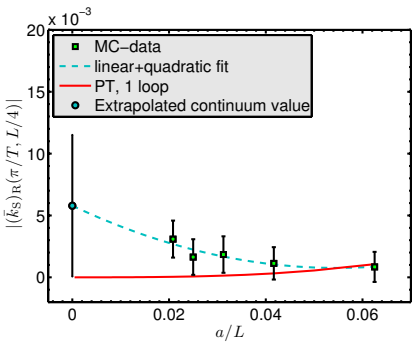

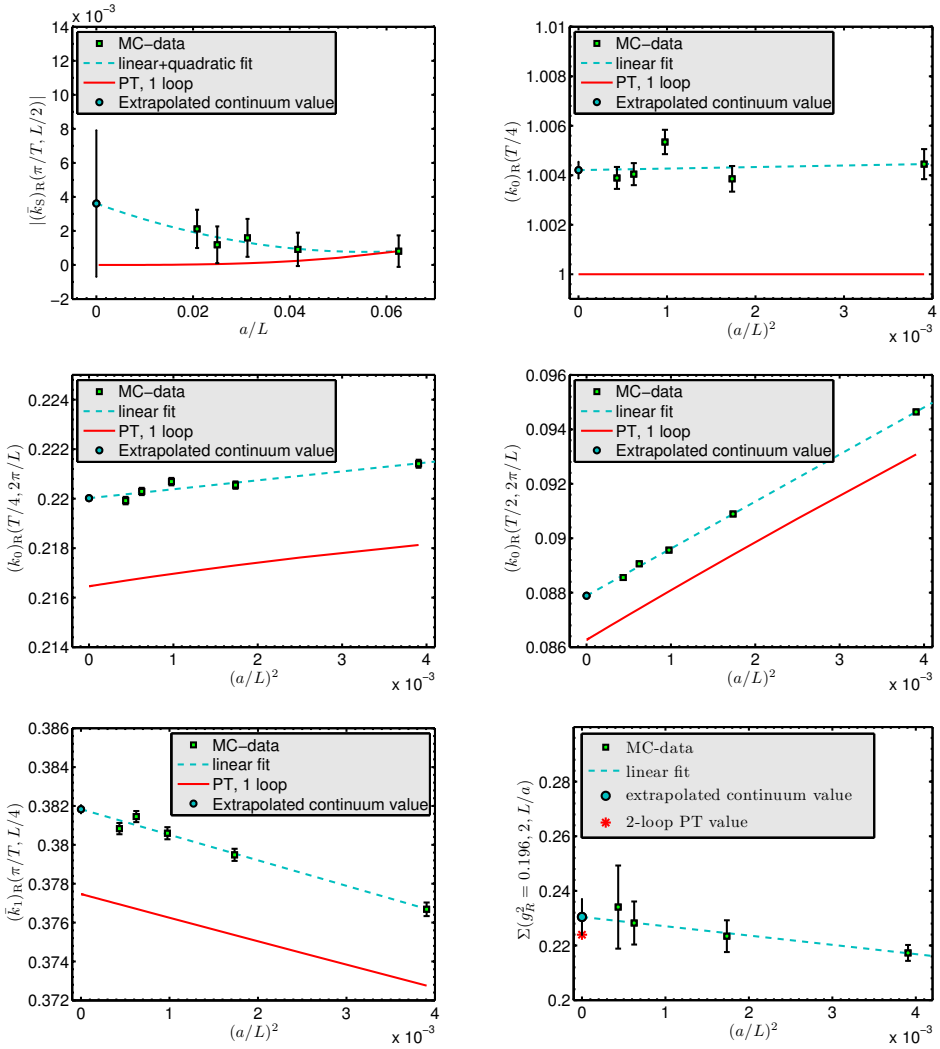

C.5.2 Thirring model at $g = 0.4$

Table C.21: Quantities that vanish in the continuum limit

L/a	$(k_S)_R(T/4, 2\pi/L)$	$(\bar{k}_S)_R(\pi/T, L/4)$	$(\bar{k}_S)_R(\pi/T, L/2)$
16	0.002805(30)	0.00122(15)	0.00098(11)
24	0.000877(43)	0.00062(20)	0.00044(15)
32	0.000421(42)	0.00049(20)	0.00025(16)
40	0.000244(53)	0.00006(26)	0.00020(20)
48	0.000146(56)	0.00013(27)	0.00013(21)

Table C.22: Quantities that do not vanish in the continuum limit

L/a	$(k_0)_R(T/4,0)$	$(k_0)_R(T/4,2\pi/L)$	$(k_0)_R(T/2,2\pi/L)$	$(\bar{k}_1)_R(\pi/T,L/4)$
16	1.00031(12)	0.218387(29)	0.093196(11)	0.373139(64)
24	1.00035(20)	0.217559(65)	0.089541(40)	0.37559(12)
32	1.00027(12)	0.217211(32)	0.088203(16)	0.376693(69)
40	1.00038(14)	0.216994(39)	0.087505(20)	0.377036(83)
48	1.00022(14)	0.216919(40)	0.087187(21)	0.377222(83)

Table C.23: Current-Current correlators

L/a	$f_{00}(T/2,0)$	$f_{11}(T/2,0)$
16	0.488507(98)	−0.50342(36)
24	0.48699(22)	−0.50199(72)
32	0.48639(15)	−0.50120(45)
40	0.48646(26)	−0.50263(79)
48	0.48590(33)	−0.50259(10)

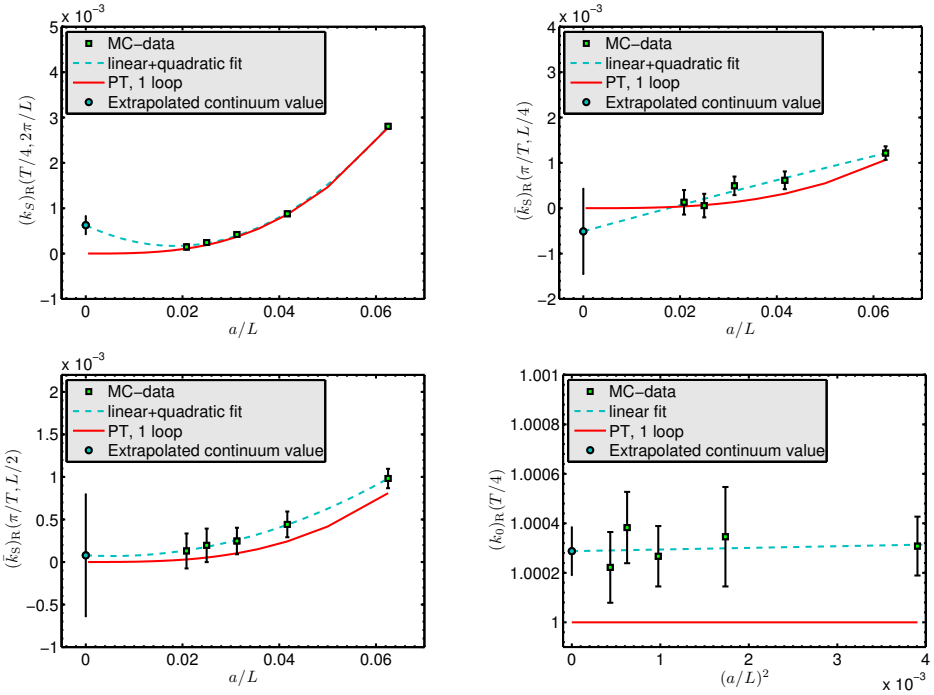

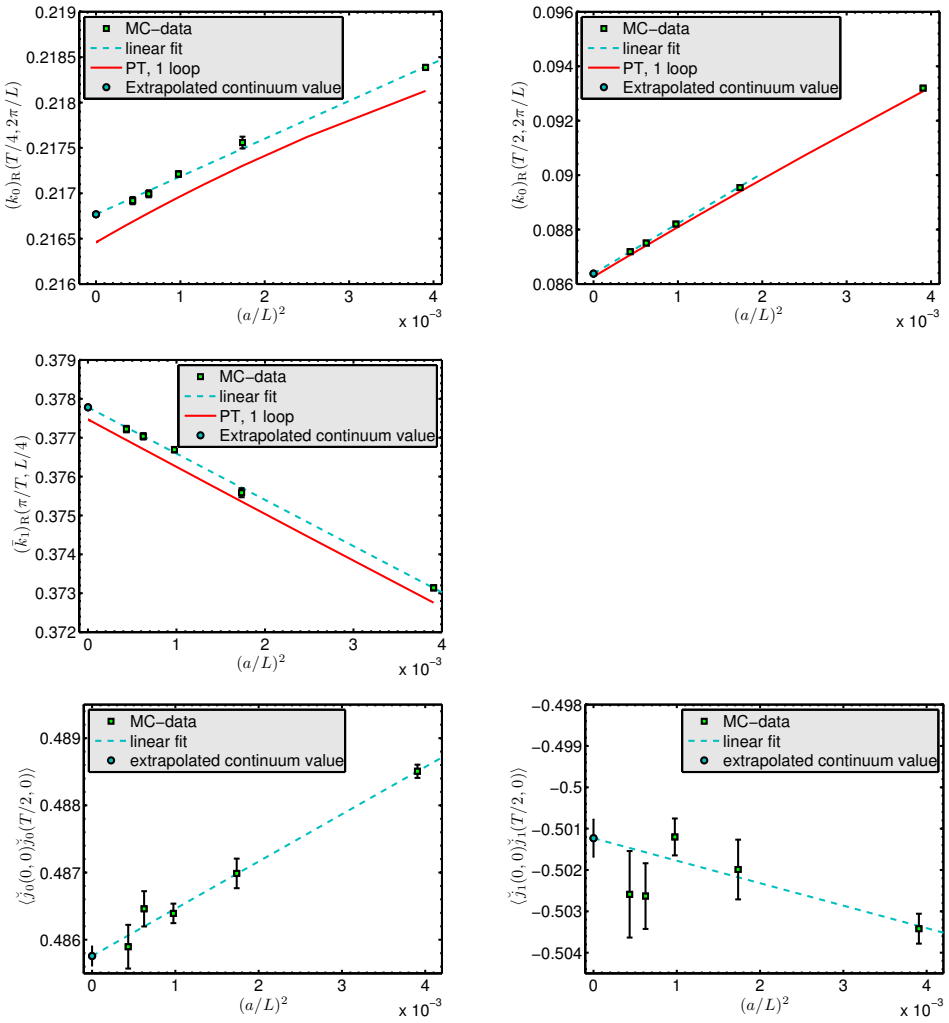

C.5.3 Thirring model at $g = 0.7$

Table C.24: Quantities that vanish in the continuum limit

L/a	$(k_S)_R(T/4, 2\pi/L)$	$(\bar{k}_S)_R(\pi/T, L/4)$	$(\bar{k}_S)_R(\pi/T, L/2)$
16	0.00286(67)	0.0020(34)	0.0000(27)
24	0.00077(40)	0.0006(20)	0.0005(15)
32	0.00080(32)	0.0021(16)	0.0009(12)
40	−0.00002(79)	0.0010(39)	0.0004(30)
48	−0.00127(92)	−0.0055(49)	−0.0044(37)

Table C.25: Quantities that do not vanish in the continuum limit

L/a	$(k_0)_R(T/4,0)$	$(k_0)_R(T/4,2\pi/L)$	$(k_0)_R(T/2,2\pi/L)$	$(\bar{k}_1)_R(\pi/T,L/4)$
16	1.0019(28)	0.22048(77)	0.09409(36)	0.3748(15)
24	1.0011(14)	0.21883(42)	0.09039(23)	0.37710(80)
32	1.0035(10)	0.21983(31)	0.08949(19)	0.37996(60)
40	1.0070(23)	0.22082(74)	0.08865(42)	0.3820(13)
48	1.0017(26)	0.21975(84)	0.08857(48)	0.3804(16)

Table C.26: Current-Current correlators

L/a	$f_{00}(T/2,0)$	$f_{11}(T/2,0)$
16	0.43519(74)	−0.4843(22)
24	0.4332(12)	−0.4804(36)
32	0.4334(12)	−0.4866(41)
40	0.4341(16)	−0.4760(51)
48	0.4344(17)	−0.4805(50)

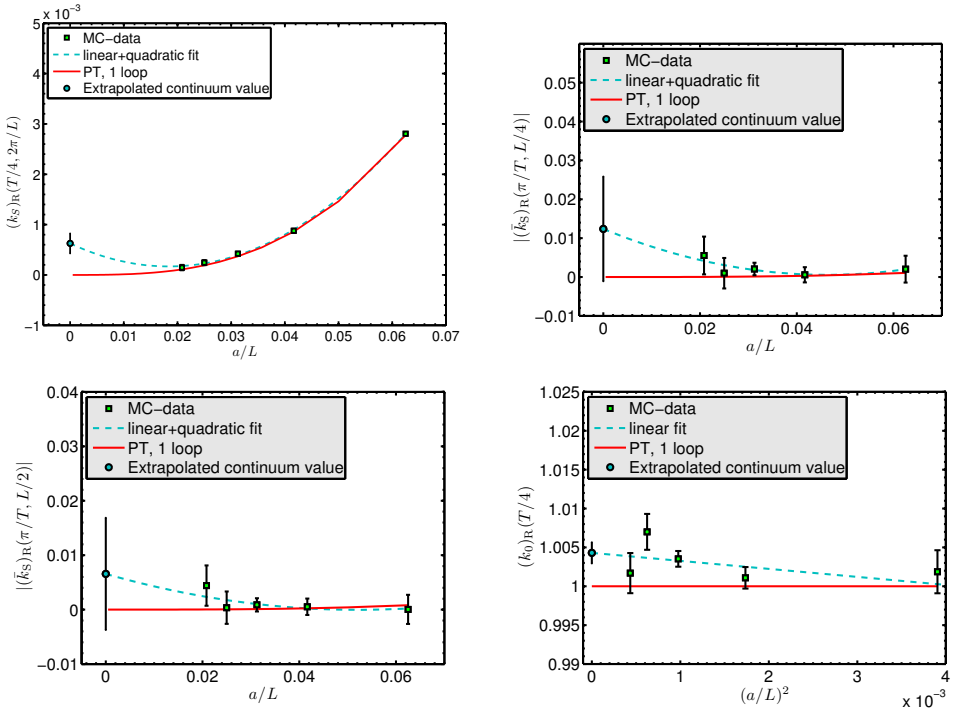

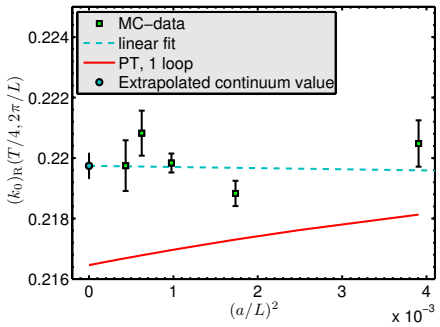
MC–data
linear fit
PT, 1 loop
Extrapolated continuum value
$(k_0)_R(T/4, 2\pi/L)$
$(a/L)^2$
x 10^{-3}

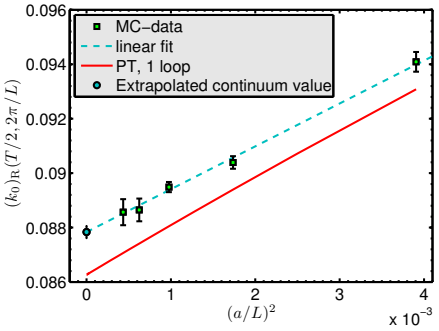
MC–data
linear fit
PT, 1 loop
Extrapolated continuum value
$(k_0)_R(T/2, 2\pi/L)$
$(a/L)^2$
x 10^{-3}

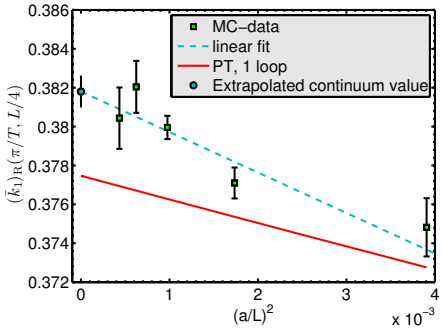
MC–data
linear fit
PT, 1 loop
Extrapolated continuum value
$(\bar{k}_1)_R(\pi/T, L/4)$
(a/L)^2
x 10^{-3}

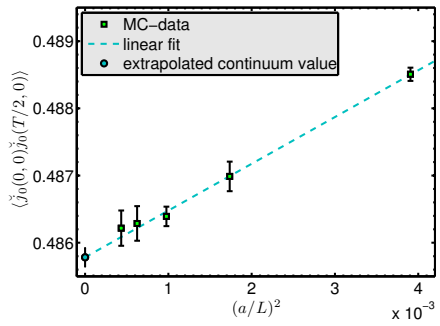
MC–data
linear fit
extrapolated continuum value
$\langle \check{j}_0(0,0)\check{j}_0(T/2,0)\rangle$
$(a/L)^2$
x 10^{-3}

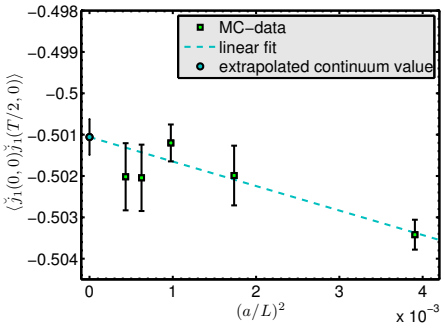
MC–data
linear fit
extrapolated continuum value
$\langle \check{j}_1(0,0)\check{j}_1(T/2,0)\rangle$
$(a/L)^2$
x 10^{-3}

Short summary in german language

Das Hauptanliegen der vorliegenden Arbeit ist es ein „Laboratorium" aufzubauen in dem Fragen, die für die Behandlung von Gitter-Eichtheorien relevant sind, untersucht werden können ohne auf überaus aufwändige Simulationen der QCD zurückgreifen zu müssen. Dazu werden zunächst das zwei dimensionale, renormierbare Gross-Neveu Modell sowie das verwandte chirale Gross-Neveu Modell eingeführt. Verschiedene Möglichkeiten der Diskretisierung beider Modelle werden vorgestellt und in einer Rechnung gegenübergestellt, in der die Zahl der Fermion-Familien N mit unendlich genähert wird. Für diesen Grenzfall lässt sich eine bestimmte universelle Größe leicht numerisch bis auf nahezu Maschinen-Genauigkeit ausrechnen. Es wird gezeigt dass die Lösung des Kontinuum-Modells sowie Kontinuumsextrapolationen der Ergebnisse die mit Wilson-, mit staggered- und mit overlap-Fermionen erzielt wurden miteinander übereinstimmen.

Die Behandlung der Modelle mit endlichem N ist weitaus schwieriger. Insbesondere in dem chiralen Modell erweist es sich aufgrund der vielen Parameter in der Wirkung als nicht praktikabel einen kontrollierten, chiralen Kontinuums-Limes zu nehmen - jedenfalls nicht wenn man die systematischen und statistischen Fehler klein halten möchte. Daher liegt das Hauptaugenmerk in diesem Teil der Arbeit auf dem gewöhnlichen Gross-Nevue Modell mit diskreter γ_5-Symmetrie. Für dieses Modell wird ein Renormierungsschema vorgeschlagen, in dem, die endliche Größe des Systems als physikalische Skala fungiert. Das Schema wird mittels Gitter-Störungstheorie mit Wilson Fermionen auf ein-Schleifen-Niveau getestet.

Im weiteren Verlauf des Textes werden die Monte-Carlo Programme die im Rahmen dieser Arbeit zur Simulation der Theorie mit Wilson und mit staggered Fermionen entwickelt wurden vorgestellt. Die Version mit Wilson Fermionen wird dazu verwendet zahlreiche universelle Größen für die Fälle $N = 1$ und $N = 4$ und verschiedene Werte der renormierten Kopplung sehr genau zu berechnen. Diese Ergebnisse können in Zukunft dazu benutzt werden andere Möglichkeiten der Fermion Diskretisierung zu testen. Darüber hinaus konnten in dem $N = 1$-Modell, welches identisch mit dem Thirring-Modell ist, Ergebnisse einer exakten analytischen Rechnung bestätigt werden.

Acknowledgments

At this point I would like to express my gratitude to a number of persons without whom this work would never have been completed.

I thank my advisor Professor Dr. Ulli Wolff for proposing the interesting topic of this thesis and giving me the opportunity to work on it in his group. His collaboration, encouragement and support throughout every stage of the project were absolutely crucial for the completion.

Francesco Knechtli has been my main collaborator during the first half of the work. I am deeply grateful for his help, for innumerable fruitful discussions and his sustained interest in my work.

Thanks to Rainer Sommer and Björn Leder for numerous rich discussions on the chiral model.

I would like to thank all past and present members of the COM-group, as well as all the guests over the last four years for creating an enjoyable working atmosphere - it has been a pleasure to have you around!

I am much obliged to the DFG for supporting me financially via the Graduiertenkolleg 271 "Strukturuntersuchungen, Präzisionstests und Erweiterung des Standardmodells der Elementarteilchenphysik".

Special thanks to my friends and family.

Lebenslauf

Name:	Tomasz Korzec
1997	Abitur am Carl-Fuhlrott-Gymnasium, Wuppertal
04.1998-02.2003	Studium an der Humboldt Universität zu Berlin in der Fachrichtung Physik Diplom am Lehrstuhl von Prof. Dr. U. Wolff
04.2003-10.2006	Promotion an der Humboldt Universität zu Berlin Lehrstuhl von Prof. Dr. U. Wolff Institut für Physik
10.2006-jetzt	Research assistant an der University of Cyprus Lehrstuhl von Prof. Dr. Constantia Alexandrou

Publications

- "Gross-Neveu model as a laboratory for fermion discretization",
  Tomasz Korzec, Ulli Wolff
  hep-lat/0609022
- "Perturbative renormalisation of the chiral Gross-Neveu model",
  Björn Leder, Tomasz Korzec
  Proc.Sci.LAT2005:266,2005. hep-lat 0509144.
- "Monte-Carlo simulation of the chiral Gross-Neveu model"
  Tomasz Korzec, Francesco Knechtli, Ulli Wolff, Björn Leder
  Proc.Sci.LAT2005:267,2005. hep-lat/0509132
- "Universality in the Gross-Neveu model"
  Francesco Knechtli, Tomasz Korzec, Björn Leder, Ulli Wolff
  Nucl.Phys.Proc.Suppl.140:785-787,2005. hep-lat/0410018
- "Comparison of analytic and numerical results in the XY model"
  Janos Balog, Francesco Knechtli, Tomasz Korzec, Ulli Wolff
  Nucl.Phys.Proc.Suppl.129:777-779,2004. hep-lat/0309052
- "Numerical confirmation of analytic predictions for the finite volume mass gap of the XY model"
  Janos Balog, Francesco Knechtli, Tomasz Korzec, Ulli Wolff
  Nucl.Phys.B675:555-566,2003. hep-lat/0309028
- "Comparison of exact and numerical results in the XY model"
  Diploma thesis by Tomasz Korzec 2003
  http://edoc.hu-berlin.de/diplom/physik/korzec-tomasz-2003-02-28/

Selbstständigkeitserklärung

Hiermit erkläre ich, die vorliegende Arbeit selbstständig ohne fremde Hilfe verfasst und nur die angegebene Literatur und Hilfsmittel verwendet zu haben.

Berlin, den 27.09.2006

Tomasz Korzec